ACIBADEM MEHMET ALI AYDINLAR UNIVERSITY
GRADUATE SCHOOL OF NATURAL AND APPLIED SCIENCES

DEVELOPMENT OF A 3D BIOPRINTED HYDROGEL MODEL FOR SPINAL CORD INJURIES

ASLIHAN AKALINLI

M.Sc. THESIS

DEPARTMENT OF BIOMEDICAL ENGINEERING

SUPERVISOR
Prof. Dr. Vasıf Nejat Hasırcı

SECONDARY SUPERVISOR
Asst. Prof. Dr. Deniz Yücel

İSTANBUL-2025

ACIBADEM MEHMET ALI AYDINLAR UNIVERSITY
GRADUATE SCHOOL OF NATURAL AND APPLIED SCIENCES

DEVELOPMENT OF A 3D BIOPRINTED HYDROGEL MODEL FOR SPINAL CORD INJURIES

ASLIHAN AKALINLI

M.Sc. THESIS

DEPARTMENT OF BIOMEDICAL ENGINEERING

SUPERVISOR
Prof. Dr. Vasıf Nejat Hasırcı

SECONDARY SUPERVISOR
Asst. Prof. Dr. Deniz Yücel

İSTANBUL-2025

DECLARATION

I declare that this thesis work is my own work, I had no unethical behavior at any stage from the planning to the writing of the thesis, I obtained all the information in this thesis in accordance with academic and ethical rules, I cited all the information and comments that were not obtained in this thesis work, and I provided resources in the list of references. I also declare that there was no violation of any patents and copyrights during the study and writing of this thesis.

30.01.2025
Aslıhan Akalınlı

PREFACE AND ACKNOWLEDGEMENT

I would like to express my deepest gratitude and sincere appreciation to my thesis advisor, Prof. Dr. Vasıf Nejat HASIRCI, who has been a constant source of guidance, encouragement, and support throughout all stages of my academic journey. From my undergraduate years to the completion of my graduate studies, his invaluable mentorship, insightful advice, and constructive feedback have played a pivotal role in shaping my scientific perspective and enhancing the quality of my work. I am truly honored and privileged to have had the opportunity to conduct my thesis under his supervision, and I will always be grateful for his patience, motivation, and unwavering belief in my abilities.

I would like to extend my indebted thanks to my secondary advisor, Asst. Prof. Deniz YÜCEL, for her invaluable guidance, support, and encouragement throughout this study. Her efforts have been instrumental in the progress and refinement of my work, and I am deeply grateful for her kindness and insight.

I would like to express my sincere gratitude to Prof. Dr. Halime KENAR for her support and motivation during my research. I feel fortunate to have had the opportunity to learn from her and to benefit from her expertise.

I sincerely thank all members of the ACU Biomaterials Center and my lab mates for their support. A special thanks to my research partner, Şeyma IŞIK[2], whose kindness and support made this journey brighter. I also extend my gratitude to METU-BIOMAT, especially Dr. Damla ARSLANTUNALI ŞAHİN, for her invaluable guidance, whose support and encouragement have been truly inspiring and reassuring.

I would like to express my heartfelt gratitude to my best friend, Nurdan ÇAM, whose friendship has been a source of strength, joy, and unwavering support. From the laughter we've shared to the memories we've created, her belief in me and genuine care have left an indelible mark. I am deeply grateful to have such a remarkable person by my side.

I would like to express my deepest gratitude to my dear master-key friend, Utku ERTETİK, whose unwavering support has been a cornerstone throughout my thesis journey. His encouragement, wisdom, and constant belief in my abilities have been an immense source of strength during the most challenging times. Utku's presence has not only made the difficult moments easier but has also been a continual source of inspiration and motivation. I am incredibly fortunate to have had him by my side, and his friendship has been one of the greatest gifts of this experience.

I am profoundly grateful to my unbiological sister, Eliz DEMİRAY, whose unwavering belief in me has been a guiding light. Her kindness, humor, and unique perspective have made challenges manageable and successes more meaningful. I am equally thankful to my dear friend, Sedat KÜRKLÜ, for his continued support and encouragement. Together, their presence has enriched this journey in ways words cannot fully capture. I am incredibly lucky to have both of them by my side.

I am deeply grateful to Kübra COŞKUN KIRATLI, whose constant support and availability, even with just a phone call, has been a true source of comfort throughout this journey. I also want to express my heartfelt thanks to Selen Ege KIRBAŞ, whose friendship has transcended distance, proving that no matter how far away, true support knows no boundaries. My sincere gratitude also goes to Tuğçe DOĞRUEL, whose encouragement, despite the time zone difference, always made me feel her presence and belief in me. Each of you has made this process smoother, and I am incredibly fortunate to have such supportive friends in my life.

I am incredibly grateful to Mehmet Mert YÜKSEL, whose support and positive energy have been a constant source of motivation throughout my journey. I also want to extend my heartfelt thanks to İpek Duygu TÜRKDEMİR, whose consistent encouragement and belief in me have made a lasting impact on my experience. Lastly, I am thankful to my dear friend, Büşra YAŞLI, for bringing so much color and joy to my life in such a short time.

I am truly grateful to Dr. Atefeh EMAMI and Dilara SİPAHİOĞLU, whose friendship and support have been invaluable throughout my master's journey. Their positive energy, insightful conversations, and unwavering encouragement have been a source of strength and inspiration.

I would like to express my deepest love and blessings to my beloved, Hurşit Emre TURAN, whose unwavering love and encouragement have been a cornerstone of my strength throughout this journey. His steadfast belief in my abilities and his constant support have made even the toughest moments feel surmountable. Sharing this path with him has brought me immense comfort and joy. He applauded me so loudly that I never even noticed who didn't.

I would like to express my deepest and most heartfelt gratitude to my beloved parents, Zülfiye Alev AKALINLI and Kemal Feza AKALINLI, for their endless love, unwavering support, and immeasurable patience throughout my life and during the completion of this thesis. Their encouragement, sacrifices, and belief in me have been my greatest source of strength. I am forever indebted to them for their constant care, trust, and guidance, which have shaped me into the person I am today. Without their unconditional love and steadfast support, none of this would have been possible. Their presence in my life is a blessing for which I will always be profoundly grateful.

I would also like to express my deepest gratitude to my beloved grandmother, Hüsniye GÜNAYDIN, who has been a pillar of love, wisdom, and strength in my life. Her unwavering support, endless encouragement, and unconditional love have been my greatest source of inspiration. I am profoundly grateful for the values she instilled in me and the countless ways she has shaped who I am today. This thesis is dedicated to her enduring belief in me and her irreplaceable presence in my life.

I would like to acknowledge to TÜBİTAK for their support through the BİDEB 2210-C Scholarship. This study was also supported by Acıbadem Mehmet Ali Aydınlar University, and I gratefully acknowledge its facilities and contributions.

TABLE OF CONTENTS

DECLARATION ..... **iii**

PREFACE AND ACKNOWLEDGEMENT ..... **iv**

TABLE OF CONTENTS ..... **vii**

ABBREVIATIONS AND SYMBOLS ..... **x**

ŞEKİLLER LİSTESİ ..... **xiii**

LIST OF TABLES ..... **xvi**

ÖZET **1**

ABSTRACT **2**

1 INTRODUCTION AND AIM **3**

2 BACKGROUND **5**

2.1 The Nervous System **5**
2.1.1 The central nervous system (CNS) **5**
2.1.1.1 Anatomy and physiology of the spinal cord **6**
2.1.2 The peripheral nervous system (PNS) **8**
2.1.3 Cells of the nervous system **9**
2.1.3.1 Glial cells **10**
2.1.3.2 Neurons **11**
2.2 Spinal Cord Injuries (SCI) **12**
2.2.1 Acute spinal cord injury **13**
2.2.2 Sub-acute spinal cord injury **15**
2.2.3 Chronic spinal cord injury **16**
2.2.4 Current treatment approaches and their limitations for spinal cord injuries **17**
2.3 Principles of Tissue Engineering and Regenerative Medicine **18**
2.3.1 Nerve tissue engineering **20**
2.3.1.1 Cell sources used in nerve tissue engineering **21**
2.3.1.1.1 Stem cells **21**
2.3.1.1.2 Schwann cells **23**
2.3.1.1.3 Induced pluripotent stem cells **25**
2.3.1.1.4 Neuronal cell lines **26**
2.3.1.2 Scaffolds used in nerve tissue engineering **27**
2.3.1.2.1 Natural materials **27**
2.3.1.2.2 Synthetic materials **30**
2.3.1.2.3 Hybrid materials **31**
2.3.1.3 Neurotrophic factors in nerve tissue engineering **33**
2.3.1.3.1 Nerve growth factor (NGF) **33**

2.3.1.3.2 Glial cell line derived neurotrophic factor (GDNF) 35
2.3.1.3.3 Brain derived neurotrophic factor (BDNF)..... 36
2.3.1.4 Three dimensional (3D) printing (additive manufacturing) 38
2.3.1.4.1 Bioprinting techniques 38
2.3.1.4.2 Multi material bioprinting 39
2.3.1.4.3 Integration of stem cells..... 39
2.3.1.4.4 *In Vitro* models and preoperative simulations..... 39
2.3.1.4.5 Challenges and future prospects 40
2.4 Approach, Aim and Novelty of the Study..... 40

3 MATERIALS AND METHODS 43

3.1 Materials..... 43
3.1.1 Chemicals 43
3.1.2 Equipments 44
3.2 Methods 44
3.2.1 Synthesis and characterization of methacrylated gelatin (GelMA) 44
3.2.1.1 Determination of methacrylation level of the methacrylated gelatin with ^{1}H-NMR..... 45
3.2.1.2 Fourier transform infrared spectroscopy (FT-IR) 46
3.2.2 Production of GelMA/HA/CS/Lmn hydrogel slabs 46
3.2.3 Characterization of GelMA/HA/CS/Lmn hydrogel slabs 47
3.2.3.1 Fourier transform infrared spectroscopy (FT-IR) 47
3.2.3.2 Determination of equilibrium water content (EWC) 47
3.2.3.3 Degradation of hydrogel slabs 48
3.2.3.4 Enzymatic degradation 48
3.2.3.5 Mechanical properties 49
3.2.3.6 Rheological examination 49
3.2.3.7 SEM examination 50
3.2.4 3D printing of hydrogel..... 50
3.2.4.1 Design of 3D bioprinted hydrogel 50
3.2.4.2 Printing of the model hydrogels 51
3.2.5 Characterization of GelMA/HA/CS/Lmn 3D printed hydrogels..... 52
3.2.5.1 Determination of equilibrium water content (EWC) 52
3.2.5.2 Degradation of 3D printed hydrogels..... 53
3.2.5.3 Enzymatic degradation 53
3.2.5.4 Mechanical properties 53
3.2.5.5 Morphological analysis..... 53
3.2.6 *In Vitro* studies 53
3.2.6.1 Cell culture of astrocytes (SVG p12 cell line)..... 53
3.2.6.2 PC 12 cell culture 54
3.2.7 Cell response and assessment of 3D bioprinted hydrogels..... 54
3.2.7.1 Cell seeded hydrogels..... 54
3.2.7.2 SVG p12 loaded 3D bioprinted hydrogel..... 55
3.2.7.3 Alamar blue assay..... 55
3.2.7.4 Live-dead cell viability assay 56
3.2.7.5 Immunostaining..... 57
3.2.7.6 Phalloidin-DAPI staining 58

3.3 Statistical Analysis 58

4 RESULTS 59

4.1 Synthesis and Characterization of Methacrylated Gelatin (GelMA) 59
4.1.1 Methacrylation efficiency of hydrogel with ^{1}H nuclear magnetic resonance (^{1}H-NMR) 59
4.1.2 Infrared spectroscopy (FT-IR) 60
4.2 Characterization of GelMA/HA/CS/Lmn Hydrogel Slabs 60
4.2.1 Infrared spectroscopy (FT-IR) 60
4.2.2 Determination of equilibrium water content (EWC) 62
4.2.3 *In Situ* degradation of hydrogel 63
4.2.4 Enzymatic degradation 64
4.2.5 Mechanical properties 65
4.2.6 Rheological examination 67
4.2.7 Morphological analysis 68
4.3 3D Printing of Hydrogels 69
4.3.1 Fabrication of 3D bioprinted hydrogels 69
4.3.2 Characterization of GelMA/HA/CS/Lmn 3D printed hydrogels 70
4.3.2.1 Determination of equilibrium water content (EWC) 70
4.3.2.2 Degradation of 3D printed hydrogels 71
4.3.2.3 Enzymatic degradation 72
4.3.2.4 Mechanical properties 72
4.3.2.5 Morphological analysis 73
4.3.3 *In Vitro* studies 74
4.3.3.1 Culture of SVG p12 cells 74
4.3.3.2 Culture of PC 12 cells 75
4.3.4 Cell response and functional evaluation of 3D bioprinted hydrogel 76
4.3.4.1 Preparation of cell loaded hydrogels 76
4.3.4.2 Cell proliferation with alamar blue assay 77
4.3.4.3 Live-dead assay for cell viability 79
4.3.4.4 Immunostaining 83
4.3.4.5 Phalloidin-DAPI staining 87

5 DISCUSSION 91

6 CONCLUSION 93

7 REFERENCES 94

8 CURRICULUM VITAE 103

ABBREVIATIONS AND SYMBOLS

2D	Two Dimensional
3D	Three dimensional
ANOVA	Analysis of Variance
ATCC	American Type Cell Collection
BDNF	Brain-derived Neurotrophic Factor
Ca	Calcium
CLSM	Confocal Laser Scanning Microscopy
cm	Centimeter
CNS	Central Nervous System
CO	Cut off
CO_2	Carbon dioxide
CS	Chondroitin sulfate
D_2O	Deuterium oxide
DAPI	4',6-Diamino-2-phenylindole
dH_2O	Distilled water
DM	Degree of Methacrylation
DMEM	Dulbecco's Modified Eagle Medium
DMSO	Dimethyl sulfoxide
DPBS	Dulbecco's Phosphate Buffered Saline
E	Young's Modulus
ECM	Extracellular matrix
EtOH	Ethanol
EWC	Equilibrium Water Content
FBS	Fetal Bovine Serum
FDM	Fused Deposition Modeling
FITC	Fluorescein isothiocyanate
Fnc	Fibronectin
FTIR	Fourier Transform Infrared
g	Gram
GAGs	Glycosaminoglycans

GDNF	Glial Cell Line derived Neurotrophic Factor
GelMA	Methacrylated gelatin
GFAP	Glial Fibrillary Acidic Protein
g	Hour
^{1}H-NMR	^{1}H-Nuclear Magnetic Resonance
HA	Hyaluronic acid
Irgacure 2959	2- (Hydroxyl)- 4- (2- hydroxyethoxy)- 2- methylpropiophenone
J	Joule
Lmn	Laminin
M	Molar
MAA	Methacrylic anhydride
MD	Methacrylation Degree
µg	Microgram
µm	micrometer
mg	Milligram
min	Minute
mL	Milliliter
mm	Millimeter
mM	Millimolar
MPa	Mega Pascal
MSCs	Mesenchymal Stem Cells
Mw	Molecular Weight
N	Newton
Na	Sodium
NGF	Nerve Growth Factor
nm	Nanometer
NSC	Neural Stem Cell
ºC	Celcius
P	Passage
P/S/A	Penicillin/Streptomycin/Amphotericin-B
PBS	Phosphate buffered saline
PDMS	Poly(dimethylsiloxane)

PFA	Paraformaldehyde
PNS	Peripheral Nervous System
rpm	Rotation per minute
RT	Room Temperature
SCI	Spinal Cord Injury
SEM	Scanning Electron Microscopy
SLA	Stereolitography
SLS	Selective Laser Sintering
TCPs	Tissue Culture Polystyrene
US	United States
UTS	Ultimate Tensile Strength
UV	Ultraviolet
v/v	volume/volume
w/v	weight/volume
W_d	Dry Weight
WHO	World Health Organization
W_w	Wet Weight

ŞEKİLLER LİSTESİ

Figure 1. Central and peripheral nervous system 5

Figure 2. The structure of the central nervous system 6

Figure 3. Anatomy and physiology of the spinal cord 7

Figure 4. Somatic and autonomic motor system 8

Figure 5. Spinal cord injury, primary and acute phase 14

Figure 6. Spinal cord injury subacute phase 15

Figure 7. Spinal cord injury chronic phase 16

Figure 8. Components of tissue engineering 19

Figure 9. Molecular structure of gelatin, a hydrolysis product of collagen 28

Figure 10. Molecular structure of hyaluronic acid 28

Figure 11. Molecular structure of chondroitin sulfate 29

Figure 12. Preparation of the SCI Model 41

Figure 13. The synthesis of GelMA 45

Figure 14. Design of 3D bioprinted SCI model 50

Figure 15. Cell proliferation with Alamar Blue Assay in cell culture procedure 56

Figure 16. 1H-NMR spectra of A) gelatin and B) methacrylated gelatin (GelMA). The peak between 7.5-6.9 ppm indicates aromatic amino acid phenylalanine signals, peak between 5.7-5.4 ppm indicates methacrylic vinyl groups and peak between 2.95-2.8 ppm indicates methacrylic vinyl groups and peak between 2.95-2.8 ppm indicates lysine methylene groups 59

Figure 17. FT-IR spectra of gelatin and methacrylated gelatin, green indicates amide I and blue indicates amide II bands 60

Figure 18 FT-IR spectra of GelMA, HA and GelMA-HA 61

Figure 19 FT-IR spectra of GelMA, HA, CS and GelMA-HA-CS 61

Figure 20. FT-IR spectra of GelMA, HA, CS and GelMA-HA-CS-Lmn 62

Figure 21. Equilibrium Water Content (EWC) (%) of GelMA, GelMA-HA, GelMA-HA-CS and GelMA-HA-CS-Lmn at the following compositions (30, 30:1, 30:1:1, and 30:1:1:0.2 in PBS). (n=3, ns: not significant, * : $p < 0.05$ and ** : $p < 0.01$) 63

Figure 22. Degradation behavior of GelMA, GelMA-HA, GelMA-HA-CS and GelMA-HA-CS-Lmn hydrogels 21 days in PBS at room temperature..... 64

Figure 23. Degradation of the hydrogels with collagenase: Weight remaining in GelMA, GelMA-HA, GelMA-HA-CS and GelMA-HA-CS-Lmn hydrogels in four different collagenase type II solutions with different concentrations (5 U/mL, 10 U/mL, 15 U/mL and 20 U/mL). 64

Figure 24. Stress- Strain curves of compression tests of GelMA, GelMA-HA, GelMA-HA-CS and GelMA-HA-CS-Lmn hydrogels days A)1, B)7 and C)14 in PBS containing 0.2% sodium azide. 66

Figure 25. Viscoelastic modulus of A) GelMA B) GelMA-HA C) GelMA-HA-CS and D) GelMA-HA-CS-Lmn. 67

Figure 26. SEM images of the slab of the 4 hydrogels used in the study. (A) GelMA, (B) GelMA-HA, (C) GelMA-HA-CS, and (D) GelMA-HA-CS-Lmn hydrogels at three different magnifications: (1) 200X, scale bar: 100 μm; (2) 500X, scale bar: 50 μm; and (3) 1000X, scale bar: 10 μm. 68

Figure 27. 3D model of spinal cord showing channels to mimic tracts of the white matter region. 70

Figure 28. Equilibrium Water Contents (%) of slabs and 3D printed form of GelMA-HA-CS-Lmn. (n=3, ns: not significant) 71

Figure 29. Degradation rates of the GelMA-HA-CS-Lmn slab and 3D Printed hydrogels in PBS (n=3). 71

Figure 30. Weight remaining percent in GelMA-HA-CS-Lmn slab and 3D-printed hydrogels after enzymatic degradation using four different concentrations of collagenase type II (20 U/mL) (n=3). 72

Figure 31. Stress- Strain curves of compression test of GelMA-HA-CS-Lmn. A) slab and B) 3D printed hydrogels in PBS containing 0.2% sodium azide. 73

Figure 32. SEM images of the GelMA-HA-CS-Lmn. (A) slab and (B) 3D printed hydrogel magnification 1000 X. 73

Figure 33. SEM images of the GelMA-HA-CS-Lmn 3D printed hydrogels. (A) top-view 31X. Microporous bulk: (B) 500 X, (C) 1000 X. Channels (D) 75X and (E) 250X. 74

Figure 34. Light microscope images of SVG p12 cells on TCPs at different magnifications: (A) 10X, (B) 20X, and (C) 40X. 75

Figure 35. Light microscopy images of PC 12 cells under different culture conditions: in the absence and presence of fibronectin, in the absence and presence of NGF (20X magnification) 76

Figure 36. Alamar Blue cell proliferation assay of SVG p12 (black) and PC 12 (grey) cells in 3D bioprinted hydrogel and slab..... 77

Figure 37. Live-Dead test of SVG p12 cells in 3D Bioprinted structure. Calcein AM stains live cells green, while Ethidium Homodimer-1 stains dead cells red. (scale bar: 50 μm) 81

Figure 38. Live-Dead assay of PC 12 loaded in the hydrogel slab Calcein AM stains live cells green, while Ethidium Homodimer-1 stains dead cells red. (scale bar: 50 μm) 82

Figure 39. Merged confocal images of 3D-printed SVG p12 cells and slab-form PC 12 cells on day 21. GFAP staining (green) shows glial cells (SVG p12), Beta III tubulin staining (red) shows axonal extensions of PC 12, and DAPI staining (blue) labels cell nuclei of both. The merged images reveal axonal outgrowth in both cell types (scale bar: 20 μm). Red arrow: indicates the cell extention along the direction of channel. Two sided arrow shows the channel direction (horizontal) 84

Figure 40. Phalloidin and DAPI staining of SVG p12 cells and PC12 cells at the junction of 3D bioprinted construct and slab between the two structures on day 7. Phalloidin staining highlights the actin cytoskeleton (green), while DAPI staining labels the cell nuclei (blue). (Scale bar: 20 μm)..... 89

LIST OF TABLES

Table 1. Molecular structure of A) GelMA, B) GelMA/HA, C) GelMA/HA/CS and D) GelMA/HA/CS/Lmn 46

Table 2. Hydrogel formulation overview 52

Table 3. Remaining weight of GelMA, GelMA-HA, GelMA-HA-CS, and GelMA-HA- CS-Lmn hydrogels after incubation in collagenase type II (5–20 U/mL) for 2 h. 65

Table 4. Young's Modulus of GelMA, GelMA-HA, GelMA-HA-CS and GelMA- HA-CS-Lmn hydrogels obtained in compression tests. 66

ÖZET

Omurilik Yaralanmaları İçin 3B Biyobasılmış Hidrojel Modeli Geliştirilmesi

Omurilik yaralanmaları (SCIs), sınırlı rejenerasyon kapasitesi nedeniyle genellikle kalıcı fonksiyon kayıplarına yol açan ciddi durumlardır. Glial skar oluşumu ve sinirsel bağlantıların bozulması bu zorlukları daha da artırmaktadır. Bu çalışmada, gri ve ak madde özelliklerini taklit eden, hidrojel tabanlı 3B biyo baskılı bir model geliştirilmiştir. Hidrojel, metakrilatlanmış jelatin (GelMA) ile sentezlenmiş ve hyaluronik asit (HA), kondroitin sülfat (CS) ve laminin (lmn) ile optimize edilmiştir. ^{1}H-NMR analizinde GelMA'nın metakrilasyon oranı %87,06 olarak belirlenmiş, FT-IR analizinde ise hidrojel bileşenlerinin başarılı şekilde sentezlenip entegre edildiği doğrulanmıştır. Hidrojelin su tutma kapasitesi %89 olarak ölçülmüş, *in situ* bozunma testlerinde 21 gün sonunda ağırlığının yaklaşık %90'ını koruduğu belirlenmiştir. Enzimatik bozunma testlerinde, 2 saatlik inkübasyonun ardından hidrojelin ağırlığının yaklaşık %76'sını koruduğu tespit edilmiştir. Mekanik testlerde, ilk gün sertlik değeri 145±11 kPa olarak ölçülmüş; reolojik incelemelerde elastik modül 10^3 ve viskoz modül 10^0 olarak bulunmuştur. Morfolojik incelemelerde, bal peteği desenli kanalların genişliği ortalama 385,07 µm olarak ölçülmüştür. *In vitro* çalışmalarda, Alamar Blue, Canlı/Ölü ve Phalloidin-DAPI analizleri, hidrojel içerisinde glial (SVG p12) ve nöronal (PC 12) hücrelerin çoğaldığını, hayatta kaldığını ve iyi organize olmuş iskelet yapıları sergilediğini göstermiştir. İmmun boyama analizleri ise hücrelerin model içerisinde nöron benzeri uzantılar verdiğini göstermiştir. Bu bulgular, geliştirilen 3B biyo baskılı hidrojel modelinin SCI araştırmaları ve omurilik onarımı için yenilikçi tedavi yaklaşımlarının geliştirilmesinde kontrollü ve tekrarlanabilir bir platform olarak potansiyele sahip olduğunu ortaya koymaktadır.

Anahtar Sözcükler: Omurilik yaralanmaları, 3B biyobasım, Hidrojel, Sinir uzantısı, Biyomürekkep

ABSTRACT

Development of a 3D Bioprinted Hydrogel Model for Spinal Cord Injuries

Spinal cord injuries (SCIs) are severe conditions that often result in permanent loss of function due to limited regenerative capacity. The formation of glial scars and disruption of neural connections further exacerbate these challenges. In this study developed a hydrogel-based 3D bioprinted model that mimics the characteristics of gray and white matter. The hydrogel was synthesized using methacrylated gelatin (GelMA) and optimized with hyaluronic acid (HA), chondroitin sulfate (CS), and laminin (lmn). ^{1}H-NMR analysis determined the degree of methacrylation of GelMA to be 87.06%, while FT-IR analysis confirmed the integration of the hydrogel components. The hydrogel had equilibrium water content of 89%. *In situ* degradation tests revealed that the hydrogel retained approximately 90% of its initial weight after 21 days. In enzymatic degradation, it maintained about 76% of its weight after 2 hours of incubation. Mechanical testing indicated a stiffness value of 145±11 kPa on the first day, while rheological analysis showed a elastic modulus (G') of 10^3 and a viscous modulus (G'') of 10^0. Morphological examinations measured the average width of the honeycomb-patterned channels as 385.07 μm. *In vitro* studies, including Alamar Blue, Live-Dead, and Phalloidin-DAPI, demonstrated the proliferation, survival, and well-organized cytoskeletal structures of glial (SVG p12) and neuronal (PC 12) cells within the hydrogel. Immunostaining analyses revealed that the cells exhibited neuron-like extensions within the model. These findings indicate that the developed 3D bioprinted hydrogel model holds significant potential as a controlled and reproducible platform for SCI research and the development of innovative spinal cord repair strategies.

Keywords: Spinal cord injuries, 3D bioprinting, Hydrogels, Neural extension, Bioink

1 INTRODUCTION AND AIM

Spinal cord injuries (SCIs) are among the most serious conditions affecting the central nervous system (CNS), leading to substantial and often irreversible impairments in sensory, motor, and autonomic functions (1). These injuries, which primarily result from traumatic events such as traffic accidents, falls, and acts of violence, affect millions of people worldwide, with a significant socioeconomic burden. The pathophysiology of SCIs is complex, involving primary mechanical damage followed by secondary injury cascades, including inflammation, oxidative stress, and apoptosis (2). These processes contribute to the formation of inhibitory glial scars and the degradation of neural networks, severely limiting the regenerative capacity of the spinal cord and impeding functional recovery (3).

Current treatment strategies for SCIs, such as surgical decompression, pharmacological interventions, and cell based therapies, offer only limited improvements in functional outcomes. Although these approaches help mitigate secondary injury and promote partial repair, they are far from providing a complete solution (4). Therefore, the development of innovative therapeutic approaches that can support neural regeneration, reduce glial scar formation, and restore functional connectivity is of critical importance (5).

Recent advancements in tissue engineering and regenerative medicine have paved the way for the development of *in vitro* models that can replicate the structural and functional characteristics of native tissues. In particular, 3D bioprinting has emerged as a powerful tool for fabricating biomimetic scaffolds with high precision and reproducibility (6). These scaffolds provide a controlled microenvironment that mimics the extracellular matrix (ECM), supporting cellular adhesion, proliferation, and migration. Moreover, 3D bioprinted models enable the integration of biochemical and mechanical cues essential for guiding neural regeneration and re-establishing functional networks (7).

This study focuses on the design and characterization of a 3D-bioprinted hydrogel model aimed at imitating the structural complexity of spinal cord tissue. Methacrylated gelatin (GelMA) was selected as the primary biomaterial due to its biocompatibility, tunable mechanical properties, and ability to support cellular functions. To enhance the hydrogel's bioactivity, hyaluronic acid (HA), chondroitin sulfate (CS), and laminin (lmn) were incorporated into the bioink formulation. These components were chosen for their roles in neural tissue repair, including promoting axonal growth, reducing inflammation, and improving cell adhesion (8).

The hydrogel-based bioink was optimized through physicochemical characterization, including analyses of gelation kinetics, equilibrium water content (EWC), and enzymatic degradation. Mechanical properties were tailored to mimic the biomechanical environment of spinal cord tissue, providing an ideal balance of stiffness and elasticity to support cellular growth. In addition, the bioprinted constructs featured specific micro architectural designs, such as honeycomb and channel patterns, to facilitate cellular alignment and guide neural network formation.

In vitro studies were conducted using glial (SVG p12) and neuronal (PC 12) cell lines to evaluate the hydrogel's biocompatibility and functionality. Key assessments, including Alamar Blue proliferation assays, Live-Dead viability tests, and immunostaining for cytoskeletal markers, confirmed the hydrogel's capacity to support cell survival, proliferation, and attachment. These results demonstrate that the hydrogel provides a supportive environment for both neuronal and glial cells, which are essential for reconstructing functional spinal cord tissue.

By combining advanced bioprinting technology with a carefully designed hydrogel system, this study aims to establish a reproducible and scalable platform for investigating SCI mechanisms and testing regenerative therapies. The findings of this research have the potential to contribute to the development of innovative treatment strategies that address the unmet clinical needs in spinal cord repair and regeneration.

2 BACKGROUND

2.1 The Nervous System

The nervous system is a highly intricate and interconnected network of specialized cells and tissues that regulates and coordinates the body's various functions. It enables the transmission of signals throughout the body, allowing us to perceive and react to our surroundings. The nervous system is primarily composed of two key components: the CNS, which includes the brain and spinal cord, and the peripheral nervous system (PNS), consisting of nerves that extend from the CNS to other parts of the body (9).

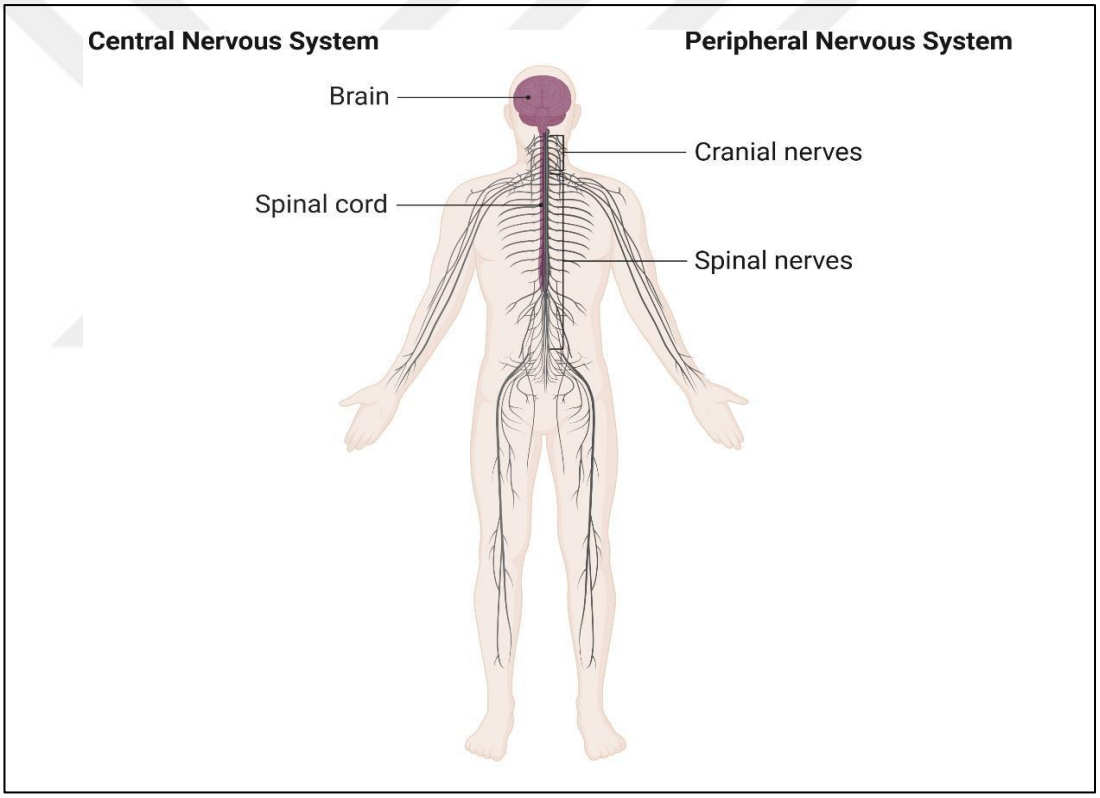

Figure 1. Central and peripheral nervous system

2.1.1 The central nervous system (CNS)

The CNS is the primary component of the human nervous system, responsible for integrating and coordinating physiological processes, sensory input, and motor

functions. It consists of the brain and spinal cord, which work in unison to interpret and respond to stimuli from both external and internal environments (10).

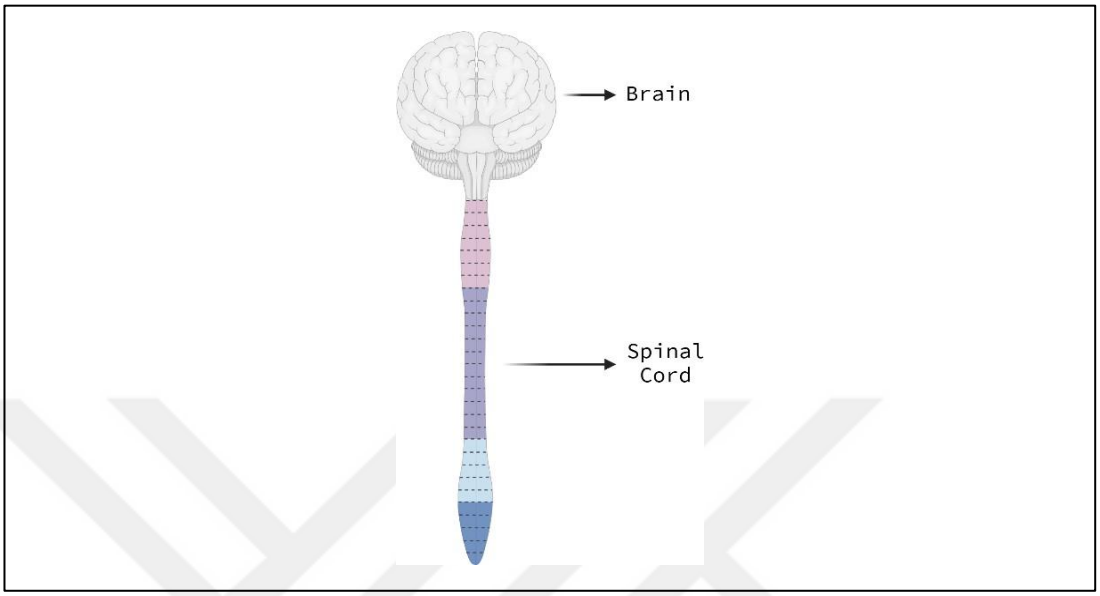

Figure 2. The structure of the central nervous system

The brain, serving as the central control unit, is divided into distinct regions with specialized roles. The cerebrum, the largest brain region, governs higher cognitive abilities, including perception, memory, and decision-making. The cerebellum, situated at the back of the brain, is crucial for coordinating voluntary movements and maintaining balance and posture (11).

The spinal cord extends from the brainstem and acts as a conduit, relaying sensory signals from the body to the brain and transmitting motor commands from the brain to the body (12). Additionally, involuntary processes such as heart rate and blood circulation are regulated by the autonomic nervous system, which is subdivided into the sympathetic and parasympathetic systems.

2.1.1.1 Anatomy and physiology of the spinal cord

The spinal cord, an essential part of the CNS, acts as the primary communication pathway between the brain and the rest of the body. It is encased within the vertebral

column, safeguarded by the bony vertebrae. Structurally, the spinal cord comprises a central region of gray matter surrounded by an outer layer of white matter (13).

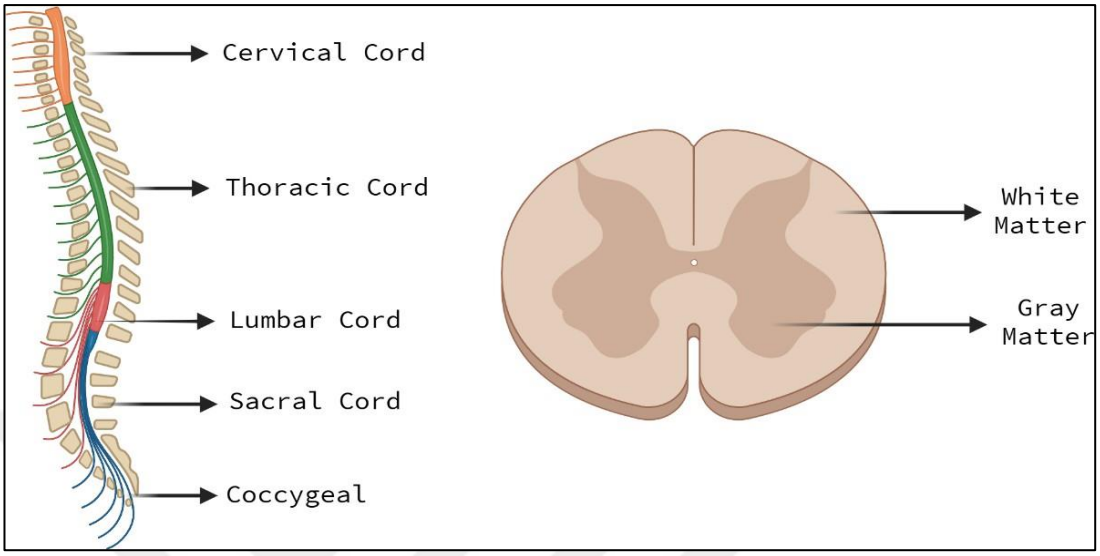

Figure 3. Anatomy and physiology of the spinal cord

The gray matter, composed of nerve cell bodies, exhibits a butterfly shaped pattern in cross-section. It contains motor neurons responsible for sending signals to muscles and interneurons that process and integrate sensory inputs. In contrast, the white matter consists mainly of myelinated axons, which facilitate the transmission of information along the spinal cord (13, 14).

The myelinated fibers in the white matter enable the rapid and efficient conduction of action potentials, crucial for maintaining coordinated body functions. These fibers are insulated by myelin sheaths, which are produced by oligodendrocytes specialized glial cells derived from oligodendrocyte precursor cells. Myelination of axons within the CNS is vital for the fast propagation of electrical signals, allowing for the seamless integration and coordination of neural activities (15).

The fatty myelin sheath insulating these axons ensures the swift and efficient transmission of electrical impulses, forming the highways and subways that interconnect various brain regions. These myelinated axons are organized into distinct tracts, each responsible for specific types of signal transmission (15, 16). The dorsal

columns convey proprioceptive and fine touch information, while the lateral and ventral columns are involved in transmitting motor and somatosensory signals. The insulating properties of the myelin sheath play a key role in maintaining the speed and efficiency of these neural transmissions. Beyond its primary functions, the spinal cord acts as a relay station for numerous ascending and descending pathways. Its posterior, lateral, and anterior columns house major tracts that transmit sensory information to the brain and deliver motor commands from the brain to the body (17). The spinal cord's connectivity with the brain, coupled with its role in processing and integrating sensory and motor information, highlights its critical significance in the CNS.

2.1.2 The peripheral nervous system (PNS)

The PNS is an intricate network of nerves and neurons that serves as a critical link between the CNS and the body's organs and structures. This system facilitates the transmission of sensory information from the body's extremities to the brain and spinal cord while conveying motor commands from the CNS to muscles, glands, and other effector organs (18).

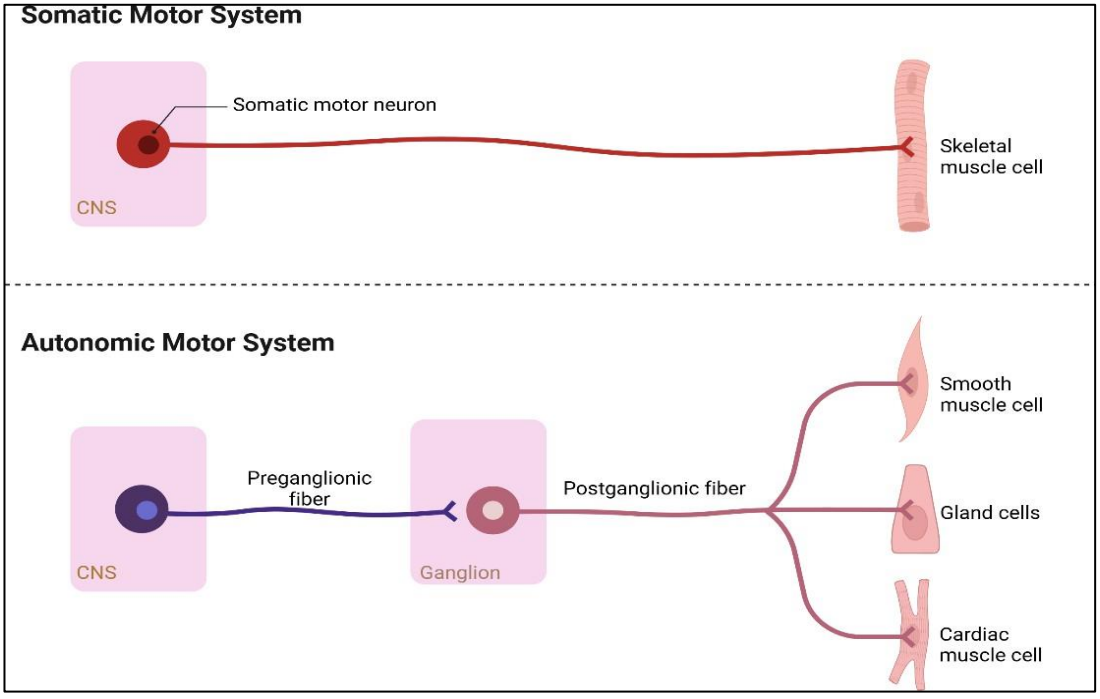

Figure 4. Somatic and autonomic motor system

The PNS consists of two main branches: the somatic nervous system and the autonomic nervous system. The somatic nervous system is responsible for voluntary control of skeletal muscles, enabling purposeful movements and physical actions. In contrast, the autonomic nervous system, which is further divided into the sympathetic and parasympathetic systems, governs involuntary functions such as heart rate, respiration, digestion, and other essential processes (18, 19).

The PNS plays a key role in the rapid conduction of electrical signals, or action potentials, through its extensive network of nerves (18, 20). These impulses are initiated by specialized receptor cells that detect various stimuli, such as touch, temperature, and pain. Once transmitted to the CNS, these signals are processed and interpreted, allowing the body to adapt and respond effectively to changes in its internal and external environments.

2.1.3 Cells of the nervous system

The nervous system is an intricate and highly organized network of interlinked cells that coordinate and regulate essential functions within the human body. It comprises two primary cell types: neuroglia (glial cells) and neurons (nerve cells) (21).

Neuroglia, or glial cells, play a vital role in supporting and maintaining the health and functionality of neurons. These cells constitute approximately 90% of the brain's total cellular population and are divided into subtypes, such as astrocytes, oligodendrocytes, and microglia (21, 22). Astrocytes are key players in maintaining the blood-brain barrier, regulating synaptic activity, and providing metabolic support to neurons (21, 23). Oligodendrocytes are responsible for producing myelin, a lipid-rich substance that insulates axons and accelerates the transmission of electrical impulses (21, 24). Microglia, the CNS's immune cells, serve as the first responders to injury or pathogens, continuously monitoring the brain for signs of damage or distress (25).

While neuroglia provide essential support, neurons are the primary functional units of the nervous system. These specialized cells generate and propagate electrical

impulses, known as action potentials, to communicate with each other and other cells. The signals travel along the axon of the neuron and are transmitted to other neurons or target cells, such as muscles or glands, via specialized junctions called synapses. The distinctive structure of neurons, comprising a cell body, axon, and dendrites, facilitates the rapid and efficient transmission of electrical signals throughout the body (21).

2.1.3.1 Glial cells

Neurons are not solitary cells; they rely on various types of glial cells for support. In many areas of the nervous system, glial cells make up more than 50% of the total cell population. These cells are broadly classified into two categories: microglia, which originate from bone marrow and populate the CNS, and macroglia, which include astrocytes, oligodendrocytes, and ependymal cells, classified based on their differentiation potential during early development (26). While there are multiple subtypes of astrocytes and microglia, the primary distinction follows their origin. Each glial cell type is localized to specific regions within the nervous system and carries out distinct functions.

Astrocytes are responsible for sequestering neurotransmitters, regulating extracellular potassium levels, and supporting the blood brain barrier's integrity. They also provide structural, nutritional, and metabolic support to neurons (27). Oligodendrocytes in the CNS are involved in myelinating numerous axons, which accelerates the transmission of electrical signals along axonal pathways (28). Ependymal cells line the brain's ventricles and the central canal of the spinal cord, where they play a key role in producing and circulating cerebrospinal fluid (29).

Microglia, derived from myeloid precursor cells in the bone marrow, mature into microglial cells and perform important tasks such as synaptic pruning (30). The aforementioned glial cells interact with one another, playing overlapping and unique roles that facilitate a continuous exchange of functions. The functions of neuroglia can

differ significantly based on their specific subtype or species, as well as other factors. Additionally, these functions are often altered in pathological conditions.

2.1.3.2 Neurons

Neurons, or nerve cells, play an essential role in connecting the cells of the nervous system to the rest of the body. Their structure is designed to perform the various complex tasks required in neural communication (31). Typically, a neuron has a central cell body, or soma, which contains the nucleus and other organelles responsible for cellular metabolism. Projected from the soma are dendrites, which receive signals from other neurons. The axon, the neuron's longest extension, transmits information away from the cell body (26). The junction between two neurons is called a synapse, particularly consisting of the axon terminal of one neuron and the dendritic spine of the next.

Neurons are specialized to conduct electrical signals, a fundamental function for communication within the nervous system. This signal conduction happens throughout the neuron. The neuron's membrane creates a barrier that controls the selective movement of ions, which generate and regulate electrical signals. The first phase of this process is graded or bioelectric, where ion movement changes the membrane potential and accumulates to decide whether an action potential will be triggered. This phase is known as summation. When an action potential is initiated, it rapidly depolarizes and repolarizes the membrane, traveling down the axon to the synaptic bouton at the junction with another neuron. The movement of ions that creates these electrical signals is driven by changes in the conformation of channel proteins along the neuron's length, a process initiated when a signal reaches the dendrite (31, 32).

A neuron is the functional unit of the nervous system and defines the capabilities of the brain. It consists of a soma, which holds most of the organelles that provide energy and structure to the cell. The soma is connected to the dendrites, which serve as receptors, receiving signals from other neurons. When these signals reach a threshold, the dendrites transmit them to the soma, which sends the information out

through the axon, acting as the neuron's mouth to communicate with other neurons (33). Axons, which can have different lengths and diameters, are classified as: unipolar, bipolar, pseudo-unipolar, and multipolar. The axon synapses with another neuron's terminal to pass on the signal, forming a complex web of interconnected systems (34).

To ensure efficient communication, the axon is insulated through myelination, where it is wrapped in myelin sheath, a substance that speeds up signal transmission. Myelin sheath is not evenly distributed along the axon; gaps called Nodes of Ranvier allow the electrical impulse to jump from segment to segment, increasing the transmission speed (35). In white matter, the axons are myelinated, while in grey matter, the lack of myelination in axonal branches gives the neurons a gray appearance. Neurons, as the communicators of the nervous system, are the core structural element of the brain. Different types of neurons are specialized for various functions, including output, planning, executive tasks, and regulation.

2.2 Spinal Cord Injuries (SCI)

SCIs are severe conditions that can profoundly affect a person's quality of life. These injuries are commonly caused by traumatic incidents such as car accidents, falls, or sports injuries, resulting in various neurological and functional impairments (36). Each year, approximately half a million people worldwide experience SCI, with most cases occurring in men during their prime years (2).

The primary and secondary damage resulting from SCIs can have extensive consequences, including the loss of sensation, motor function, autonomic function, and neurological capacity (37). The primary injury, typically caused by the initial trauma, may lead to cell death, biochemical disruptions, and tissue damage, while the secondary injury often worsens the primary damage through inflammation, ischemia, and other detrimental processes (38).

In recent years, there has been significant advancement in understanding the complex mechanisms of SCIs and exploring therapeutic strategies. Research has increasingly pointed to the potential of biomaterials in promoting neuronal regeneration and functional recovery after SCI (39). Innovative approaches, such as hydrogel-based scaffolds, have shown promise in supporting the recovery of neuronal tissue.

SCIs are life-altering neurological conditions with lasting effects on an individual's physical, emotional, and social well-being. These injuries are usually classified into three phases: acute, sub-acute, and chronic, each with its distinct pathophysiology and clinical significance (40).

2.2.1 Acute spinal cord injury

The acute phase of a SCI marks the immediate aftermath of the traumatic event, where the body experiences severe consequences such as cell death, neuronal disconnection, and a permanent halt in both the ascending and descending transmission of signals within the spinal cord. This stage, often triggered by sudden and high-impact accidents such as motor vehicle collisions, violent encounters, or sports-related injuries, represents the initial damage to the spinal cord that sets the stage for further complications. During this critical period, the primary injury occurs, leading to a disruption in the integrity of the spinal cord’s structure and function (40).

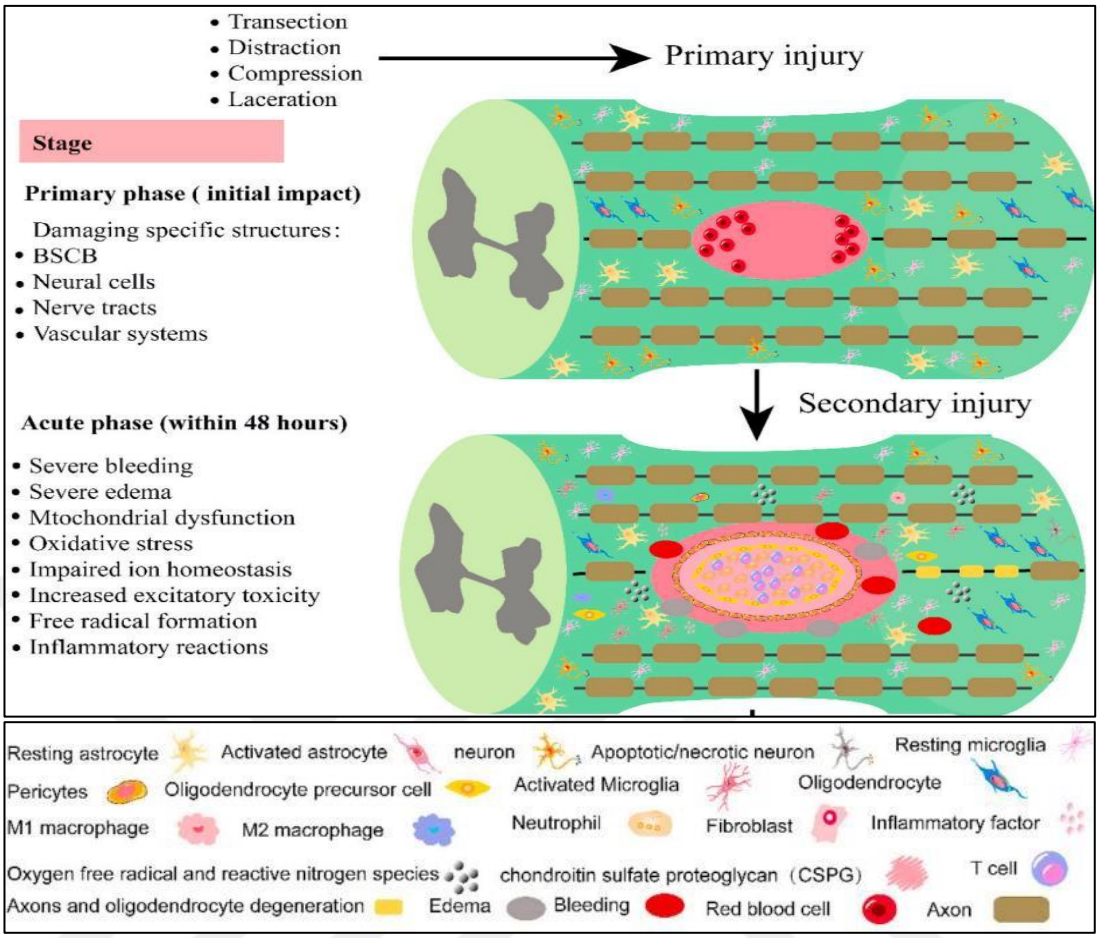

Figure 5. Spinal cord injury, primary and acute phase (41)

Following this, a cascade of secondary injury events unfolds, including inflammation, ischemia (reduced blood flow), and the progressive death of cells, which exacerbate the damage caused by the initial trauma in blood-spinal cord barrier (BSCB). These secondary events can extend the injury zone and complicate the body's ability to heal (41).

As the body struggles to contain the initial damage, the inflammation caused by immune responses can worsen the injury and impair cellular repair mechanisms. In some cases, the ischemic processes resulting from the disruption of blood flow to the affected regions of the spinal cord can lead to additional tissue necrosis, further hindering recovery. During the acute phase, timely medical intervention and appropriate emergency care are essential for stabilizing the patient and minimizing the long-term consequences of the injury. Rehabilitation efforts during this time are

equally important, as they can significantly impact the likelihood of improving motor function and minimizing complications, thus reducing the chances of premature death and lifelong disability. The severity of the initial trauma and the subsequent events highlight the need for both immediate and long-term therapeutic approaches to prevent irreversible damage and enhance the potential for recovery.

2.2.2 Sub-acute spinal cord injury

The sub-acute phase of SCI typically spans the months following the initial trauma and is marked by significant changes in the biological and pathophysiological processes occurring within the injured spinal cord. During this phase, the body's acute inflammatory response, which is crucial for initiating repair mechanisms, begins to reduce, allowing for the commencement of several reparative processes (40, 42). Among these processes, the formation of a glial scar plays a key role in attempting to isolate the damaged tissue from surrounding healthy areas. Additionally, various growth factors are activated, which contribute to the body's efforts to promote healing. However, despite these repair mechanisms, the restoration of neurological function is often limited during this period.

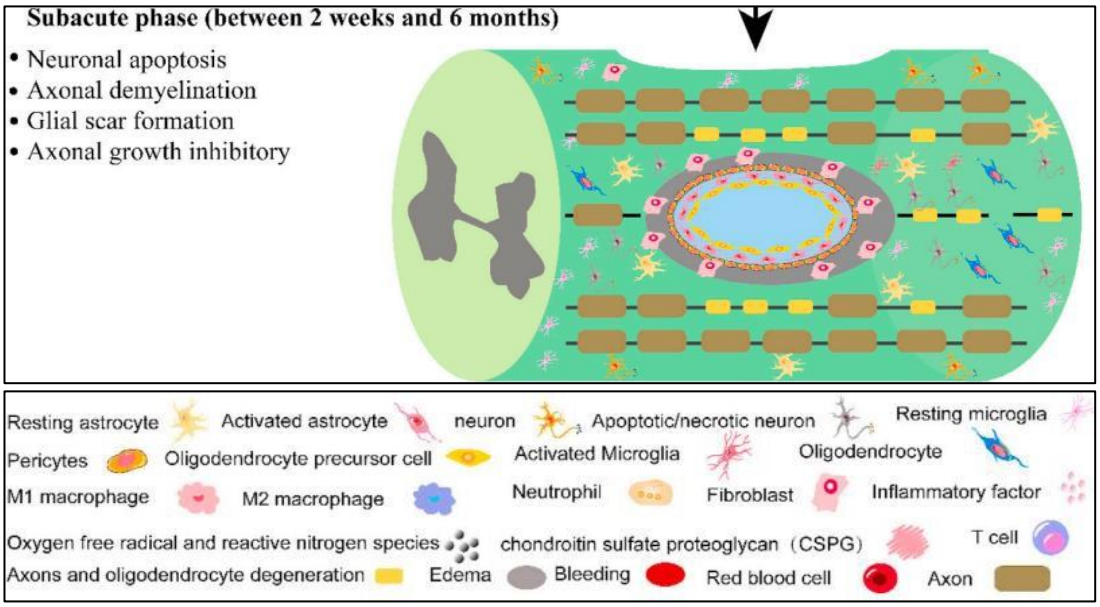

Figure 6. Spinal cord injury subacute phase (41)

This is largely due to the hostile environment created within the spinal cord following injury, which presents numerous challenges to effective neural regeneration and plasticity (42, 43). The formation of the glial scar, while essential in protecting the uninjured parts of the spinal cord, can act as a barrier to axonal growth, further hindering recovery. Thus, while the body does initiate recovery processes, the extent of functional restoration remains constrained, making the sub-acute phase a critical window for intervention to enhance the chances of neurological recovery.

2.2.3 Chronic spinal cord injury

As the SCI advances into the chronic phase, which can persist for years or even a lifetime, the biological landscape within the injured area continues to undergo significant changes. During this phase, the glial scar that initially formed in response to the injury matures, becoming more fibrous and rigid (44). This maturation of the scar tissue further complicates the healing process by creating an increasingly hostile environment for axonal regrowth. The injury site becomes even less conducive to neural repair, as the glial scar can act as a physical and biochemical barrier to the growth of new nerve fibers.

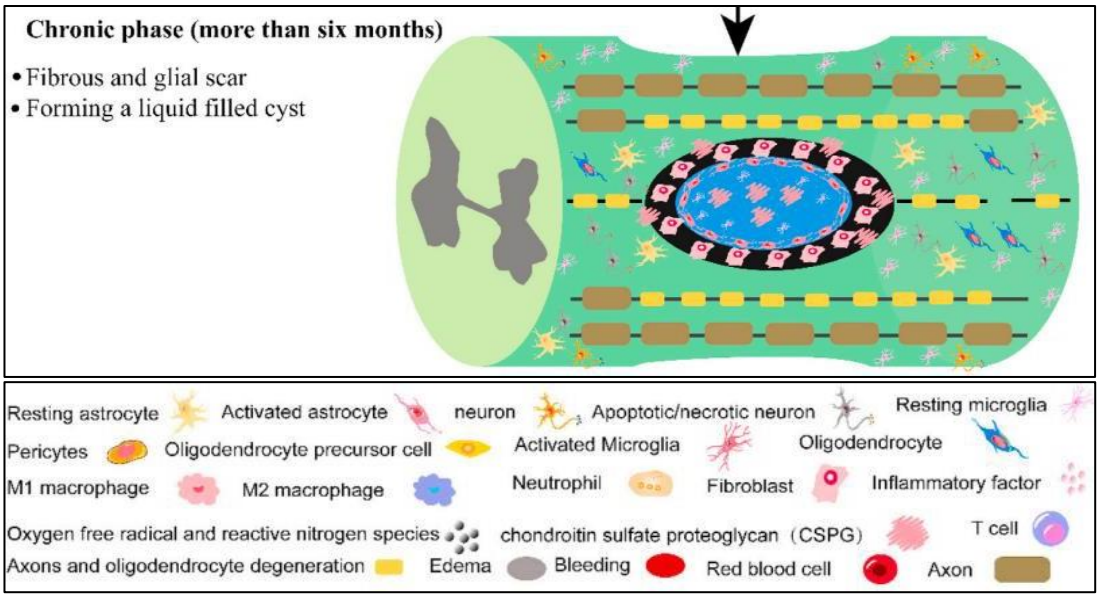

Figure 7. Spinal cord injury chronic phase (41)

This structural impediment not only prevents the restoration of damaged neural connections but also limits the potential for functional recovery (44, 45). Consequently, the chronic phase presents a major challenge to therapeutic efforts, as the body's ability to promote regeneration is severely compromised, leading to persistent deficits in motor, sensory, and autonomic functions.

2.2.4 Current treatment approaches and their limitations for spinal cord injuries

Despite significant advancements in medical and rehabilitative interventions, effectively treating SCIs remains a considerable challenge due to the complex nature of the spinal cord environment. The spinal cord is a highly specialized structure, containing an intricate network of cells, neurons, and vascular systems, all of which are susceptible to both primary and secondary injury-induced damage. After traumatic SCI, a cascade of pathophysiological events, such as inflammation, glial scarring, and progressive tissue degeneration, occurs, further exacerbating the initial structural and functional damage. The recovery process is hindered by the challenges of managing these cascading events and promoting regeneration in such a unique environment (46).

In response to these challenges, various treatment approaches have been explored, including pharmacological interventions, cell based therapies, and engineered biomaterials. Pharmacological treatments, such as neuroprotective agents and anti-inflammatory drugs, have shown some promise in preclinical studies (47). However, their effectiveness in clinical trials has often been limited, highlighting the difficulty of translating these treatments into widespread clinical applications.

Cell-based therapies have also garnered attention as a potential treatment strategy, particularly through the transplantation of autologous or allogeneic cells to promote neuroprotection and axonal regeneration (48). Specific strategies, such as utilizing neural stem/progenitor cells, Schwann cells, or olfactory ensheathing cells, have demonstrated potential in preclinical models. However, challenges related to sourcing clinically suitable stem/progenitor cells, ensuring cell survival, integration into the

host tissue, and controlling differentiation have limited the success of these therapies in clinical settings. Engineered biomaterials represent a promising avenue for overcoming the complex challenges posed by SCIs. Biomaterials can be designed to mimic the extracellular matrix (ECM) of the spinal cord, creating a more supportive environment for cell growth, axonal regeneration, and tissue repair (49). They can also serve as drug delivery systems, enabling the localized, controlled release of therapeutic agents to promote healing. Recent studies have shown promising results for biomaterial-based strategies, such as 3D constructs embedded with cells derived from oral mucosa, which have induced functional recovery in animal models of SCI. Moreover, combining biomaterials with cellular therapies and/or pharmacological interventions has been explored as a means to further enhance treatment efficacy and address the multifaceted nature of SCI (50).

Despite these innovative approaches, the treatment of SCIs remains a significant challenge, and the development of clinically viable therapies continues to be an area of ongoing research. The unique complexity of the spinal cord, the diverse responses to injury, and the need for comprehensive strategies that address both the structural and functional impairments of the injury site remain central to the pursuit of effective treatments. As research progresses, these challenges are likely to drive new developments and breakthroughs in SCI therapies.

2.3 Principles of Tissue Engineering and Regenerative Medicine

Tissue engineering and regenerative medicine have emerged as transformative fields with immense potential for restoring, maintaining, and enhancing the function of damaged or diseased tissues and organs. By combining the principles of engineering, materials science, stem cell biology, and developmental biology, these fields focus on developing biological substitutes capable of regenerating and repairing tissues to restore normal function (50).

Central to the concept of tissue engineering is the tissue engineering triad, which includes cells, scaffolds, and bioactive factors. Stem cells or progenitor cells, which

have the potential to differentiate into various types of tissue, are seeded onto porous, three-dimensional scaffolds that mimic the ECM of natural tissues (51, 52). These scaffolds provide both the structural and mechanical support necessary for the growth, proliferation, and differentiation of cells into the desired tissue type. Additionally, bioactive factors such as growth factors are often incorporated into the scaffolds to stimulate and direct the tissue regeneration process, ensuring that cells not only survive but also thrive and integrate within the scaffold.

A critical component of tissue engineering is the design and fabrication of scaffolds. Scaffolds are essential for the success of tissue regeneration, as they act as temporary templates that support the growth and organization of new tissue (53). The materials chosen for scaffolds, including natural and synthetic biomaterials such as polymers, hydrogels, and ceramics, must meet specific requirements in terms of biocompatibility, biodegradability, and mechanical properties. The ability to create scaffolds with controlled pore size, geometry, and interconnectivity is crucial to the efficient formation of new tissue.

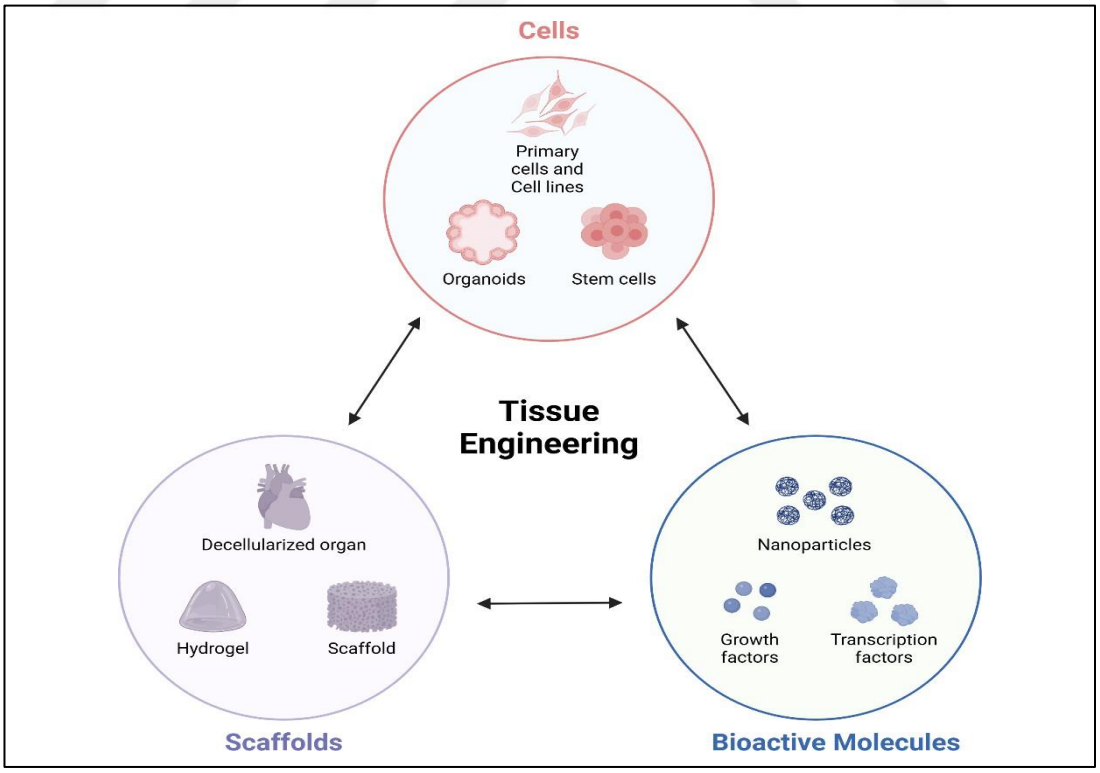

Figure 8. Components of tissue engineering

In recent years, biomimetic hydrogels that form *in-situ* have gained attention as a promising strategy for tissue regeneration (54). These hydrogels can be injected or implanted with minimal invasiveness and undergo gelation when exposed to environmental changes such as pH or temperature shifts. This characteristic allows hydrogels to be used for localized tissue regeneration, as they can encapsulate cells, growth factors, and other bioactive molecules to create a tailored microenvironment conducive to tissue healing and regeneration (55).

The design and fabrication of scaffolds continue to be at the forefront of tissue engineering research. Traditional techniques for scaffold fabrication, including solvent casting, gas foaming, and freeze-drying, have limitations in terms of controlling the pore size, geometry, interconnectivity, and mechanical properties of the scaffolds. To overcome these limitations, advanced manufacturing techniques such as 3D and 4D printing have gained popularity in the field. These technologies enable the precise fabrication of scaffolds with customized microarchitectures, optimized porosity, and the ability to incorporate bioactive factors, leading to enhanced outcomes in tissue regeneration. 3D and 4D printing technologies offer a new level of control in creating scaffolds tailored to the specific needs of the patient, further advancing the potential of tissue engineering in clinical applications (56).

2.3.1 Nerve tissue engineering

A primary objective of nerve tissue engineering is to regenerate and repair neural tissues that have been lost or damaged due to injury or disease. In the CNS, the loss of function resulting from damage to the brain or spinal cord presents a significant challenge for millions of individuals around the world (57). Although damage to the PNS tends to have a less severe impact on patients, it still represents a considerable concern both for the individuals affected and for society due to the economic burden it places on healthcare systems. Despite ongoing advancements, current therapeutic options for nervous system injuries and diseases remain far from ideal. In the PNS, nerve autografting remains the gold standard clinical approach for repair, whereas the

treatment of CNS injuries largely focuses on mitigating inflammation, encouraging nerve regeneration, and promoting neuroplasticity in the damaged areas (57, 58).

Nerve tissue engineering, an emerging interdisciplinary field within tissue engineering and regenerative medicine, specifically addresses the challenges associated with nerve regeneration. The goal of this field is to develop solutions that can effectively repair or regenerate nerve tissues in both the PNS and CNS (59). There are critical issues that nerve tissue engineering must overcome to achieve these goals.

- The identification and use of appropriate regenerative cell sources, such as glial cells, which are essential for supporting nerve regeneration and repair.
- The development of scaffolds that mimic the architecture of the native tissue environment, providing the necessary support for the directional regeneration of damaged nerves. These scaffolds must create a conducive environment for cells to grow, differentiate, and organize into functional tissue structures.
- The application of neurotrophic factors that can stimulate and accelerate nerve regeneration, helping to guide and promote the repair of damaged neural tissues.

By addressing these key issues, nerve tissue engineering aims to improve current treatments and offer more effective solutions for individuals suffering from nerve injuries or diseases, with the ultimate goal of restoring nerve function and enhancing quality of life.

2.3.1.1 Cell sources used in nerve tissue engineering

2.3.1.1.1 Stem cells

Stem cells are a unique group of undifferentiated cells that possess the remarkable ability to both self-renew and differentiate into a variety of specialized cell types. This capacity distinguishes them from other cell types (60). Stem cells can maintain an unspecialized state while also retaining the potential for numerous divisions, allowing them to continuously produce more of themselves as well as develop into various

specialized cell types. These two fundamental characteristics make stem cells invaluable for medical research and therapeutic applications.

Since the discovery of embryonic stem cells and adult stem cells, there has been significant progress in understanding their distinct properties and how they can be harnessed for various medical purposes. Over the past two decades, numerous cell sources have been identified that possess the ability to reprogram spontaneously, develop tissue-specific phenotypes, and serve as potential precursors for neural tissue. These include embryonic stem cells, adult stem cells, and induced pluripotent stem cells (iPSCs) (61).

Embryonic stem cells have long been used as a model to study the mechanisms of self- renewal and cellular differentiation (62). There are two main classes of adult stem cells for nervous tissue: Type 1, which refers to NSCs derived from postnatal or adult mice, and Type 2, which includes postnatal clonogenic multipotent cells that can differentiate into neurons, astrocytes, and oligodendrocytes (63). In 2006, the groundbreaking achievement of reprogramming adult mouse fibroblasts into pluripotent stem cells was demonstrated, followed by successful replication of the process in human cells (64). This discovery led to a rapid shift in stem cell research, with much of the focus now directed toward human-derived induced pluripotent stem cells, largely moving away from the ethical and scientific concerns surrounding of embryonic stem cells.

The plasticity and versatility of iPSCs, which are biologically similar to embryonic stem cells, have generated significant interest in their potential applications in regenerative medicine. iPSCs offer the advantage of studying differentiation pathways for all three germ cell layers without the ethical challenges associated with embryonic stem cells (65). Notable advances include the ability to reprogram skin fibroblasts from patients with genetic diseases into iPSCs. These iPSCs then inherit the specific disease phenotype when induced to differentiate into the appropriate mature cell type. This capability enables the study of genetic and epigenetic traits at the localized level, offering the possibility of generating patient-specific cells for disease

modeling and personalized medicine. Furthermore, iPSCs represent an ideal source of autologous cells, which could minimize the risk of immune rejection in therapeutic applications.

Mesenchymal stem cells (MSCs), another type of adult stem cell, have also become a focus of significant research in the field of tissue engineering and regenerative medicine. MSCs are already being explored for a wide range of applications due to their ease of isolation, self-renewal capacity, immunosuppressive properties, and ability to regenerate damaged tissues (66). In particular, MSCs have shown promise for differentiation into neural phenotype cells and have the potential to treat both degenerative and trauma-related diseases. Their ability to support the growth of neural tissues makes them an exciting tool for advancing treatments in neurodegenerative conditions and traumatic injuries to the nervous system.

Together, the ongoing research and development of stem cells, including iPSCs and MSCs, hold tremendous potential for advancing regenerative medicine, offering new avenues for repairing damaged tissues, treating genetic disorders, and providing personalized therapeutic options for patients.

2.3.1.1.2 Schwann cells

Schwann cells are the primary glial cells of the PNS, and their role in myelination has been extensively studied. When the peripheral nerve is injured, a series of events unfold, leading to the loss of the axon distal to the injury site, primarily due to the lack of trophic support (67). This process of axonal degeneration is a central feature in the pathology of many types of nerve injuries. The ability to restore the continuity of the peripheral nerve largely depends on the myelination of regenerated axons within the proximal stump by Schwann cells. Without Schwann cells, regenerating axons are unable to function properly, both in terms of structural integrity and electrical signaling (68).

Schwann cells are responsible for forming the myelin sheath that insulates axons, and they represent the most prevalent cell type in the PNS. Numerous studies have highlighted the critical role of Schwann cells in supporting and facilitating the recovery of peripheral nerve function following injury (69). This has spurred ongoing research into optimizing the interaction between Schwann cells and damaged neural tissue to enhance regeneration.

For successful repair of nerve injuries and full restoration of PNS function, it is essential that Schwann cells exhibit long-term survival, proliferation, differentiation, and migration. Their interaction with regenerating axons plays a pivotal role in the recovery process. Therefore, in nerve tissue engineering, careful preparation, maturation, and purification of Schwann cells are critical for facilitating successful regeneration (70). Schwann cell isolation and cultivation methods have been well established, with techniques for isolating these cells from rat nerve tissues and culturing them in purified Schwann cell medium to ensure high purity (71).

In artificial peripheral nerve systems, Schwann cells serve as the main functional cell type, providing support and promoting the regeneration of nerve fibers. Artificial nerve constructs often consist of various scaffolds embedded with Schwann cells. Both natural and synthetic biodegradable materials have been employed to culture Schwann cells *in vitro* and *in vivo*, offering the potential to mimic the natural environment of the PNS.

Furthermore, Schwann cell activity can be enhanced by incorporating neurotrophic factors, which stimulate their growth and function. However, challenges remain in nerve tissue engineering, such as optimizing the alignment and regrowth of axons, overcoming immunogenic reactions to synthetic biomaterials, and addressing other unresolved issues (72). Despite these challenges, experiments involving Schwann cells combined with synthetic biomaterial scaffolds have demonstrated the feasibility of using these cells in nerve repair applications. This research has shown promise in advancing therapeutic strategies for nerve regeneration and holds significant potential for improving the treatment of nerve injuries in the future.

2.3.1.1.3 Induced pluripotent stem cells

Pluripotent stem cells, including both embryonic stem cells and induced pluripotent stem cells (iPSCs), have the remarkable ability to self-renew indefinitely and differentiate into all three germ layers: ectoderm, mesoderm, and endoderm (73). While embryonic stem cells offer significant potential for cell therapy, their use is hindered by several limitations. These include ethical concerns surrounding the use of human embryos, the risk of immune rejection by patients, and potential immune responses (74). In contrast, induced pluripotent stem cells, which are derived from somatic cells such as human dermal fibroblasts through the reprogramming of specific factors, offer several key advantages over embryonic stem cells (75). Notably, iPSCs do not raise immunogenic concerns and are free from the ethical issues associated with embryo use.

Induced pluripotent stem cells have been shown to differentiate into a variety of cell types across different lineages both *in vitro* and *in vivo* (76). For instance, when iPSCs were induced to form embryoid bodies in mice, motor cortex formation, development of perivascular cells in the brain, and the expression of neural markers were observed, even though the iPSCs themselves were not integrated into the mice's brain tissue (77). This underscores the capacity of iPSCs to contribute to complex tissue development, further enhancing their potential for therapeutic applications.

The applications of iPSC technology have grown rapidly in recent years, with notable advancements in areas such as disease modeling, drug screening, and cell-based therapies. For example, iPSCs have been used to create the first psychiatric disease model derived from monozygotic twins discordant for schizophrenia (78). In addition, 3D brain organoid models have been developed from iPSCs harboring disease-specific mutations or derived from patient samples. These models have successfully replicated aspects of neural maturation and early embryonic development seen in human brains, further highlighting the potential of iPSCs in nervous system disease research (79).

Importantly, strategies for neural differentiation, mixed differentiation, and clinical applications of iPSCs have been significantly refined. These advancements include the modulation of neural morphogen pathways, the use of small molecules to target specific pathways, and the optimization of efficient differentiation protocols (80). Such improvements have greatly enhanced the potential of iPSCs for treating nervous system diseases. Collectively, iPSCs represent a promising and versatile source for developing innovative treatments for a wide range of neurological conditions, with ongoing research paving the way for their clinical application in regenerative medicine (81).

2.3.1.1.4 Neuronal cell lines

Electrical signaling in both the CNS and PNS is essential for transmitting sensory information, integrating data, and facilitating movement by enabling rapid communication between various target tissues (82). However, due to the elongated and delicate nature of nerve fibers, nerve regeneration is typically slow and frequently incomplete. *In vivo*, nerve regeneration often proves ineffective because damaged nerves contain multiple microenvironments that complicate the repair process. Moreover, the loss of these microenvironments in *in vitro* conditions further hampers the regeneration of nerve tissue.

To overcome these challenges, numerous tissue engineering approaches have been developed to promote nerve regeneration. These strategies involve the careful selection of cell sources, the design of appropriate microenvironments, and the use of scaffolds and proteins that support nerve repair. By tailoring these factors, researchers are exploring new avenues for enhancing nerve regeneration in tissue engineering applications. A key focus is on creating and preserving microenvironments that mimic the natural conditions needed for optimal nerve function and repair. Such advancements may provide valuable support to researchers working in this field (83).

Neuron-like cell lines are commonly employed for preliminary studies, particularly when tissue volume is limited (84). These cell lines are useful because

they can form neuronal-like networks on culture plates, making them ideal for *in vitro* research. Among the most frequently used neural cell lines are Neuro-2a, PC 12, and SH-SY5Y, all of which originate from neural tumors (85). To further enhance the network formed by these cells, co-culturing them with Schwann cells has proven beneficial. For example, implanting a combination of Neuro-2a cells and Schwann cells into a polymer scaffold has shown promising results in promoting nerve repair, particularly in severe lesion models (86). This approach led to the increased expression of neurofilament and glyceraldehyde-3-phosphate dehydrogenase (GAPDH), suggesting significant improvements in nerve regeneration and function (87). These findings highlight the potential of combining neuronal and Schwann cells with scaffold materials for improving the outcomes of nerve repair strategies.

2.3.1.2 Scaffolds used in nerve tissue engineering

2.3.1.2.1 Natural materials

Natural materials, including gelatin, HA, and CS, have become pivotal in the development of nerve tissue engineering, thanks to their unique advantages such as biocompatibility, biodegradability, and their ability to closely mimic the ECM of native tissues. These materials offer promising solutions for addressing the challenges associated with nerve regeneration, as they not only provide structural support but also create a favorable environment for cellular activities crucial for recovery.

Gelatin, for example, is a naturally derived polymer that has gained widespread attention in tissue engineering. Due to its excellent biocompatibility and the ability to be easily modified, gelatin is often utilized to fabricate scaffolds that can support cell adhesion, proliferation, and differentiation. Its ability to be functionalized further enhances its potential for promoting nerve regeneration (88). The incorporation of growth factors into gelatin scaffolds has also proven to be beneficial, as it helps to stimulate the repair and regeneration of nerve tissues. This makes gelatin a versatile and reliable material in nerve tissue engineering applications, especially in cases of peripheral nerve injury where regeneration is crucial for recovery (89).

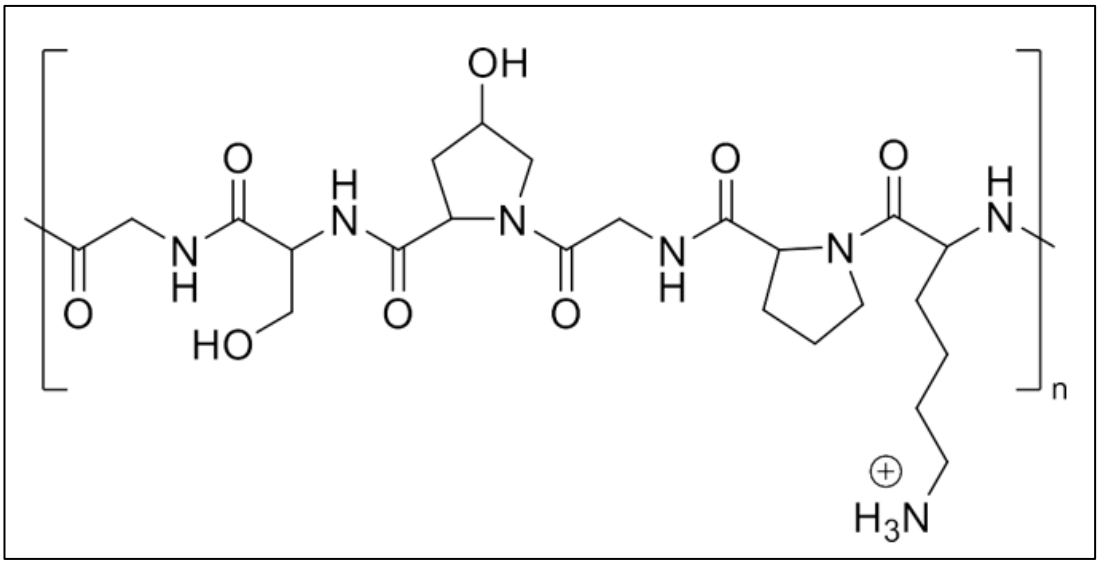

Figure 9. Molecular structure of gelatin, a hydrolysis product of collagen

Similarly HA, a glycosaminoglycan, plays a significant role in supporting nerve regeneration. One of its remarkable features is its antimicrobial properties, which help to prevent infections at the injury site a critical concern in nerve repair (90). HA has been shown to support the proliferation and differentiation of neural cells, making it an attractive candidate for creating hydrogels or scaffolds for nerve tissue engineering (91). Furthermore, HA can help modulate the ECM environment, enhancing the growth and survival of nerve cells. The ability of HA based scaffolds to encourage cell migration and tissue formation further underscores its value in regenerative medicine.

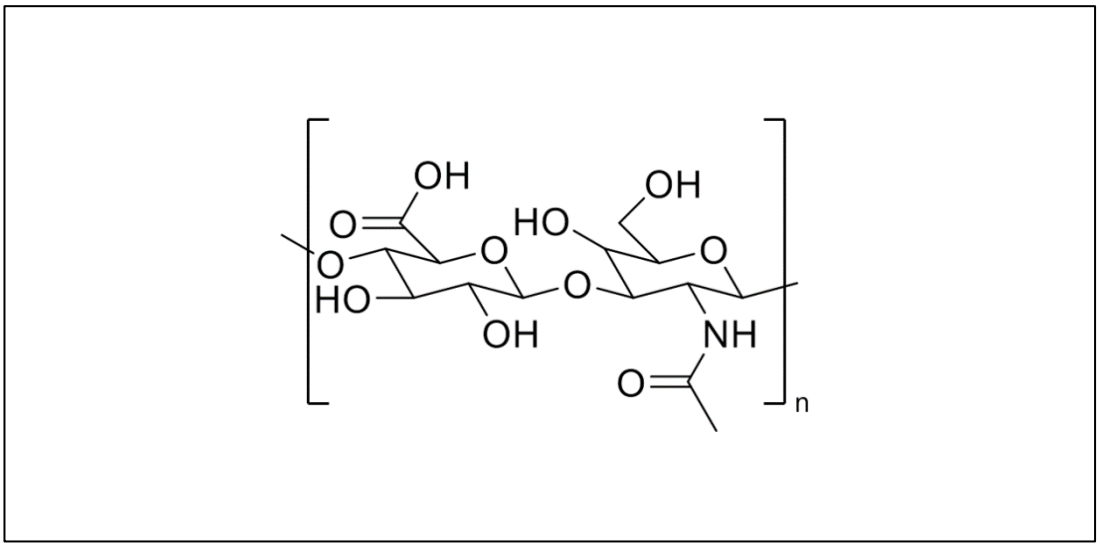

Figure 10. Molecular structure of hyaluronic acid

CS, another key natural material, has been explored for its role in nerve repair. It is a component of the ECM and plays a critical role in the regulation of cellular processes such as migration and differentiation (92). In nerve tissue engineering, CS has been incorporated into hydrogel-based scaffolds that provide both structural support and a platform for controlled release of growth factors. These scaffolds can help deliver bioactive molecules to the site of injury, which can significantly enhance nerve regeneration. Notably, CS is also involved in the modulation of the inhibitory environment around the injury site, which can aid in overcoming the barriers to axonal regrowth (93).

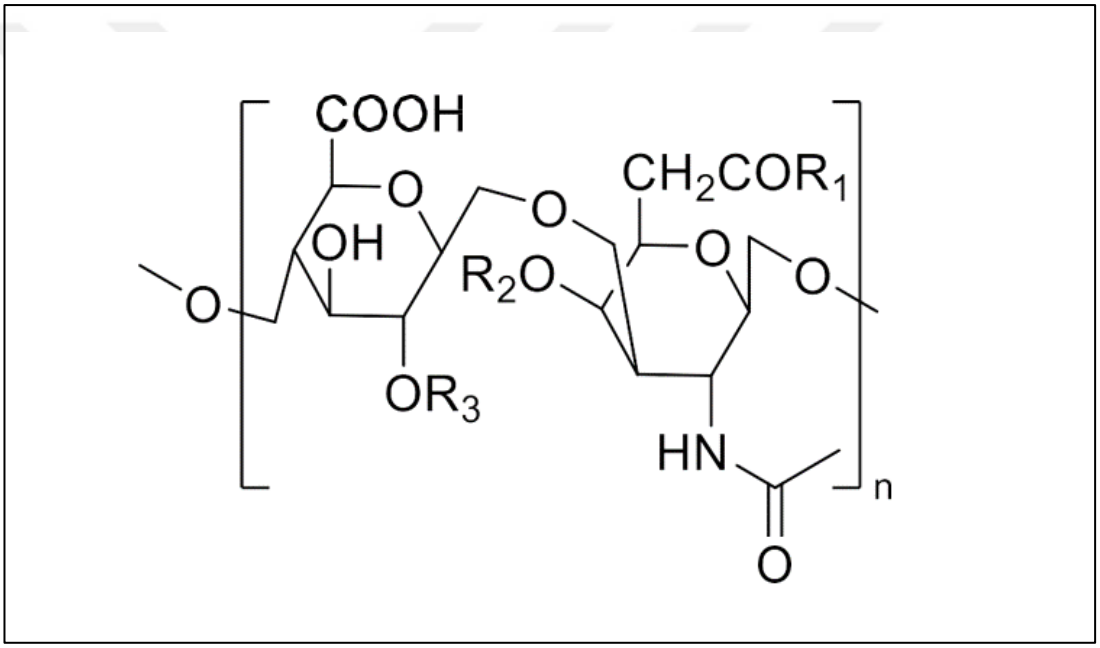

Figure 11. Molecular structure of chondroitin sulfate

In summary, natural materials like gelatin, HA, and CS are emerging as key players in the field of nerve tissue engineering. By providing the necessary support for cell growth and differentiation, as well as delivering therapeutic molecules that enhance regeneration, these materials are contributing to the development of more effective and functional treatments for nerve injuries. As research continues, the combination of these natural materials with advanced techniques such as 3D printing and scaffold fabrication promises to revolutionize regenerative therapies for nerve damage.

2.3.1.2.2 Synthetic materials

Synthetic materials, such as polyesters, polycaprolactone (PCL), and poly(lactic acid- co-glycolic acid) (PLGA), have gained considerable attention in the field of nerve tissue engineering due to their ability to be tailored for specific applications (94). These materials offer a range of desirable characteristics, including tunable mechanical properties, controlled degradation rates, and the ability to modify their surface chemistry for enhanced interactions with cells. These advantages make synthetic polymers highly versatile for creating scaffolds and other structures designed to support nerve regeneration.

Polyesters, such as poly(lactic acid-co-glycolic acid), are particularly popular in nerve tissue engineering because of their excellent biocompatibility and biodegradability. The key advantage of PLGA lies in its ability to control the degradation rate, allowing for a gradual breakdown of the material that can match the rate of tissue regeneration (95). This characteristic is critical for nerve repair, as it ensures that the scaffold remains intact long enough to support nerve regrowth, but eventually degrades without causing an inflammatory response or hindering the healing process. PLGA-based scaffolds can also be engineered to carry bioactive molecules, such as growth factors, which can further promote nerve regeneration at the injury site.

Polycaprolactone (PCL), another biodegradable polyester, has also garnered significant attention due to its relatively slow degradation kinetics. This slow degradation rate is particularly beneficial for nerve tissue engineering applications where long-term support is needed. PCL's ability to maintain structural integrity over extended periods makes it an ideal candidate for nerve scaffolds, especially in cases where nerve regeneration is slow or when the injury is extensive (96). Moreover, PCL can be easily processed into a variety of forms, such as fibers, films, and scaffolds, allowing for customizable designs that optimize tissue ingrowth and axonal regrowth (97). Beyond polyesters, other synthetic polymers have shown promise in nerve tissue engineering. Methacrylates, polyanhydrides, polycarbonates, and polyvinyls, among others, are frequently used in the development of advanced biomaterials for nerve

repair. For instance, polymers such as poly(lactic acid) (PLA) and poly(p-phenylene vinylene) are commonly employed to create scaffolds with controlled mechanical properties that mimic the stiffness and flexibility of native nerve tissue (98). These materials can be modified to achieve specific surface chemistries that promote cell adhesion, which is crucial for effective regeneration and integration of the scaffold with the surrounding tissue.

Additionally, hydrogels, such as those based on poly(ethylene glycol) (PEG), sulfonated polystyrene, and poly(norbornene), have shown specific advantages in nerve tissue engineering (99). Hydrogels are highly hydrated, making them suitable for creating environments that closely resemble the natural ECM found in nerve tissues. Their properties, such as high water retention and tunable mechanical stiffness, make them an attractive option for promoting cell survival, proliferation, and migration in nerve regeneration applications. Furthermore, these hydrogels can be functionalized with various bioactive molecules to enhance cellular behaviors and guide tissue formation.

In summary, synthetic materials like PLGA, PCL, and various other polymers have proven to be invaluable in nerve tissue engineering due to their customizable properties. By offering precise control over mechanical strength, degradation rates, and surface chemistry, these materials can be tailored to meet the specific requirements of nerve regeneration. As research continues to progress, the development of novel synthetic materials and hybrid systems combining natural and synthetic components holds great potential for improving the effectiveness of nerve repair strategies and advancing the field of regenerative medicine.

2.3.1.2.3 Hybrid materials

To harness the strengths of both natural and synthetic materials, researchers have been investigating the creation of hybrid scaffolds that combine the bioactive properties of natural polymers with the customizable attributes of synthetic polymers. These hybrid materials are designed to overcome the limitations of individual materials

and offer a more versatile platform for tissue engineering, particularly in nerve regeneration (100). By integrating natural and synthetic components, hybrid scaffolds can better mimic the complex microenvironment of native nerve tissue, supporting both the mechanical requirements and the biochemical cues necessary for effective cell growth, proliferation, and differentiation.

One such approach involves combining gelatin based hydrogels with synthetic polymers. Gelatin, derived from natural collagen, is biocompatible, biodegradable, and provides inherent bioactivity, promoting cell adhesion and tissue regeneration. However, its mechanical properties alone may not be sufficient to support the structural integrity needed for nerve tissue engineering (101). By combining gelatin with synthetic polymers like methacrylic anhydride (MAA), researchers can enhance the mechanical strength of the scaffold without compromising its biocompatibility. This combination also allows for the tunability of key properties such as degradation rate, porosity, and surface chemistry, which are critical for creating an optimal environment for neural cell growth.

The addition of synthetic components, such as MAA, further enables the modification of scaffold properties to achieve a balance between flexibility and rigidity, making the scaffold more suitable for nerve regeneration applications (102). These enhanced mechanical properties help to provide the necessary structural support for axonal growth, while the gelatin component ensures that the scaffold remains conducive to cell attachment and differentiation. Additionally, scaffolds can be further tailored by incorporating growth factors, such as nerve growth factor (NGF), to stimulate nerve cell proliferation and guide axonal regeneration, creating a scaffold that not only mimics the physical properties of native tissue but also supports its biological functions (103).

This synergy between natural and synthetic materials offers several advantages over single material scaffolds. The approach allows for better control over the scaffold's mechanical and biochemical properties, ensuring that it can provide both the structural support needed for nerve regeneration and the bioactive cues that promote

cellular activity. By more closely replicating the native nerve tissue environment, scaffolds hold great promise for improving the outcomes of nerve repair and enhancing the potential for functional recovery following nerve injuries.

As research in this area continues, the development of scaffolds that combine the best features of natural and synthetic materials is expected to play a significant role in advancing nerve tissue engineering and regenerative medicine. These materials could pave the way for more effective treatments for various nerve related conditions, from peripheral nerve injuries to more complex CNS disorders.

2.3.1.3 Neurotrophic factors in nerve tissue engineering

Nerve tissue engineering is a dynamic and rapidly advancing field, offering significant potential for treating a wide range of neurological disorders and injuries. One of the most critical aspects of this field is the strategic use of neurotrophic factors, which are essential for the survival, growth, and regeneration of nerve cells (104). These proteins or molecules not only support neuronal development but also enhance the ability of nerve cells to recover from damage and regenerate functional connections (105). Their role is crucial in overcoming the challenges of nerve repair, particularly in cases where traditional healing mechanisms fail or are inadequate.

Among the various neurotrophic factors that have been extensively studied for their therapeutic potential in nerve tissue engineering, NGF, Glial Cell Line derived Neurotrophic Factor (GDNF), and Brain derived Neurotrophic Factor (BDNF) stand out as some of the most promising (106). Each of these factors plays a distinctive role in neural health and regeneration, making them ideal candidates for incorporation into engineered nerve tissues (107).

2.3.1.3.1 Nerve growth factor (NGF)

NGF is a well-studied and highly regarded neurotrophic factor that has been extensively investigated for its potential in nerve tissue engineering. Its importance

lies in its essential role in promoting the survival, maintenance, and regeneration of neurons, particularly in response to injury (108). NGF has been shown to stimulate various key processes involved in neural recovery, including neurite outgrowth, neuronal differentiation, and the overall repair of damaged neural tissues (109).

One of the most significant functions of NGF is its ability to promote neurite outgrowth, which is crucial for the restoration of neural networks following injury (110). Neurite outgrowth refers to the extension of nerve cell processes, such as axons and dendrites, which are necessary for the reconnection of neurons and the restoration of functional communication between them (111). NGF stimulates the elongation of these processes, contributing to the regeneration of damaged nerves and the re-establishment of lost neural connections.

In addition to supporting neurite outgrowth, NGF plays an important role in neuron differentiation. This process involves the transformation of precursor or stem cells into fully differentiated neurons, a critical aspect of neural regeneration (112). NGF has been shown to induce differentiation of neural progenitor cells into mature neurons, helping to replace lost or damaged neuronal populations and improve functional recovery.

NGF also exerts indirect effects by promoting the proliferation and differentiation of cell lines that are important for nerve regeneration (113). For example, NGF has been demonstrated to stimulate the proliferation and differentiation of PC 12 cells (a pheochromocytoma cell line derived from rat adrenal medulla) and SH-SY5Y cells (a human neuroblastoma cell line) (114). These cell lines are widely used in research as models for neuronal differentiation and neuroregeneration. NGF's ability to enhance the proliferation and differentiation of these cells is particularly valuable in studying spinal cord regeneration and repairing other parts of the CNS and PNS.

The regenerative potential of NGF has made it a cornerstone of research in nerve tissue engineering, particularly for SCIs and other types of neuronal damage (115). NGF's ability to enhance both the growth and differentiation of neurons, as well as its

role in supporting neuronal health, make it an invaluable tool in the development of therapeutic strategies aimed at repairing damaged nerve tissues. Researchers continue to explore new ways to deliver NGF effectively to injury sites, often through incorporation into engineered scaffolds, biomaterials, and cell based therapies, to enhance the outcomes of nerve regeneration.

2.3.1.3.2 Glial cell line derived neurotrophic factor (GDNF)

Glial Cell Line derived Neurotrophic Factor (GDNF) is another critical neurotrophic factor that has garnered significant attention in the field of nerve tissue engineering (116). GDNF is known for its potent effects on the survival and regeneration of motor neurons, making it a highly promising candidate for the treatment of a variety of neurodegenerative diseases and SCIs (117).

GDNF was originally identified for its role in promoting the survival of dopaminergic neurons, particularly in the context of Parkinson's disease (118). However, its benefits extend beyond dopaminergic neurons, and it has been shown to have a broad effect on several types of motor neurons and sensory neurons, including those in the PNS and CNS. In particular, GDNF has demonstrated remarkable efficacy in promoting the survival of motor neurons, which are particularly vulnerable in diseases such as Amyotrophic Lateral Sclerosis (ALS), spinal muscular atrophy (SMA), and after SCIs (119).

GDNF's primary mechanism of action involves activating specific receptors on neurons, leading to the activation of intracellular signaling pathways that promote cell survival and axonal growth (120). It is particularly known for enhancing neuroprotection and neurogenesis, which are essential for restoring function after nerve damage. In animal models, GDNF has been shown to significantly reduce neuronal death and promote functional recovery following SCI, as well as in the treatment of various neurodegenerative conditions.

In spinal cord injuries, GDNF has demonstrated the ability to promote axonal regeneration, which is crucial for the repair of damaged nerve fibers (121). The spinal cord's natural regenerative capacity is limited, particularly in the context of CNS injuries, where the environment is more inhibitory than in the PNS (122). GDNF's role in overcoming some of these inhibitory signals by enhancing axonal outgrowth and fostering an environment conducive to regeneration has made it an attractive therapeutic candidate for SCI repair.

Research in nerve tissue engineering has also explored methods of incorporating GDNF into biomaterials and scaffolds to enhance its delivery to injured sites. These strategies aim to provide sustained and localized release of GDNF, ensuring its effectiveness in stimulating neural repair over time. The use of gene therapy and cell based therapies, where cells are engineered to produce and release GDNF in response to injury, has further enhanced its potential in treating SCIs and neurodegenerative diseases.

The ability of GDNF to promote motor neuron survival, axonal growth, and functional recovery positions it as a critical tool in the development of regenerative therapies for various neurological disorders, especially those involving motor neuron degeneration and spinal cord trauma. Researchers continue to focus on improving the targeted delivery and sustained release of GDNF in clinical applications, aiming to translate these findings into effective treatments for patients suffering from neurological diseases and SCIs (123).

2.3.1.3.3 Brain derived neurotrophic factor (BDNF)

BDNF is a neurotrophic factor that plays a pivotal role in the survival, differentiation, and plasticity of a broad range of neuronal cell types, including both sensory and motor neurons (124). As one of the most extensively studied neurotrophic factors, BDNF has been shown to promote the health and regeneration of neurons in the CNS and the PNS (125).

BDNF is crucial in enhancing neurogenesis and neuroplasticity, which are fundamental for the recovery and repair of neuronal circuits following injury or disease (126). In the context of nerve tissue engineering, BDNF has shown great promise due to its ability to stimulate nerve regeneration and contribute to functional recovery in various models of nerve injury, particularly in the PNS (127). BDNF plays an essential role in axonal growth, synaptic plasticity, and the remodeling of neural networks, which are critical for restoring the function of injured nerves.

In animal models of peripheral nerve injury, BDNF has been shown to enhance nerve regeneration, stimulate neurite outgrowth, and improve functional recovery by promoting the survival of neurons and supporting the growth of axons (128). BDNF also has a profound effect on the differentiation of neural progenitor cells and the maturation of neurons. These properties make it an important factor for nerve repair, especially in cases where the nervous tissue has been damaged due to injury or disease (129).

BDNF's regenerative potential extends beyond the PNS. In the CNS, BDNF has been shown to support the survival of neurons, enhance synaptic plasticity, and even counteract neurodegeneration in several models of CNS disorders (130). Its role in promoting neuronal survival and synaptic remodeling has made it a key target in the development of therapies for diseases such as Parkinson's disease, Alzheimer's disease, and Huntington's disease (131).

In nerve tissue engineering, BDNF is often utilized in biomaterials and scaffolds designed to mimic the natural ECM, where it is incorporated to support the regeneration of damaged nerves (132). Research has focused on the controlled delivery of BDNF to the site of injury, using techniques such as gene therapy, protein delivery systems, and nanostructured scaffolds. These approaches aim to provide sustained and localized release of BDNF, thereby enhancing its effectiveness in promoting nerve regeneration and functional recovery.

Furthermore, BDNF has been studied in combination with other neurotrophic factors, such as NGF and GDNF, to further enhance the therapeutic effects of nerve tissue engineering strategies. The synergistic effects of these factors could offer a more comprehensive approach to repairing nerve injuries and restoring normal function (133).

Overall, the potential of BDNF in nerve tissue engineering is vast, as it not only supports the survival and differentiation of neurons but also plays an integral role in promoting nerve regeneration and functional recovery (134). With ongoing research and advances in drug delivery systems and scaffold technologies, BDNF is poised to play a key role in the development of innovative therapies for nerve injuries and neurodegenerative diseases.

2.3.1.4 Three dimensional (3D) printing (additive manufacturing)

Recent advancements in 3D bioprinting for SCI have dramatically expanded the potential for effective repair and regeneration of damaged neural tissues. These innovations promise to offer novel therapeutic approaches that could transform the treatment of SCI (135). There are some key developments in this promising field:

2.3.1.4.1 Bioprinting techniques

With the advent of personalized manufacturing, researchers can now tailor scaffold designs to suit the anatomical needs of individual patients. 3D imaging technologies such as MRI and CT scanning are integrated with bioprinting techniques to produce highly customized scaffolds that precisely fit the injury profiles of SCI patients (136, 137). This level of anatomical fidelity ensures that the scaffolds align with the complex structures of the spinal cord, potentially improving the efficacy of the repair process and maximizing outcomes.

2.3.1.4.2 Multi material bioprinting

The introduction of multi nozzle technology in 3D bioprinting has allowed for the simultaneous printing of various materials, enabling the creation of complex, heterogeneous scaffold structures that more accurately replicate the multi layered nature of spinal cord tissue (138). This technique allows researchers to embed bioactive agents such as neurotrophic factors and stem cells within the scaffold, which can further enhance the regenerative potential of the engineered tissue (139, 140). These scaffolds can guide axon growth, support neuron survival, and promote the formation of neural networks, crucial for repairing the damaged spinal cord.

2.3.1.4.3 Integration of stem cells

The combination of stem cell therapy with 3D bioprinting represents a major breakthrough in SCI treatment (141). By embedding NSCs within bioprinted scaffolds, researchers aim to create an environment that supports the survival and differentiation of stem cells into functional neurons (142). These neuronal progenitors can aid in the restoration of neural pathways and promote axon regeneration, which is vital for functional recovery after SCI (143). Additionally, the use of stem cells enables the development of personalized therapeutic approaches, as stem cells derived from the patient or suitable donor sources can be used to minimize immune rejection (144).

2.3.1.4.4 *In Vitro* models and preoperative simulations

One of the key advantages of 3D bioprinting is its ability to rapidly create *in vitro* models that simulate SCIs. These models serve as invaluable tools for researchers to test and refine therapeutic strategies before clinical application (145). By using bioprinted models, scientists can simulate various injury scenarios and evaluate the efficacy of different regenerative treatments, including stem cell therapy, gene therapy, and bioactive molecule delivery (146). These preoperative simulations are vital for optimizing therapeutic approaches, ensuring better results once applied in human clinical settings.

2.3.1.4.5 Challenges and future prospects

Despite these advancements, there remain several challenges in the application of 3D bioprinting to SCI repair. Issues related to printability, cell material interactions, and cell survival within the bioprinted scaffolds continue to hinder progress. For instance, ensuring that printed cells maintain high survival rates and function properly after implantation is critical for the success of these approaches. Additionally, overcoming immune rejection and achieving long term integration of bioprinted tissues with native spinal cord tissue is another significant hurdle.

Ongoing research efforts are focused on addressing these limitations, with particular emphasis on improving bioprinting precision, enhancing bioink formulations, and exploring new strategies to increase cell viability and functional integration. As 3D bioprinting continues to evolve, the development of advanced biomaterials, coupled with stem cell based therapies, holds the promise of delivering more effective and personalized treatments for SCIs. The future of 3D bioprinting in SCI repair looks incredibly promising, as continued innovation in bioprinting technologies, material science, and regenerative medicine will likely lead to more effective treatments that can improve functional recovery, restore lost neural functions, and ultimately enhance the quality of life for SCI patients.

2.4 Approach, Aim and Novelty of the Study

The objective of this study is to develop a hydrogel based microenvironment model that effectively simulates the complex conditions of SCI while addressing the key challenges in nerve regeneration and glial scar formation. The creation of an *in vitro* model is essential for studying the intricate cellular and molecular mechanisms underlying SCIs and testing potential therapeutic approaches before clinical application. To achieve this goal, GelMA was chosen as a core material for the hydrogel, due to its ability to mimic the natural composition of the spinal cord ECM. The degree of methacrylation (DM) was carefully optimized to enhance the hydrogel's functionality, providing the ideal balance between stiffness and flexibility, while

maintaining the capability for cell attachment and growth. Key components of the ECM, including HA, CS, and lmn, were integrated into the hydrogel formulation. These molecules are naturally abundant in the spinal cord and play pivotal roles in promoting cellular adhesion, neuroprotection, and nerve regeneration. HA, for instance, supports cell migration and facilitates tissue repair, while CS helps modulate inflammation and is involved in axonal growth and neurogenesis. Lmn, a critical ECM protein, is known to support neuronal survival and axon extension, particularly in injury repair models.

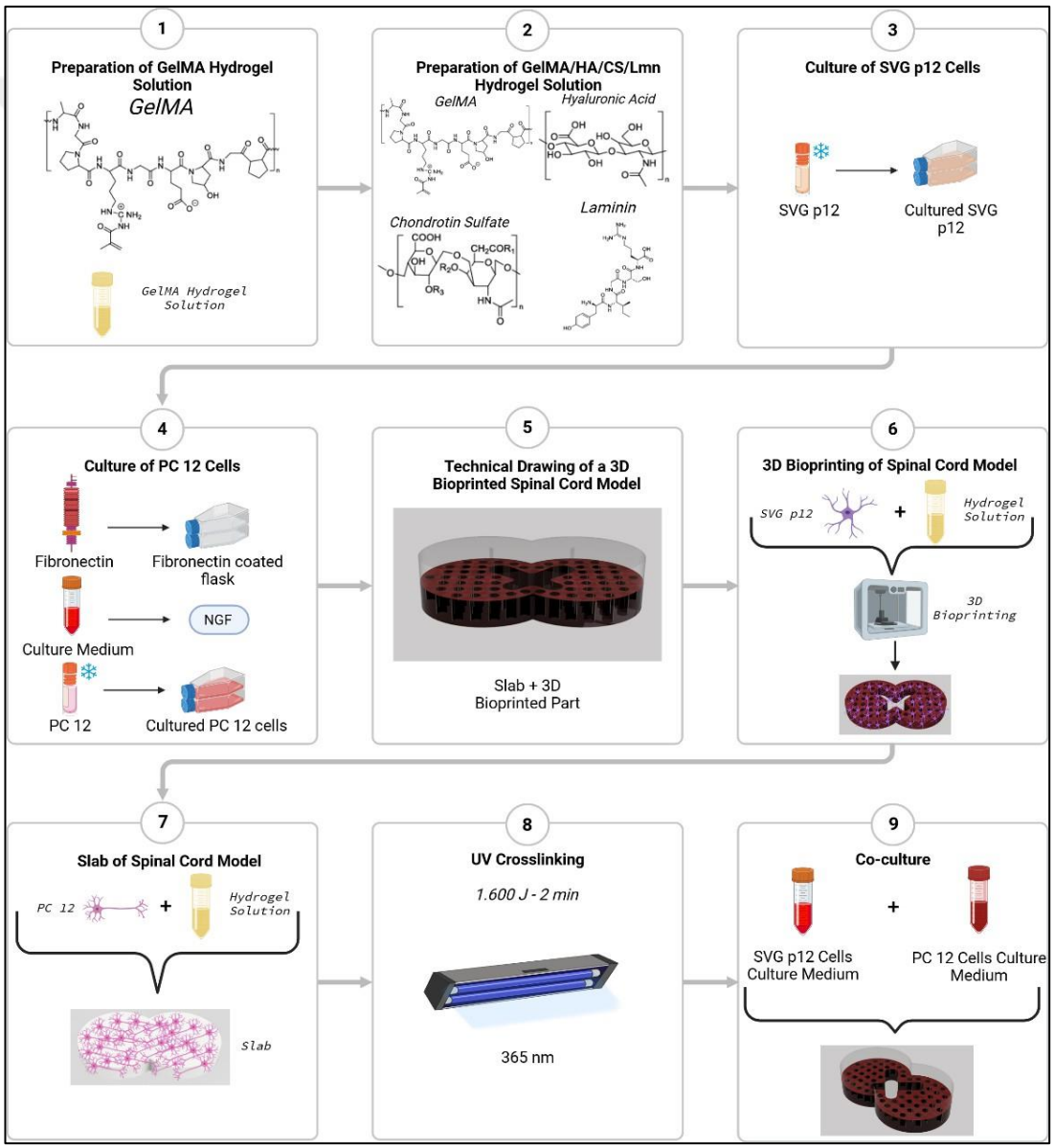

Figure 12. Preparation of the SCI Model

Additionally, a 3D printed honeycomb structure was employed to replicate the spatial architecture of the spinal cord, including the tracks found within it. This structure is designed to enhance cellular interaction and promote tissue-like behavior, encouraging cells to form organized structures similar to the native spinal cord tissue. The honeycomb configuration also aids in nutrient distribution, oxygen diffusion, and the creation of microenvironments that support cellular function and nerve regeneration, while mimicking the tracks in the spinal cord that are essential for nerve conduction.

A significant aspect of this study is the inclusion of astrocyte-laden bioinks, which are integrated into the hydrogel matrix and 3D printed to form the scaffolds. Astrocytes, the predominant glial cell type in the spinal cord, play an essential role in maintaining the integrity of the blood-brain barrier, supporting neuron survival, and modulating neuroinflammation. By incorporating these cells directly into the hydrogel bioink, their interactions with neurons are facilitated, allowing them to imitate their natural function, particularly in scar formation and axonal regeneration following injury.

Through this integrated approach, the study aims to evaluate cell viability, proliferation, and functional behavior within the engineered platform. The ultimate goal is to provide a robust *in vitro* model that closely mimics the SCI microenvironment, offering an invaluable tool for advancing SCI research. This model will serve as a critical platform for testing therapeutic interventions, including the evaluation of neurotrophic factors, stem cell therapies, and drug treatments, with the potential to contribute to the development of effective strategies for promoting nerve regeneration and functional recovery after SCI.

3 MATERIALS AND METHODS

3.1 Materials

3.1.1 Chemicals

In this study, various chemicals and reagents were employed for material preparation, cell culture, and analytical assays. For material synthesis, gelatin from porcine skin (80-120g Bloom, Type A, Sigma-Aldrich), methacrylic anhydride (Sigma-Aldrich), and hyaluronic acid sodium salt from *Streptococcus equi* (Sigma-Aldrich) were used, alongside CS and mouse laminin (Sigma-Aldrich). Dialysis processes utilized Snake Skin Dialysis Tubing (10,000 MWCO, Thermo Scientific) to purify the materials. Cell culture was conducted using Dulbecco's Phosphate Buffered Saline (DPBS, Gibco), Dulbecco's Modified Eagle's Medium (DMEM, Sigma-Aldrich) and RPMI 1640 (PAN Biotech), all supplemented with fetal bovine serum (FBS, Sigma-Aldrich), penicillin-streptomycin (Gibco), NGF-β (Sigma-Aldrich) and trypsin-EDTA (Gibco). For cryopreservation, dimethyl sulfoxide (DMSO, Sigma-Aldrich) was used, while ethanol (EtOH, Isolab) and sodium azide (Sigma-Aldrich) were applied in additional protocols.

Analytical and viability assays were performed using Alamar Blue and Live-Dead assay kits (Thermo Fisher Scientific), and immunostaining was conducted with GFAP(Invitrogen), beta tubulin (Abcam), FITC-Phalloidin and 4',6-Diamino-2-phenylindole (DAPI) (Sigma-Aldrich). The combination of these materials and methods provided a comprehensive framework for investigating SCI *in vitro*, facilitating the evaluation of cell viability, proliferation, and functional behavior within engineered hydrogel scaffolds. In addition, secondary antibodies conjugated with Alexa Fluor 488 and Alexa Fluor 555 were purchased from Thermo Fisher. This robust approach aimed to advance the development of novel strategies for nerve regeneration and tissue engineering in SCI research.

3.1.2 Equipments

In this study, various advanced instruments and laboratory devices were employed to conduct experiments and analyses. Imaging studies were performed using a Confocal Microscopy (Zeiss LSM 900) and a Stereomicroscope (Zeiss Stereomicroscope Stemi 2000) for detailed visualization of samples. Structural and morphological characterizations were carried out with a Scanning Electron Microscope (Zeiss Evo 10 SEM) to observe fine details of the samples and an FT-IR spectrometer (Shimadzu IR Tracer 100) for chemical composition analysis. Quantitative measurements were obtained using an Absorbance-Fluorescence Plate Reader (Victor Nivo: Flex Station 3, Molecular Devices) to assess cell viability and proliferation. The fabrication of hydrogel based scaffolds was performed using a 3D Bioprinter (Envisiontec 3D- Bioplotter Developer), while freeze drying was carried out with a Freeze Dryer (Labconco 6L) to preserve sample integrity. Additional devices for precise control and analysis included a UV Cabin (Witec Imaging UV System BLX 365) for UV irradiation, a Mechanical Tester (Shimadzu AGS-X Series Universal Test Machine) for mechanical properties testing, Centrifuges (Beckman Coulter Allegra X-30R) for sample separation, and an Autoclave (Nüve NC 90 M) for sterilization. For storage and preparation of reagents, a Deep Freeze (Kirsch) and a Pure Water Device (MilliQ) were utilized. Routine laboratory operations were supported by a Vortex (Thermo Scientific), Biosafety Cabinets (Thermo Scientific) for safe handling of cell cultures, an Orbital Shaker (Ohaus) for mixing, and a CO2 Incubator (PHCbi) to maintain cell culture conditions. These instruments and devices provided essential capabilities for the successful execution of experiments in the study.

3.2 Methods

3.2.1 Synthesis and characterization of methacrylated gelatin (GelMA)

Porcine skin gelatin (100 Bloom, Sigma) was dissolved at a concentration of 10% (w/v) in phosphate buffered saline (PBS) at 60°C under continuous stirring until complete dissolution was achieved. MAA was then introduced into the gelatin solution

at a controlled rate of 0.5 mL/min, with the temperature maintained at 50°C. The reaction was allowed to proceed for 1 hour (h) while stirring. To stop the reaction, the solution was diluted with PBS at 40°C.

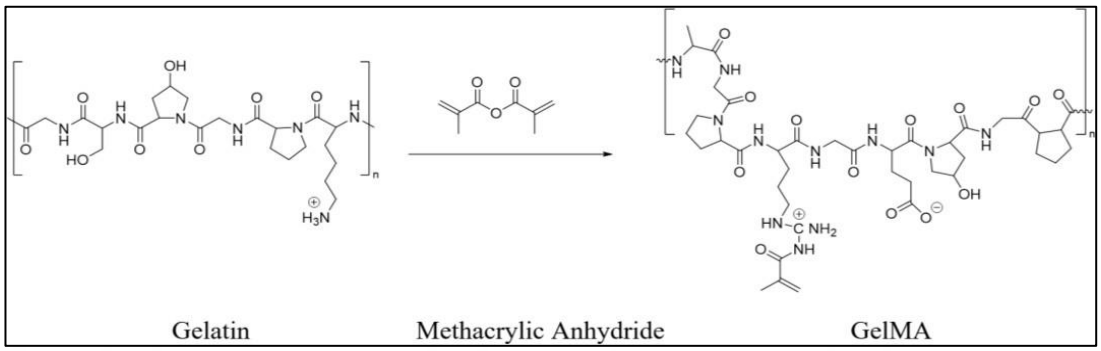

Figure 13. The synthesis of GelMA

The resulting mixture was filtered and placed into dialysis membranes, followed by dialysis at 37°C for 10 days to remove residual salts and unreacted methacrylic acid. After dialysis, the solution was filtered through filter paper and transferred into large Petri dishes, then frozen at -80°C. The frozen solution underwent lyophilization for one week, resulting in a white, porous foam that was ready for further processing and use in the study.

3.2.1.1 Determination of methacrylation level of the methacrylated gelatin with ^{1}H-NMR

^{1}H-NMR spectrometer was employed for the determination of the methacrylation level of GelMA. The analysis was conducted using a Bruker DPX 400 spectrometer operating at a ^{1}H resonance frequency of 400 MHz, with 16 scans performed for each sample. The GelMA samples were solubilized in D_2O at a concentration of 30 mg/mL. The methacrylation degree (MD) was determined using the MestreNova NMR analysis software (version 6.0.2, Mestrelabs Research, SL, Spain). The MD of gelatin is defined as the ratio of the methacrylate group protons to the total protons in the polymer chain.

$$\boldsymbol{DM}(\%) = (\mathbf{1} - \frac{\boldsymbol{Lysine\ methylene\ of\ GelMA}}{\boldsymbol{Lysine\ methylene\ of\ Gelatin}})\ \boldsymbol{x100} \quad (1)$$

3.2.1.2 Fourier transform infrared spectroscopy (FT-IR)

FT-IR analysis was conducted using a spectrometer (Perkin Elmer, Inc., UK) to confirm the presence of specific peaks of Gelatin and GelMA to determine their presence. The analysis was performed in the wavelength range of 450-4000 cm^{-1} with a resolution of 4 cm^{-1}.

3.2.2 Production of GelMA/HA/CS/Lmn hydrogel slabs

GelMA (15%, w/v), GelMA-HA 30:1, GelMA-HA-CS 30:1:1, and GelMA-HA-CS- Lmn 30:1:1:0.2 solutions containing 0.5% (w/v) Irgacure 2959 photoinitiator were prepared. The solutions were then placed into poly(dimethylsiloxane) (PDMS) molds and exposed to ultraviolet (UV) light at a wavelength of 365 nm for 2 min.

Table 1. Molecular structure of A) GelMA, B) GelMA/HA, C) GelMA/HA/CS and D) GelMA/HA/CS/Lmn

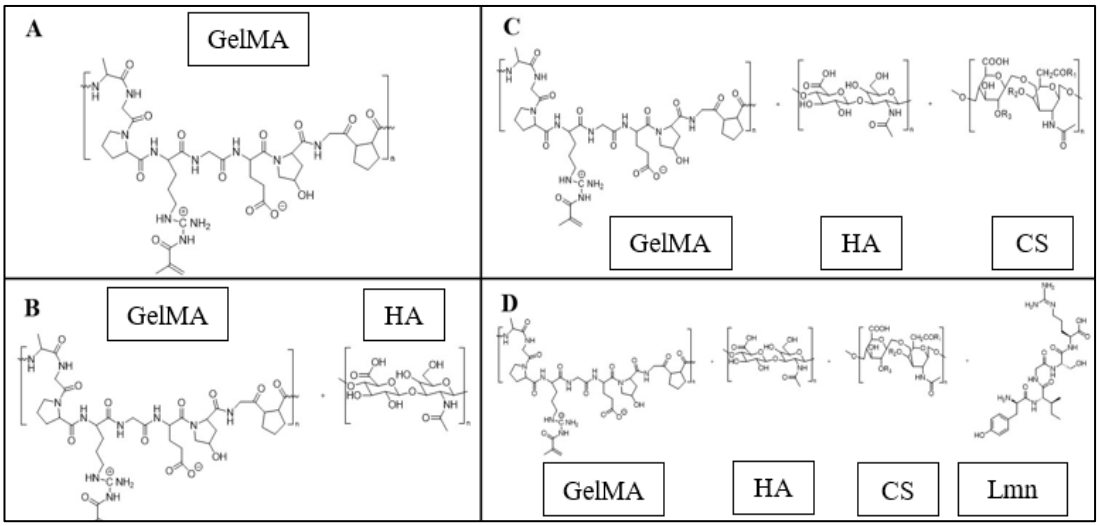

3.2.3 Characterization of GelMA/HA/CS/Lmn hydrogel slabs

3.2.3.1 Fourier transform infrared spectroscopy (FT-IR)

FTIR analysis was performed using a Perkin Elmer L1600401 spectrometer (Perkin Elmer, Inc., UK) to determine the presence of specific peaks corresponding to absorbances by GelMA, GelMA-HA, GelMA-HA-CS, and GelMA-HA-CS-Lmn hydrogel slabs. The analysis was conducted over a wavenumber range of 450–4000 cm^{-1}. The spectra data obtained were analyzed to assess the chemical interactions and the degree of modification achieved in the hydrogel networks.

3.2.3.2 Determination of equilibrium water content (EWC)

The EWC (%) of GelMA, GelMA-HA, GelMA-HA-CS, and GelMA-HA-CS-Lmn hydrogel slabs was assessed at 37 °C using a shaking incubator (Ohaus) set at 150 rpm. Initially, the hydrogels were incubated in PBS with 0.2% (w/v) sodium azide for 24 h to allow for equilibration. After the incubation, excess water on the surface was carefully removed with filter paper, and the wet weight (W_{wet}) of the hydrogels was recorded. In order to remove salts and any remaining PBS, the hydrogels were washed with distilled water (dH_20) and subsequently lyophilized. The dry weight (W_{dry}) of the lyophilized hydrogels was then measured. The EWC (%) of each hydrogel was calculated using the following equation:

$$\boldsymbol{EWC}(\%) = \frac{\boldsymbol{W_{wet} - W_{dry}}}{\boldsymbol{W_{wet}}} \boldsymbol{x100} \quad (2)$$

This calculation provided the percentage of water content retained by the hydrogels after the equilibration and drying process, offering insight into the hydrophilicity and swelling behavior of the hydrogel formulations.

3.2.3.3 Degradation of hydrogel slabs

GelMA, GelMA-HA, GelMA-HA-CS, and GelMA-HA-CS-Lmn hydrogel slabs (n=3) were rinsed with dH_20, lyophilized, and weighed to record their initial dry weights (W_0). They were then incubated in PBS (pH 7.4, 10 mM) containing 0.2% (w/v) sodium azide at 37 °C in a shaking incubator for 28 days to simulate long term incubation under physiological conditions. On days 1, 7, 14, 21, and 28, samples were rinsed with dH_20, lyophilized, and weighed (W_t). The final weight loss over time was used to calculate the remaining weight (W) as a percentage, using the following equation:

$$\boldsymbol{W}(\%) = [\frac{\boldsymbol{W_0} - \boldsymbol{W_t}}{\boldsymbol{W_0}}] \boldsymbol{x100} \quad (3)$$

This calculation allowed for the assessment of the degradation behavior of the hydrogels and their stability in a simulated biological environment, providing insight into their potential for long term use in tissue engineering applications.

3.2.3.4 Enzymatic degradation

Collagenase type II was utilized to assess the degradability of GelMA, GelMA-HA, GelMA-HA-CS, and GelMA-HA-CS-Lmn hydrogel slabs (n=3). The initial dry weights of the hydrogel slabs were recorded (W_0), in an accelerated fashion the samples were then incubated in various concentrations of collagenase type II (5, 10, 15, and 20 U/mL) in PBS (pH 7.4, 10 mM). The hydrogel slabs were incubated at 37 °C, and at 2h, the samples were removed, washed and lyophilized. The dry weights of the hydrogels (W_t) were determined at each time point. Degradation (%) of the hydrogels was calculated using the following equation:

$$\boldsymbol{Degradation}(\%) = [\frac{\boldsymbol{W_0} - \boldsymbol{W_t}}{\boldsymbol{W_0}}] \boldsymbol{x100} \quad (4)$$

W_t: dry weight at time t, W_0: initial dry weight

3.2.3.5 Mechanical properties

The mechanical properties of GelMA, GelMA-HA, GelMA-HA-CS, and GelMA-HA- CS-Lmn hydrogel slabs were assessed using compression tests. The tests were conducted with a Shimadzu AGS-X Series Universal Testing Machine (Japan) equipped with a 20 kN load cell. The hydrogel slabs were subjected to compression at a constant speed of 1 mm/s, allowing for the determination of their mechanical strength, including parameters such as stiffness, elasticity, and compressive modulus. This analysis provides crucial information on the structural integrity and suitability of the hydrogels for applications in tissue engineering, where the mechanical properties of scaffolds must closely match those of the target tissue to promote proper cellular behavior and functionality.

$$Strain(\varepsilon) = \frac{\Delta l}{l} \tag{5}$$

$$Stress(\sigma) = \frac{F}{A} \tag{6}$$

$$Compressive\ Modulus = \frac{\sigma}{\varepsilon} \tag{7}$$

3.2.3.6 Rheological examination

The rheological properties of GelMA, GelMA-HA, GelMA-HA-CS, and GelMA-HA- CS-Lmn hydrogel slabs were evaluated using a Malvern Kinexus Ultra+ rheometer at 25°C room temperature (RT). The shear rate was increased logarithmically from 1 to 1000 s^{-1} to assess the viscosity of each hydrogel (n=3). The testing involved determining both the elastic modulus (G') and the viscous modulus (G") of the hydrogels, which reflect their ability to resist deformation and flow under applied stress. The elastic modulus indicates the solid like behavior of the material, while the viscous modulus provides insight into its liquid like characteristics. These measurements are critical for understanding the flow behavior and mechanical stability of the hydrogels, which are important factors in their performance as scaffolds in tissue

engineering applications. Frequency-dependent storage modulus (G') and loss modulus (G") were measured using an 8 mm diameter plate with a gap of 0.5 mm. Oscillation frequency analysis was conducted at 1% strain within the range of 0.1–10 Hz. The linear viscoelastic region was determined through a strain sweep test performed at 25 °C, with strain logarithmically increasing from 0.1% to 100%. Before each measurement, the samples were equilibrated at 25 °C for 3 minutes to ensure consistent testing conditions. All experiments were performed in triplicate to ensure reproducibility and reliability of the results.

3.2.3.7 SEM examination

Dry GelMA, GelMA-HA, GelMA-HA-CS, and GelMA-HA-CS-Lmn hydrogel slabs were examined under a Scanning Electron Microscope (SEM, EVO 10, Zeiss, Germany) to examine their surface morphology and microstructure. In order to prepare the samples, the hydrogel slabs were placed onto aluminum stubs and coated with gold.

3.2.4 3D printing of hydrogel

3.2.4.1 Design of 3D bioprinted hydrogel

The primary objective was to create a biomimetic scaffold for the spinal cord. The scaffold model was based on histological features of the spinal cord.

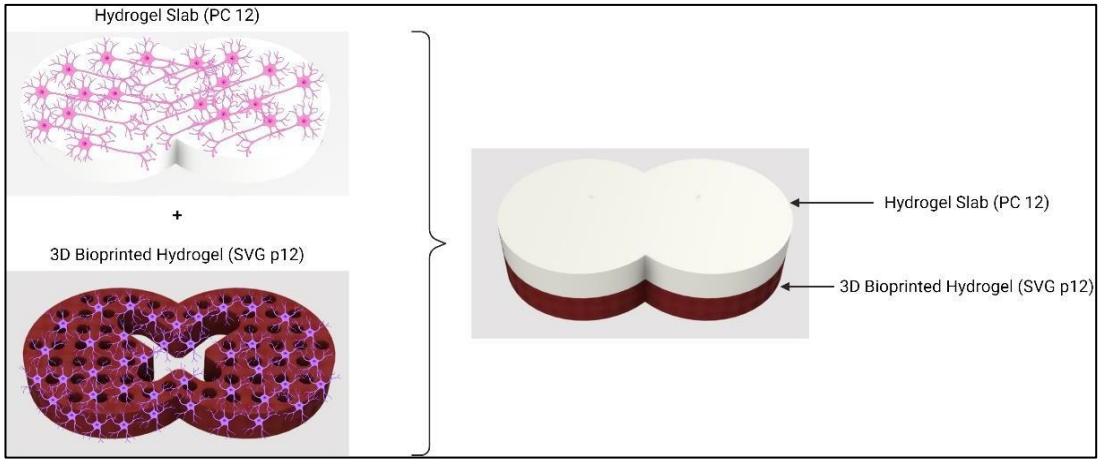

Figure 14. Design of 3D bioprinted SCI model

In this study, a three-dimensional model was designed to mimic the structural organization of the spinal cord using software, including Fusion 360, Perfactory, and Visual Machine. The primary goal was to mimic the characteristic structure with white matter region at the periphery and the gray matter at the center.

Initially, the spinal cord's shape was modeled in Fusion 360 with dimensions of 13 mm in length and 8 mm in width. The design was then imported into Perfactory software, where it was digitally sliced into 200-micron layers.

The resulting cell suspension was loaded into the cartridge, at 18°C for 20 min prior to printing. The GelMA/HA/CS/Lmn solution (3 mL) was loaded into the cartridge, which was then positioned into the printer's head, maintained at 20°C. The precise printing parameters included a cartridge temperature and chiller temperature both set to +20°C, with a needle offset of 0.160 mm, pressure of 1.1 bar, printing speed of 20.0 mm/s, and a pre-flow time of 0.09 s. The design pattern used for the construct was the honeycomb configuration, with continuous strands. The distance from the contour was 0.05 mm, and between strands 0.60 mm, and the period between patterns 1.20 mm. The build contour was included in the design. Following the printing, it was UV crosslinked. The UV parameters were adjusted to a distance of L/2, with a power of 1.600 J and a time of 1.30 min for each side, ensuring effective crosslinking of the material.

Finally, the sliced design was processed in Visual Machine software, where additional structural features were incorporated to mimic the white matter region's microarchitecture. The honeycomb pattern was selected for its mechanical strength, interconnected pathways, and ability to enhance cellular alignment, promoting a biomimetic environment conducive to tissue regeneration.

3.2.4.2 Printing of the model hydrogels

The GelMA/HA/CS/Lmn hydrogel was prepared as in Table 2 and reaction was initiated with Irgacure 2959 (0.5% w/v).

Table 2. Hydrogel formulation overview

Sample Name	Final ratio of GelMA:HA:CS:Lmn	GelMA (w/v)	HA (w/v)	CS (w/v)	Laminin (w/v)
GelMA-HA-CS-Lmn	30:1:1:0.2	15%	0.5%	0.5%	0.14%

The GelMA-HA-CS-Laminin (Lmn) hydrogel was fabricated using an EnvisionTEC 3D printer. A total of 3 mL of the prepared GelMA-HA-CS-Lmn solution was loaded into the bioprinter cartridge. In order to ensure optimal viscosity for printing, the cartridge was placed in the print head and maintained at a constant temperature of +18°C for 20 min prior to the start of the process.

The cartridge and chiller temperatures were set at +18 °C to stabilize the hydrogel solution. The needle offset was adjusted to 0.160 mm, while the extrusion pressure was maintained at 1.1 bar to ensure smooth flow. The printing speed was set at 20.0 mm/s, with a pre-flow duration of 0.09 s.

Continuous strand printing was employed, with a contour distance of 0.05 mm and a strand-to-strand spacing of 0.60 mm, ensuring uniformity. The period of the honeycomb structure was set to 1.20 mm, and a build contour was applied to maintain structural integrity. Post-printing, the hydrogel was crosslinked using ultraviolet (UV) irradiation. Distance L/2 from the light source, power 1.600 J, exposure duration 1.30 min, each side.

3.2.5 Characterization of GelMA/HA/CS/Lmn 3D printed hydrogels

3.2.5.1 Determination of equilibrium water content (EWC)

The equilibrium water content (EWC) of the 3D printed GelMA-HA-CS-Lmn hydrogels was measured, following the procedure outlined in Section 3.2.3.2.

3.2.5.2 Degradation of 3D printed hydrogels

Degradation of the 3D printed GelMA-HA-CS-Lmn hydrogels was investigated in accordance with the method described in Section 3.2.3.3.

3.2.5.3 Enzymatic degradation

The enzymatic degradation of the 3D printed GelMA-HA-CS-Lmn hydrogels was studied based on the protocol detailed in Section 3.2.3.4.

3.2.5.4 Mechanical properties

The mechanical properties of the 3D printed GelMA-HA-CS-Lmn hydrogels were determined through compression testing, as described in Section 3.2.3.5.

3.2.5.5 Morphological analysis

The surface morphology and microstructure of the 3D printed GelMA-HA-CS-Lmn hydrogels were examined with following the methodology specified in Section 3.2.3.7.

3.2.6 *In Vitro* studies

3.2.6.1 Cell culture of astrocytes (SVG p12 cell line)

SVG p12 cells were cultured in Dulbecco's Modified Eagle's Medium (DMEM), which was supplemented with 10% fetal bovine serum (FBS) and 1× penicillin/streptomycin/amphotericin B (P/S/A). These cells were maintained in tissue culture polystyrene (TCPs) flasks at 37 °C in an CO_2 incubator (5% CO_2).

The growth medium was refreshed every two days. When the cells reached confluence, the medium was removed, and the cells were gently rinsed with phosphate-

buffered saline (PBS). The adherent cells were then detached using Trypsin-EDTA (0.05%), which was prepared by diluting a 0.25% stock solution in PBS. The cells were incubated with trypsin at 37 °C for 5 min. After detachment, DMEM high glucose medium containing 10% serum and penicillin/streptomycin was added. The cell suspension was then collected and transferred into fresh culture vessels for continued growth or experimental procedures.

3.2.6.2 PC 12 cell culture

PC 12 cells were cultured in RPMI 1640 medium supplemented with 10% FBS and 1× P/S/A to promote cell. The cells were subjected to four different experimental conditions to investigate the effects of surface coating and the presence of NGF. These conditions included cells grown on uncoated and fibronectin (fnc)-coated TCPs with or without NGF (50 ng/mL). The PC 12 cells were incubated at 37 °C in a humidified atmosphere with 5% CO_2. The growth medium was changed every two days.

For passaging, the medium was removed, and the cells were washed with PBS then treated with Trypsin-EDTA (0.05%), and incubated at 37 °C for 5 min. After detachment, RPMI 1640 medium was added containing 10% FBS and 1× P/S/A, and the detached cells were collected for further analysis or passaging into new culture vessels.

3.2.7 Cell response and assessment of 3D bioprinted hydrogels

3.2.7.1 Cell seeded hydrogels

The GelMA-HA-CS-Lmn solution was filtered through a 0.22 μm syringe filter under a laminar flow hood. Once the cells reached confluency, they were detached from the TCPs flasks using 0.025% Trypsin-EDTA, followed by centrifugation at 1500 rpm for 5 min. The resulting cell pellet was resuspended in 1 mL of culture medium for further processing. Cell counting was performed using a Thoma counter chamber (ISOLAB, Germany) to determine the required cell density.

For cell entrapment, 3×10^6 cells were collected and centrifuged. The pellet was then resuspended in 3 mL of GelMA-HA-CS-Lmn solution. The hydrogel solution was pipetted gently to ensure a uniform distribution of cells throughout the hydrogel matrix.

3.2.7.2 SVG p12 loaded 3D bioprinted hydrogel

The hydrogel solution carrying SVG p12 cells was transferred into a cartridge, which was then placed in the bioprinting head. In order to maintain the viscosity, the cartridge was kept at +20 °C for 20 min. Following this, the hydrogel material was crosslinked under UV (365 nm, 1.6 Joule/cm²) for 2 min.

3.2.7.3 Alamar blue assay

A 10% Alamar Blue solution was prepared by mixing 1 mL of Alamar Blue with 9 mL of DMEM High Glucose colorless medium supplemented with Penicillin/Streptomycin and was covered with aluminum foil.

The samples in the wells were washed twice with sterile PBS to remove any residual medium before 1 mL of the prepared Alamar Blue solution was added to each well to completely cover the scaffolds. The 24-well plate was then wrapped in aluminum foil and incubated in a CO_2 incubator for 1 h. Then, 200 µL of solution from each well was transferred to a 96-well plate for optical density (OD) measurements at 570 nm and 595 nm using a multi plate reader.

The percentage reduction of the dye was calculated using the absorbances at 570 nm and 595 nm. Extinction coefficients (ε) were: λ_1 = 570 nm and for λ_2 = 595 nm, as well as the observed absorbance readings for the test wells (A_{λ_1} , A_{λ_2}) and the negative control wells (A'_{λ_1} , A'_{λ_2}). $(\varepsilon_{ox})_{\lambda 2}$ = 117.216, $(\varepsilon_{ox})_{\lambda 1}$ = 80.586, $(\varepsilon_{red})_{\lambda 1}$= 155.677 and $(\varepsilon_{red})_{\lambda 2}$ = 14.652

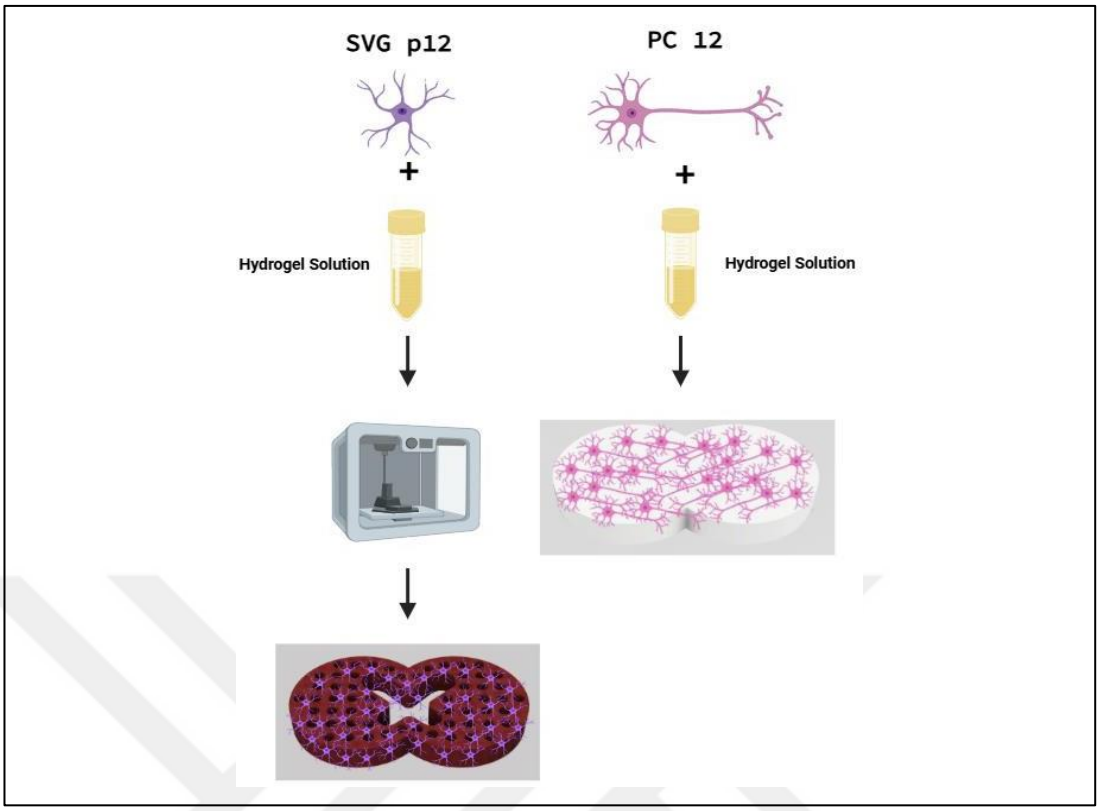

Figure 15. Cell proliferation with Alamar Blue Assay in cell culture procedure

To determine the proliferation of SVG p12 and PC12 cells, cell-loaded samples were cultured separately under appropriate conditions (Figure 15). This approach ensured that the growth characteristics of each cell type could be accurately assessed without interference from the other.

3.2.7.4 Live-dead cell viability assay

Following a 21 day culture period, a Live-Dead Cell Viability Assay was performed to assess the viability of cells within 3D bioprinted hydrogels. The assay solution was prepared in DPBS, incorporating calcein AM (1:2000) for live cells (green) and ethidium homodimer-1 (1:500) for dead cells (red). Following the removal of the culture media, Live-Dead test solution was introduced into the wells, and the samples were incubated at 37°C for 30 min. Following incubation, the test solution was discarded, and DMEM-High Glucose devoid of Phenol Red was introduced to the

samples, which were subsequently analyzed using a Confocal Laser Scanning Microscope (CLSM) (Zeiss LSM 900, Germany).

3.2.7.5 Immunostaining

Following the 21day culture, immunostaining for β-tubulin and GFAP was performed to evaluate the expression of neuronal and glial markers in the 3D bioprinted hydrogels. The samples were first washed with dPBS (with Mg^+ Ca^+) to remove any residual culture media. They were then fixed with 4% paraformaldehyde (PFA) for 1 h at RT. After fixation, the samples were washed three times with dPBS. Next, the samples were permeabilized with 0.1% Triton X-100 in dPBS for 10 min at RT. The samples were incubated with 100 mM glycine at RT for 15 min and washed three times with dPBS. Next, using 0.1% Triton X-100 in dPBS for 10 min at RT. Following permeabilization, the samples were blocked with 1% BSA in dPBS for 30 min at 37°C to prevent non-specific binding. The primary antibody, GFAP (1:200, invitrogen) for glial cells, was diluted in %0.1 BSA and applied to the samples, which were incubated overnight at +4°C. After primary antibody incubation, the samples were washed with dPBS. The secondary antibody, anti-chicken conjugated with fluorescent dyes (AlexaFluor 488, 1:200), was applied to the samples, which were incubated for 1 h at +37°C in the dark. After secondary antibody incubation, the samples were washed again with PBS. The primary antibody, β-tubulin (1:500, Abcam) for neurons, were diluted in %0.1 BSA and applied to the samples, which were incubated overnight at +4°C. After primary antibody incubation, the samples were washed with dPBS. The secondary antibodies, anti-mouse conjugated with fluorescent dyes (AlexaFluor 555, 1:200), were applied to the samples, which were incubated for 1 h at +37°C in the dark. After secondary antibody incubation, the samples were washed again with dPBS. Finally, the samples were stained with DAPI (1:5000 in dPBS) for 10 min to label the cell nuclei. After washing, the samples were mounted on glass slides with mounting medium. Immunofluorescence imaging was performed using Confocal Laser Scanning Microscopy (CLSM, Zeiss LSM 900, Germany) to visualize the expression of β- tubulin (orange) and GFAP (green), along with the DAPI-stained nuclei (blue).

3.2.7.6 Phalloidin-DAPI staining

To assess the cytoskeletal organization and cell morphology within the 3D bioprinted hydrogels, Phalloidin-DAPI staining was performed. Following the 21-day culture period, the samples were first washed with dPBS (with Mg^+ Ca^+) to remove any residual culture media. The samples were then fixed using 4% PFA for 1 h at RT. After fixation, the samples were washed three times with dPBS. The samples were subsequently permeabilized using 0.1% Triton X-100 in dPBS for 5 min at RT. This step allowed the Phalloidin to access the actin filaments within the cells. The samples were washed three times with dPBS. After permeabilization, the samples were blocked with 1% BSA in dPBS for 30 min at 37°C to prevent non-specific binding. Then samples were washed with 0.1% BSA in dPBS. Phalloidin-FITC, conjugated with a fluorescent dye (AlexaFluor 488, 1:100, in 0.1%BSA), was applied to the samples and incubated for 1 h at 37°C in the dark to stain the F-actin filaments. Following incubation, the samples were washed three times with dPBS. The samples were stained with DAPI (AlexaFluor 555, 1:5000,in dPBS) for 10 min at RT. After staining, the samples were washed with dPBS and mounted on glass slides with mounting medium. The stained samples were analyzed using CLSM to visualize the actin filaments (green) and the nuclei (blue) of the cells within the hydrogels.

3.3 Statistical Analysis

All statistical analyses were conducted using GraphPad Prism 5.0 (GraphPad Software, San Diego, CA, USA). Experiments were performed in triplicates unless otherwise stated. The data were presented as the mean ± standard deviation (SD) to reflect variability within the measurements. Statistical comparisons between groups were evaluated using either one-tailed or two-tailed Student's t-tests, depending on the hypothesis being tested. A p-value of less than 0.05 was considered to indicate statistical significance, suggesting that the observed differences were unlikely due to chance.

4 RESULTS

4.1 Synthesis and Characterization of Methacrylated Gelatin (GelMA)

4.1.1 Methacrylation efficiency of hydrogel with ^{1}H nuclear magnetic resonance (^{1}H-NMR)

In order to determine the degree of methacrylation, the ^{1}H-NMR spectra of both the gelatin used for GelMA synthesis and the methacrylated GelMA polymer were analyzed. The spectra (Figure 16) were processed using MestreNova NMR analysis software (version 6.0.2, Mestrelabs Research) to calculate the methacrylation degree. Methacrylate groups produced two peaks between 5.4–5.7 ppm, while the aromatic amino acid phenylalanine exhibited a peak between 6.9–7.5 ppm. Since the phenylalanine peak remains unaffected during methacrylation, it was used for normalization across the spectra. The lysine methylene peaks, located within the orange region (2.8–2.95 ppm), were integrated to calculate the methacrylation degree based on the formula provided in Section 3.2.1.1. The methacrylation degree of the synthesized GelMA in this study was determined to be 87.06%.

$$\boldsymbol{DM}\ (\%) = \mathbf{1} - \left(\frac{\mathbf{0.15}}{\mathbf{1.16}}\right)\boldsymbol{x}\mathbf{100} \tag{9}$$

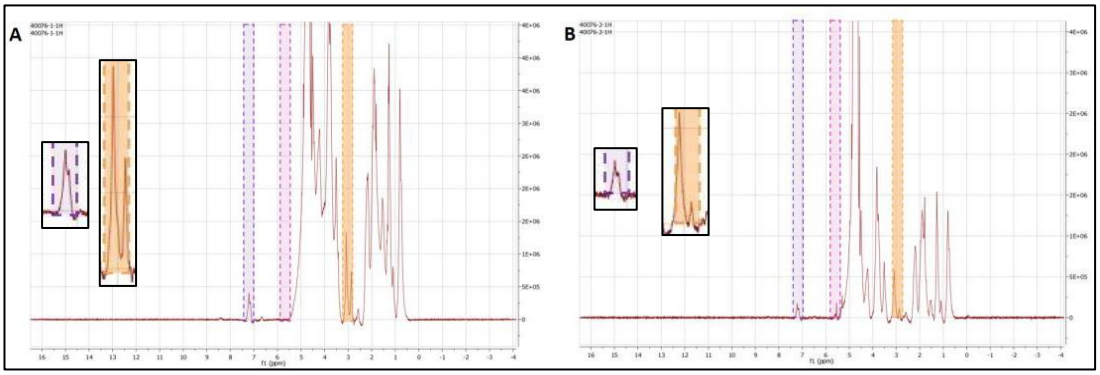

Figure 16. 1H-NMR spectra of A) gelatin and B) methacrylated gelatin (GelMA). The peak between 7.5-6.9 ppm indicates aromatic amino acid phenylalanine signals, peak between 5.7-5.4 ppm indicates methacrylic vinyl groups and peak between 2.95-2.8 ppm indicates methacrylic vinyl groups and peak between 2.95-2.8 ppm indicates lysine methylene groups

4.1.2 Infrared spectroscopy (FT-IR)

The FT-IR spectra of gelatin and GelMA were obtained using a Shimadzu (IR Tracer 100) device to examine their functional groups and confirm the methacrylation process. The spectrum of gelatin displayed characteristic bands at typical amide I (1640 cm^{-1}, C=C stretching) and amide II (1540 cm^{-1}, N–H bending) bands, along with differences in C–H stretching and bending regions between gelatin and GelMA, confirming the introduction of methacrylate groups to the lysine residues of gelatin.

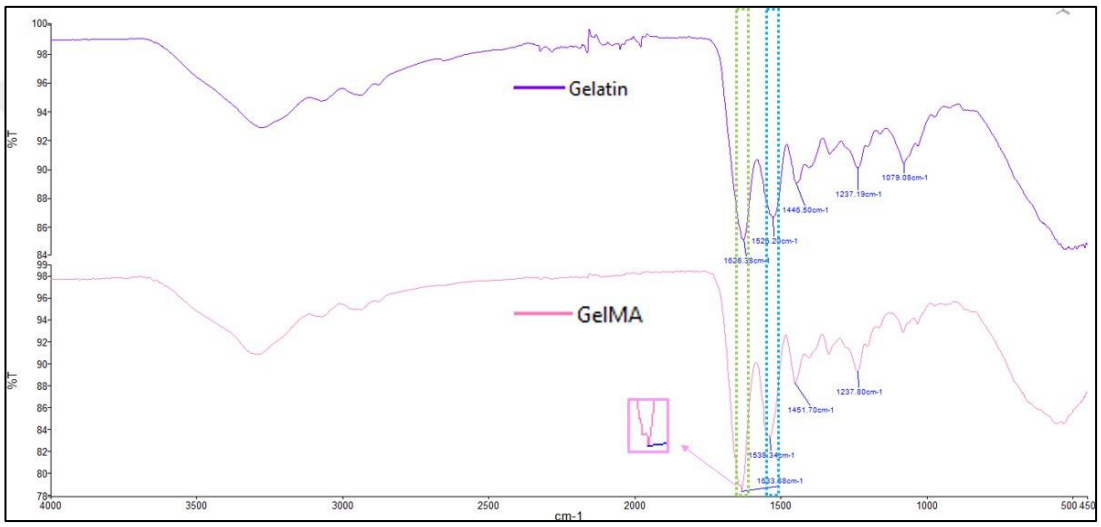

Figure 17. FT-IR spectra of gelatin and methacrylated gelatin, green indicates amide I and blue indicates amide II bands

4.2 Characterization of GelMA/HA/CS/Lmn Hydrogel Slabs

4.2.1 Infrared spectroscopy (FT-IR)

The FT-IR spectra of GelMA-HA, GelMA-HA-CS and GelMA-HA-CS-Lmn were analyzed using a Shimadzu IR Tracer 100 device to check the incorporation of HA, CS and Lmn into the GelMA hydrogel.

The FT-IR spectra of hyaluronic acid (HA) exhibits distinct characteristic peaks. A broad peak around 3400 cm^{-1} corresponds to the O–H stretching vibration due to hydroxyl groups present in HA. The peak at 2920 cm^{-1} is associated with C–H

stretching vibrations originating from the polysaccharide backbone. The peak at 1640 cm^{-1} represents C=O stretching vibrations related to N-acetyl groups in HA. Additionally, a peak at 1550 cm^{-1} is because of the N–H bending vibrations. The peak at 1410 cm^{-1} is from C–H bending and COO^- symmetric stretching vibrations. Finally, the region between 1030–1150 cm^{-1} shows C–O–C and C–O stretching vibrations, which are typical of saccharide structures.

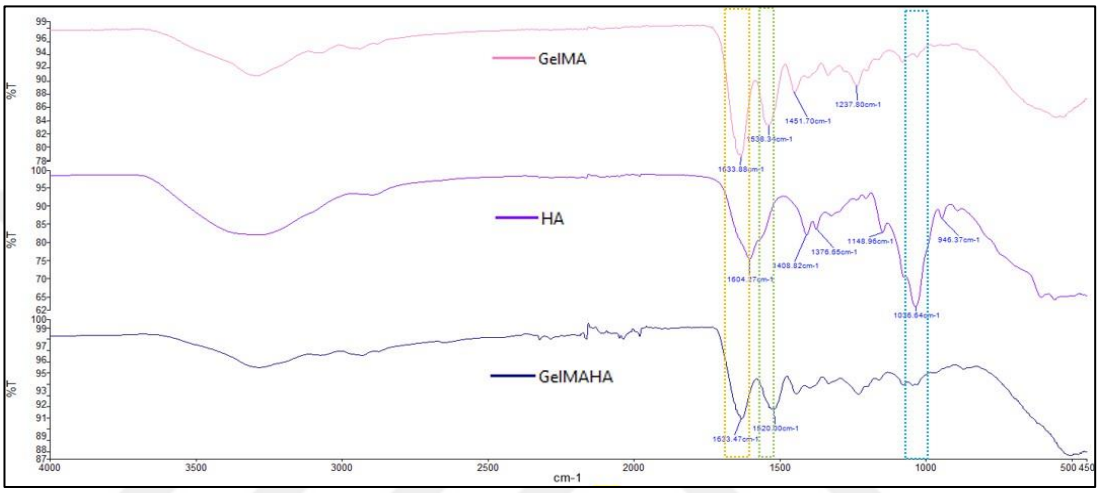

Figure 18 FT-IR spectra of GelMA, HA and GelMA-HA

These bands also indicate the presence of carboxylic acid groups in HA. Peaks corresponding to amide I and II bonds were present in both the GelMA and GelMA-HA spectra, confirming the successful incorporation of HA into GelMA.

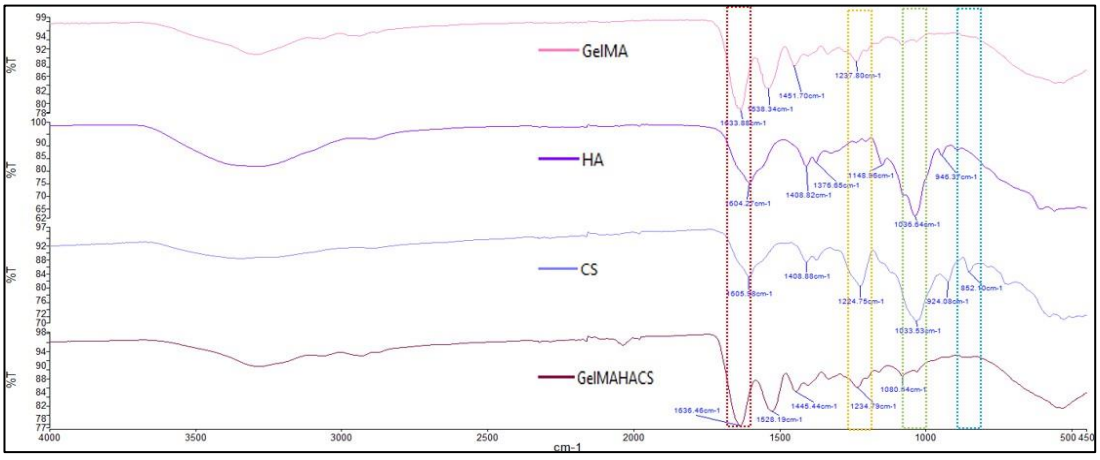

Figure 19 FT-IR spectra of GelMA, HA, CS and GelMA-HA-CS

The FT-IR spectra of chondroitin sulfate (CS) exhibits peaks associated with sulfate groups, such as asymmetric S=O stretching observed at 1230–1260 cm^{-1} and C–O–S vibrations at 810–850 cm^{-1}. Peaks corresponding to carboxylic acid groups (C=O stretching) are observed at 1610–1650 cm^{-1}, confirming the presence of carboxyl functional groups. Glucosidic bonds (C–O–C stretching) appear at 1030–1070 cm^{-1}. These spectra indicated the incorporation of CS and HA into GelMA.

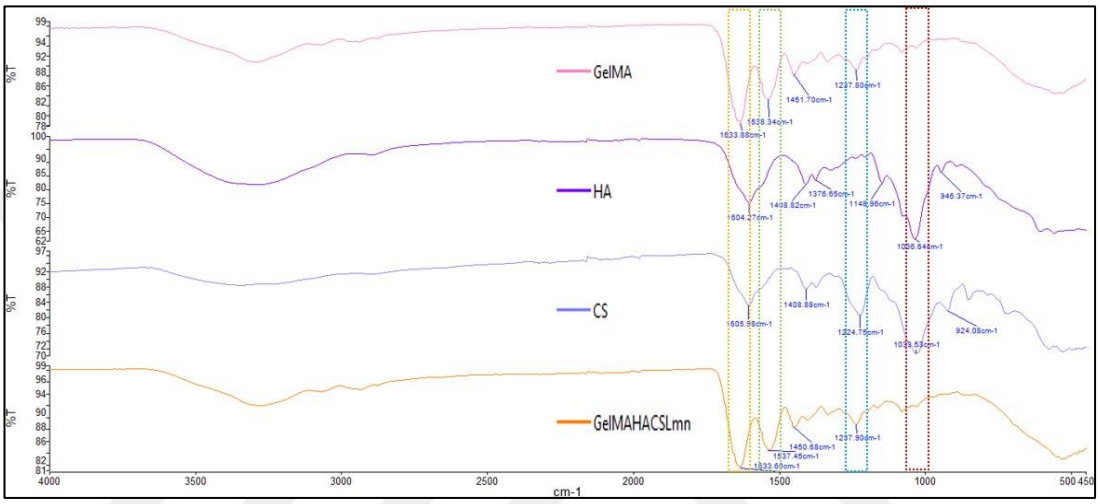

Figure 20. FT-IR spectra of GelMA, HA, CS and GelMA-HA-CS-Lmn

In the FTIR spectra of laminin, the Amide I band (1600–1700 cm^{-1}), Amide II band (1500–1600 cm^{-1}) and the Amide III band (1200–1300 cm^{-1}) prove the presence of laminin in the final construct.

These results validate the successful incorporation of hyaluronic acid, chondroitin sulfate and laminin into GelMA.

4.2.2 Determination of equilibrium water content (EWC)

The EWC of GelMA, GelMA-HA, GelMA-HA-CS, and GelMA-HA-CS-Lmn hydrogels, prepared with the following compositions 30, 30:1, 30:1:1, and 30:1:1:0.2, respectively, were determined using the equation provided in Section 3.2.3.2.

The results of the EWC measurements were GelMA 85.48%, GelMA-HA 89.31%, GelMA-HA-CS 87.63%, and GelMA-HA-CS-Lmn 88.70%. These indicate that the addition of HA, CS, and laminin to the GelMA base hydrogel did not result in changes in the water contents either due to similarity in the molecules or their amounts in the final mixtures are insignificant, with GelMA-HA achieving the highest water retention.

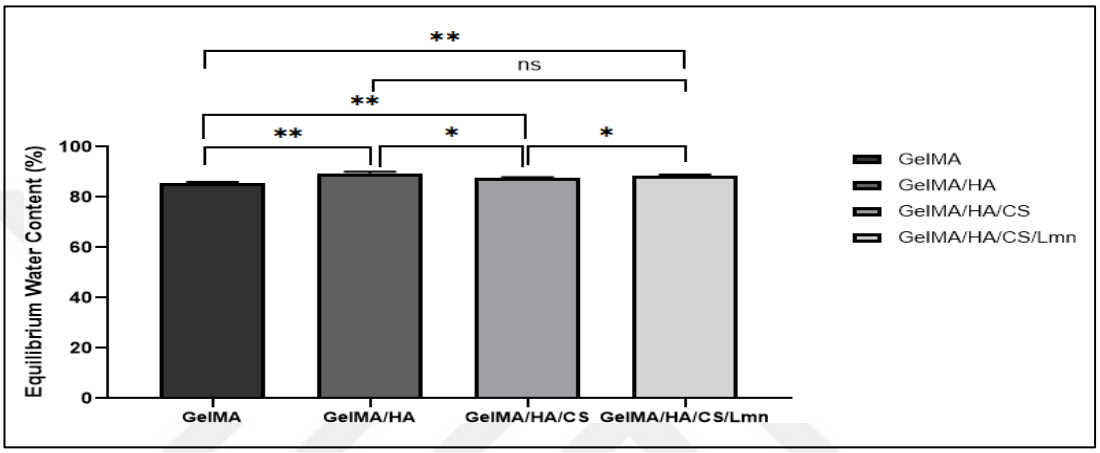

Figure 21. Equilibrium Water Content (EWC) (%) of GelMA, GelMA-HA, GelMA-HA-CS and GelMA-HA-CS-Lmn at the following compositions (30, 30:1, 30:1:1, and 30:1:1:0.2 in PBS). (n=3, ns: not significant, * : $p < 0.05$ and ** : $p < 0.01$)

4.2.3 *In Situ* degradation of hydrogel

Weight loss data obtained as a result of the 21 day degradation test are presented in Figure 22. The hydrogels were incubated in PBS to determine their degradation profiles over time. After 21 days, the weight loss of each hydrogel was measured and were found to be around 10% for all. GelMA exhibited a weight loss of 10.06%, GelMA-HA 9.29%, GelMA-HA-CS 10.02%, and GelMA-HA-CS-Lmn 8.57%. These results indicate that the addition of HA, CS and Lmn at the low amounts did not significantly change the weight loss, while the inclusion of laminin (Lmn) apparently enhanced the hydrogel's structural stability. The degradation rates suggest that increasing the structural complexity of the hydrogels did not lead to changes in degradation. The EWC data show that the model that will be created with these compositions will be unchanged during the testing period and will therefore reliable in this sense.

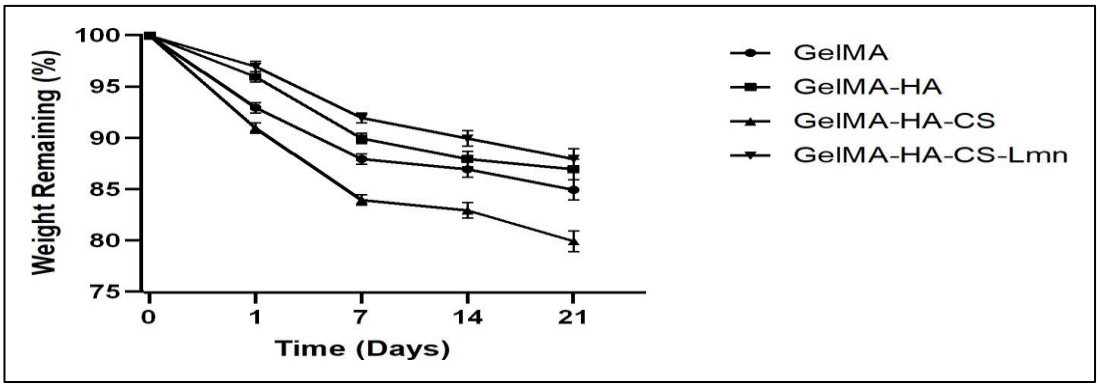

Figure 22. Degradation behavior of GelMA, GelMA-HA, GelMA-HA-CS and GelMA-HA-CS-Lmn hydrogels 21 days in PBS at room temperature.

4.2.4 Enzymatic degradation

GelMA, GelMA-HA, GelMA-HA-CS, and GelMA-HA-CS-Lmn hydrogels were also subjected to enzymatic degradation using collagenase type II at concentrations of 5 U/mL, 10 U/mL, 15 U/mL, and 20 U/mL for a duration of 2 h in order to accelerate the degradation test. Degradation was determined at both the first and second hours of incubation.

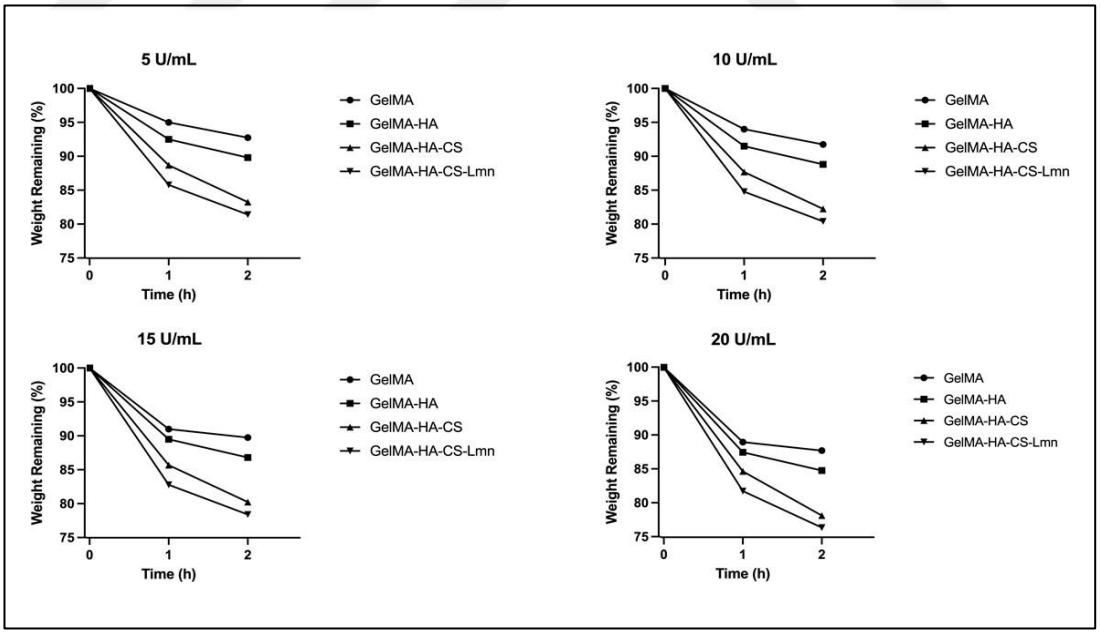

Figure 23. Degradation of the hydrogels with collagenase: Weight remaining in GelMA, GelMA-HA, GelMA-HA-CS and GelMA-HA-CS-Lmn hydrogels in four different collagenase type II solutions with different concentrations (5 U/mL, 10 U/mL, 15 U/mL and 20 U/mL).

The results demonstrated as the concentration of collagenase type II increased, the rate of degradation for all hydrogel groups also increased in a very small extent. Among the hydrogel types, GelMA-HA-CS-Lmn exhibited the highest rate of degradation, while the pure GelMA hydrogel showed the lowest.

Table 3. Remaining weight of GelMA, GelMA-HA, GelMA-HA-CS, and GelMA-HA- CS-Lmn hydrogels after incubation in collagenase type II (5–20 U/mL) for 2 h.

	5 U/mL	**10 U/mL**	**15 U/mL**	**20 U/mL**
GelMA	94%	93%	91%	89%
GelMA-HA	92%	90%	88%	85%
GelMA-HA-CS	83%	83%	81%	78%
GelMA-HA-CS-Lmn	81%	81%	79%	76%

4.2.5 Mechanical properties

Compression tests were conducted on GelMA, GelMA-HA, GelMA-HA-CS, and GelMA-HA-CS-Lmn hydrogels on days 1, 7, and 14 to determine their mechanical properties after incubation in PBS containing 0.2% sodium azide.

The Young's modulus values for day 1 were 101.55, 113.65, 129.44, and 131.15 kPa, respectively in the given complexity of composition sequence (Figure 24 and Table 4). These indicate that the addition of each component (HA, CS, and Lmn) to GelMA resulted in a progressive increase in the Young's modulus. Slopes indicate the Young's moduli of an individual composition.

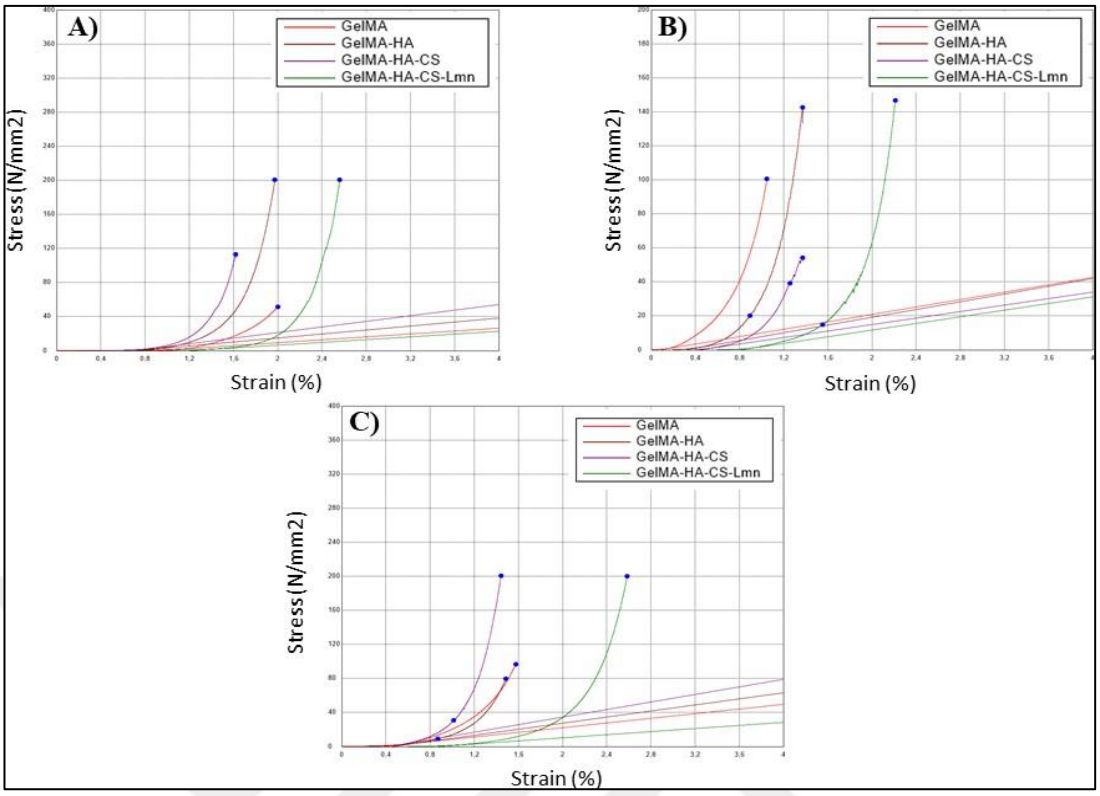

Figure 24. Stress- Strain curves of compression tests of GelMA, GelMA-HA, GelMA-HA-CS and GelMA-HA-CS-Lmn hydrogels days A)1, B)7 and C)14 in PBS containing 0.2% sodium azide.

On day 7, the measured Young's modulus values were 116.21, 124.26, 140.02, and 146.69 kPa, respectively, showing an increase. Day 14 showed a higher Young's moduli for each even though they gradually degraded as the duration of incubation in dH_2O increased (Table 4).

Table 4. Young's Modulus of GelMA, GelMA-HA, GelMA-HA-CS and GelMA- HA-CS-Lmn hydrogels obtained in compression tests.

	TIME (Days)		
Slabs	**1**	**7**	**14**
GelMA	101±12 kPa	116±13 kPa	125±15 kPa
GelMA/HA	113±10 kPa	124±10 kPa	133±17 kPa
GelMA/HA/CS	129±14 kPa	140±13 kPa	149±16 kPa
GelMA/HA/CS/Lmn	131±13 kPa	146±14 kPa	156±12 kPa

4.2.6 Rheological examination

Rheological characterization revealed that all hydrogel samples exhibited shear-thinning behavior, with viscosity decreasing as the shear rate increased from 1 to 1000 s^{-1}. This property, shown in Figure 25, supports their suitability for use as bioinks in FDM (Fused Deposition Modelling). The viscoelastic properties of the hydrogels were frequency-dependent, with both storage modulus (G') and loss modulus (G") increasing with frequency across all samples. The elastic modulus (G') of each hydrogel was significantly higher than its viscous modulus (G"), as indicated by tan δ values less than 1, confirming the dominance of gel-like behavior before crosslinking. Among the hydrogel groups, the addition of HA to GelMA led to an increase in viscous modulus (G"), reflecting the influence of HA on the hydrogel's viscoelastic properties. However, the subsequent addition of CS to GelMA-HA did not result in a significant difference in either G' or G". Notably, the incorporation of Lmn into GelMA-HA-CS led to an increase in elastic modulus (G') while causing a decrease in viscous modulus (G"), indicating a more pronounced gel- like behavior and enhanced structural stability.

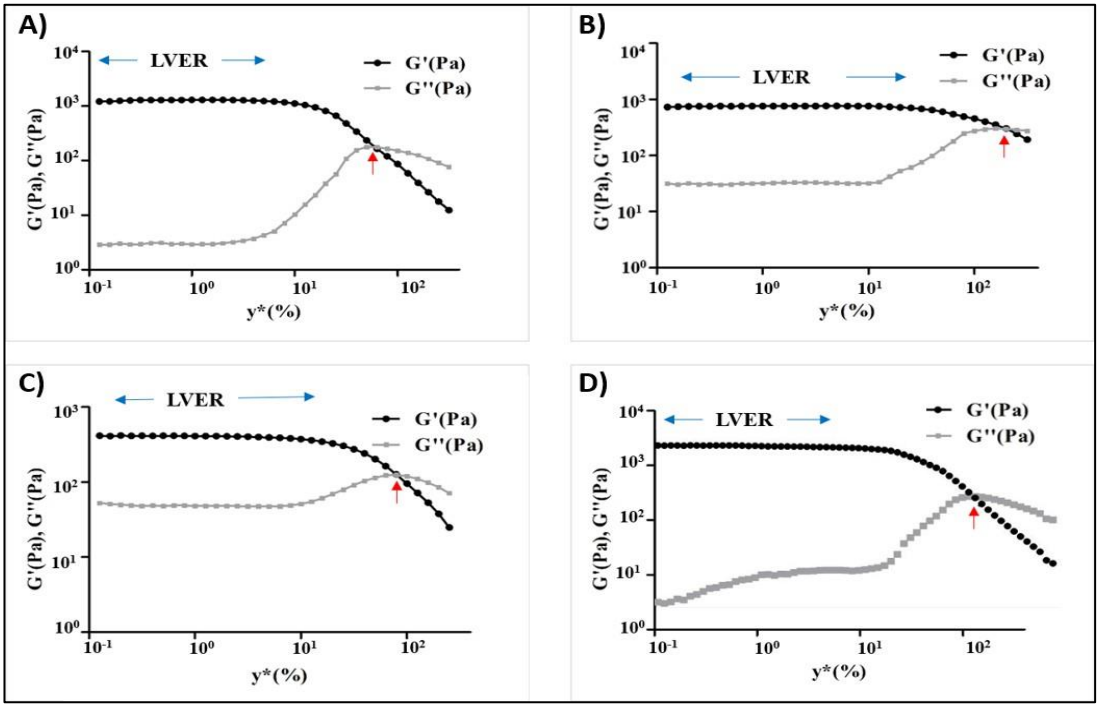

Figure 25. Viscoelastic modulus of A) GelMA B) GelMA-HA C) GelMA-HA-CS and D) GelMA-HA-CS-Lmn.

These results demonstrate that the inclusion of HA and Lmn influences the viscoelastic properties of the hydrogels, with Lmn providing the most robust viscoelastic profile. This makes GelMA-HA-CS-Lmn a promising candidate for tissue engineering applications requiring mechanically stable and supportive scaffolds. Overall, the rheological data provide valuable insights into the suitability of these hydrogels for extrusion-based bioprinting and their potential for maintaining structural integrity during the regenerative process.

4.2.7 Morphological analysis

SEM imaging was utilized to investigate the microstructural differences among GelMA, GelMA-HA, GelMA-HA-CS, and GelMA-HA-CS-Lmn hydrogels at various magnifications (200X, 500X, and 1000X).

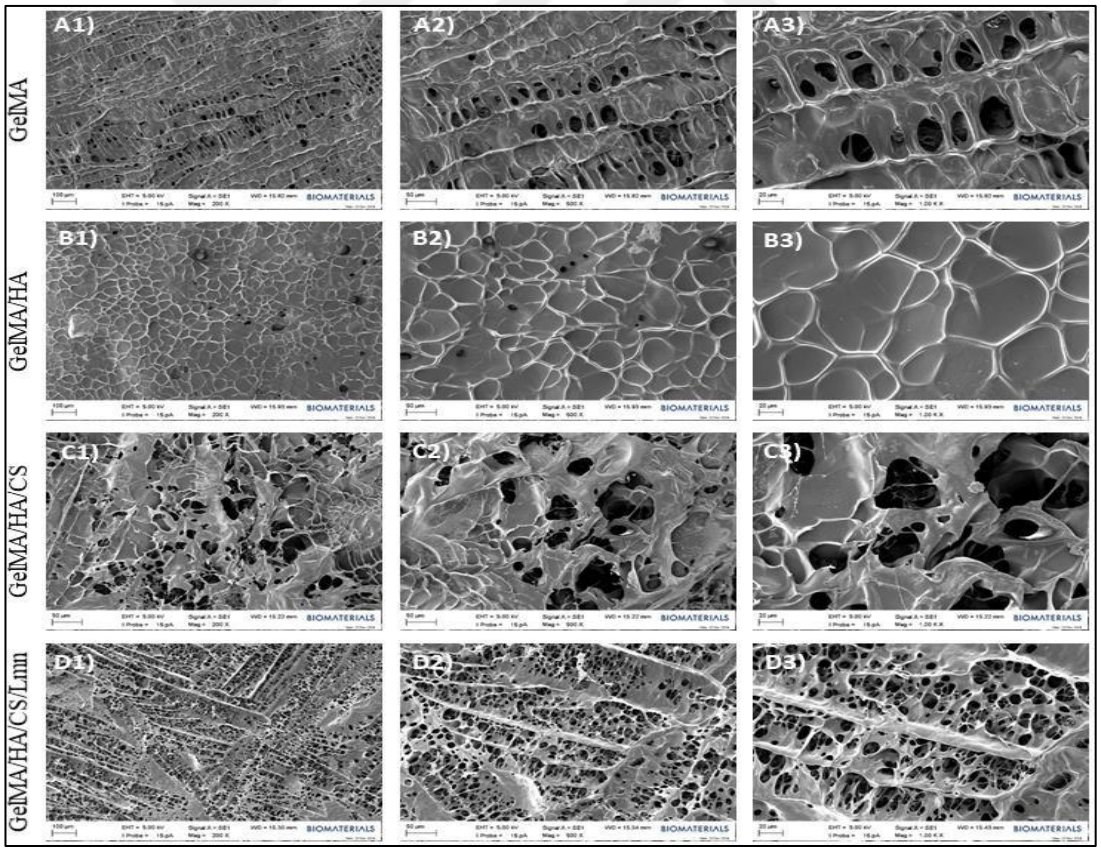

Figure 26. SEM images of the slab of the 4 hydrogels used in the study. (A) GelMA, (B) GelMA-HA, (C) GelMA-HA-CS, and (D) GelMA-HA-CS-Lmn hydrogels at three different magnifications: (1) 200X, scale bar: 100 μm; (2) 500X, scale bar: 50 μm; and (3) 1000X, scale bar: 10 μm.

The results revealed that there were differences in the porous architecture with the addition of other components to the GelMA hydrogel. The SEM images of pure GelMA hydrogel (Figures A) exhibited a highly porous structure, characterized by large, interconnected pores. This structure is favorable for facilitating nutrient and oxygen diffusion, as well as cell infiltration. However, upon incorporation of HA into the GelMA matrix (Figures B), the porous structure was largely diminished. The GelMA-HA hydrogel appeared denser and more compact, indicating that HA contributes to the reduction of porosity, possibly due to its ability to form tighter networks through increased hydrogen bonding. However, it should not be forgotten that the EWC of all the hydrogels are around 85%. Therefore, this dry form does not represent the real wet swollen state.

When CS was added to the GelMA-HA hydrogel, a significant change in the microstructure was observed (Figures C). The GelMA-HA-CS hydrogel displayed the reappearance of a porous architecture; however, the pore size distribution is broad.

The addition of Lmn, a glycoprotein, to the GelMA-HA-CS hydrogel (Figures D) resulted in a highly organized and densely packed porous structure. The GelMA-HA-CS-Lmn hydrogel exhibited small, uniform, and evenly distributed pores, indicative of improved structural regularity and stability. It is interesting that a ratio of 30-to-0.01 for GelMA and Lmn could still influence a 1/3000 contribution of Lmn. In conclusion, incorporation of HA, CS, and Lmn into the GelMA matrix significantly altered the hydrogel's dry microstructure. The wet microstructure is the important state in 3D printed scaffolds and the cell numbers will probably affected much less.

4.3 3D Printing of Hydrogels

4.3.1 Fabrication of 3D bioprinted hydrogels

In this study, a three-dimensional model was prepared to mimic the spinal cord. The primary goal was to a lateral section of the spinal cord, which consists of gray and white matter regions.

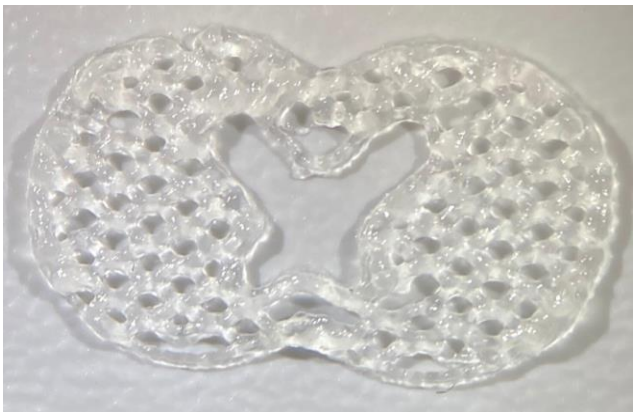

Figure 27. 3D model of spinal cord showing channels to mimic tracts of the white matter region.

The GelMA-HA-CS-Laminin (Lmn) hydrogel was fabricated using an EnvisionTEC 3D bioprinter, GelMA-HA-CS-Lmn solution (3 mL) was loaded into the bioprinter cartridge, and the cartridge was kept at temperature +18 °C for 20 min. The cartridge and chiller temperatures: +18 °C, the needle offset 0.160 mm, extrusion pressure 1.1 bar, the printing speed 20.0 mm/s, pre-flow duration 0.09 s. Continuous strand printing was employed, with a contour distance of 0.05 mm, strand-to-strand spacing 0.60 mm, and a build contour was applied. Post-printing, the hydrogel was crosslinked with UV with 1.30 min for each side.

4.3.2 Characterization of GelMA/HA/CS/Lmn 3D printed hydrogels

4.3.2.1 Determination of equilibrium water content (EWC)

The equilibrium water contents (EWC) of GelMA-HA-CS-Lmn in slab and 3D printed form were calculated according to Section 3.2.3.2.

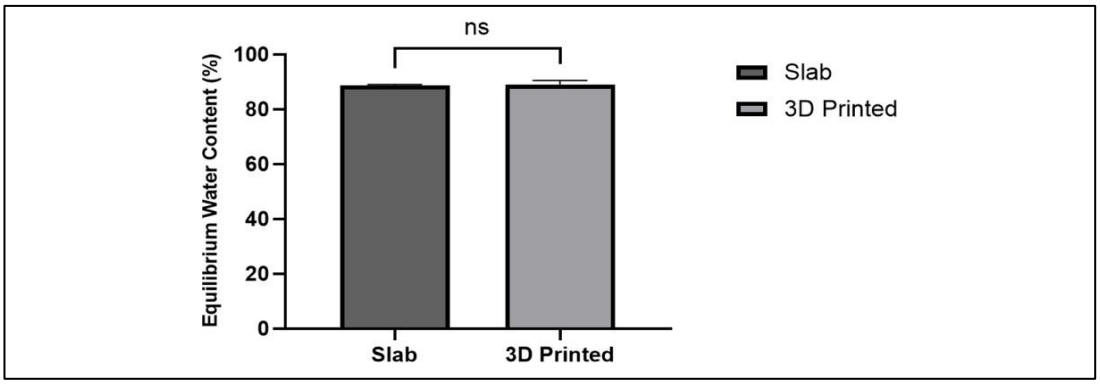

Figure 28. Equilibrium Water Contents (%) of slabs and 3D printed form of GelMA-HA-CS-Lmn. (n=3, ns: not significant)

For the slab configuration, which was designed to mimic the properties of gray matter, an EWC of 88.69% was obtained. The 3D printed hydrogel, tailored for white matter applications, demonstrated very similar EWC of 89.01%.

4.3.2.2 Degradation of 3D printed hydrogels

The degradation profiles of the GelMA-HA-CS-Lmn hydrogel were obtained after a 21 day degradation test for both its slab and 3D-printed forms. For the slab configuration, the weight loss in PBS was 8.57%, consistent with the previous data. However, the 3D-printed form exhibited a significantly lower weight loss of 6.73% compared to each other at the end of the 21-day period. This difference is not important as both are very small degradation results.

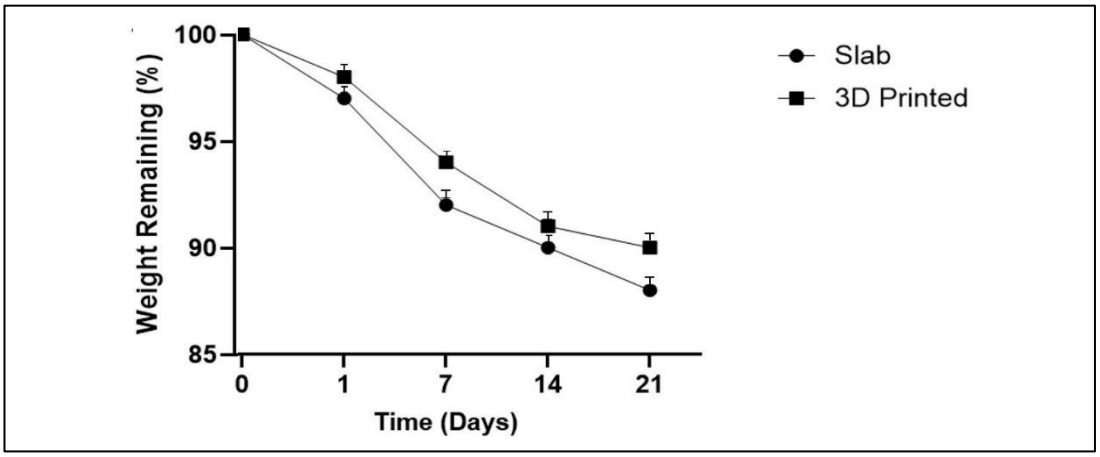

Figure 29. Degradation rates of the GelMA-HA-CS-Lmn slab and 3D Printed hydrogels in PBS (n=3).

4.3.2.3 Enzymatic degradation

GelMA-HA-CS-Lmn hydrogels in both slab and 3D printed forms were subjected to enzymatic degradation tests using collagenase type II at concentrations of 5 U/mL, 10 U/mL, 15 U/mL, and 20 U/mL for a duration of 2 h. Degradation was calculated at the end of 1h and 2h. Similar to previous findings, an increase in collagenase concentration led to a corresponding increase in the rate of degradation for both hydrogel forms.

In the slab form, a weight loss of around 30% was observed after 2 h of incubation in an enzymatic environment indicating a similar degradation rate.

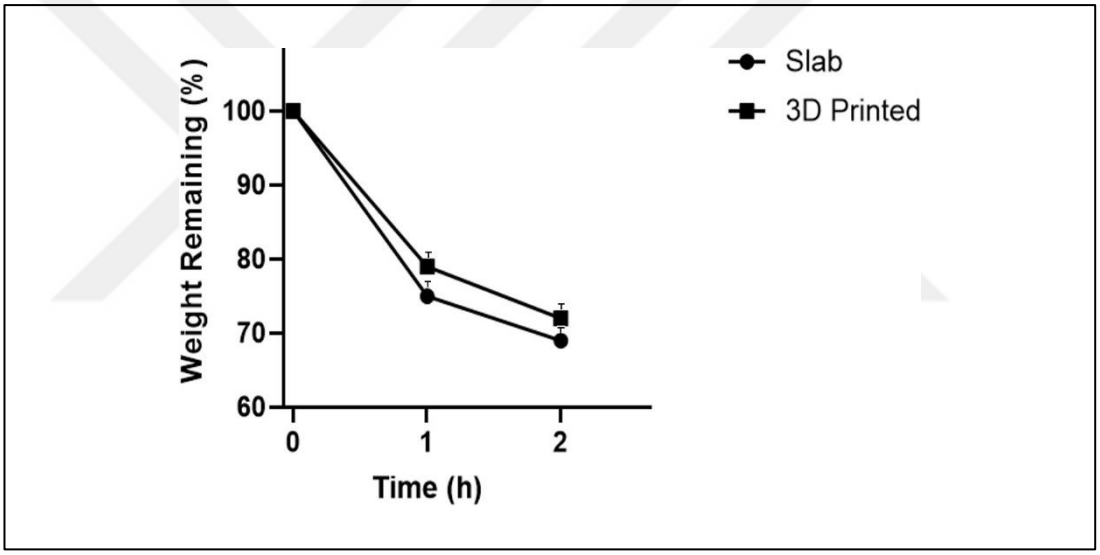

Figure 30. Weight remaining percent in GelMA-HA-CS-Lmn slab and 3D-printed hydrogels after enzymatic degradation using four different concentrations of collagenase type II (20 U/mL) (n=3).

4.3.2.4 Mechanical properties

Compression tests were conducted on GelMA-HA-CS-Lmn hydrogels in both slab and 3D printed forms to evaluate their mechanical properties on day 1. The results showed that the Young's modulus for the slab hydrogel was calculated as 131±13 kPa, while the 3D printed hydrogel exhibited almost identical Young's modulus of 145±11

kPa. The higher Young's modulus in the 3D printed form suggests improved mechanical stability.

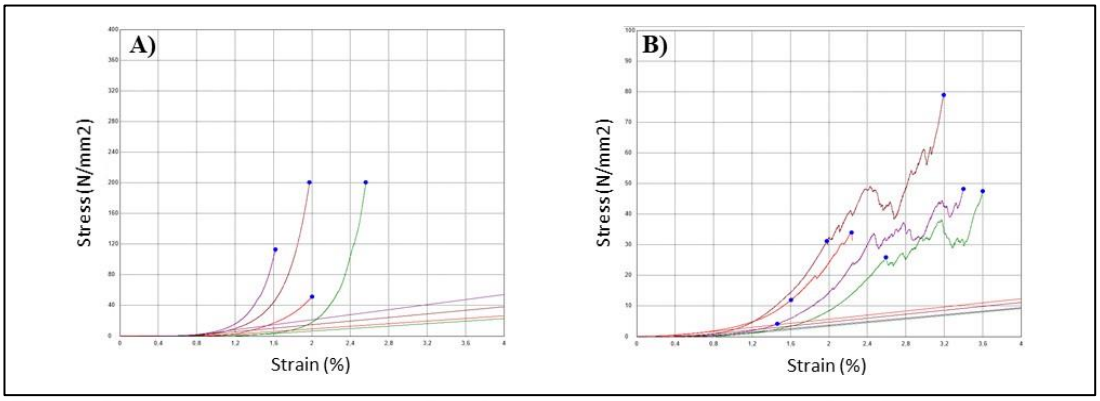

Figure 31. Stress- Strain curves of compression test of GelMA-HA-CS-Lmn. A) slab and B) 3D printed hydrogels in PBS containing 0.2% sodium azide.

4.3.2.5 Morphological analysis

SEM imaging was employed to investigate the microstructural features of GelMA- HA-CS-Lmn hydrogels in both slab and 3D-printed forms at various magnifications (500X, and 1000X). The results demonstrated that both forms exhibited a similar microporous structure, indicative of interconnected porous network.

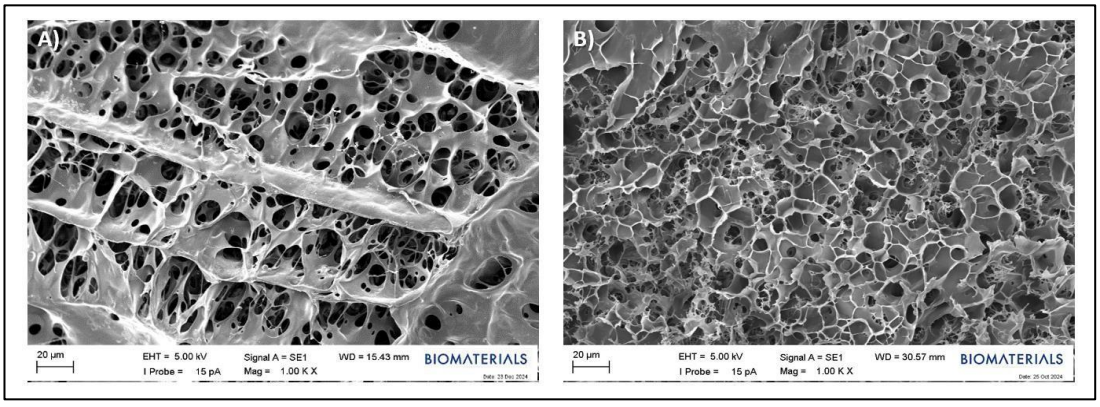

Figure 32. SEM images of the GelMA-HA-CS-Lmn. (A) slab and (B) 3D printed hydrogel magnification 1000 X.

Additionally, in the 3DP samples, honeycomb shaped channels were observed, specifically designed to mimic the structural organization of spinal cord tracts. These channels had diameters smaller than 450 μm, in agreement with dimensions reported to support axonal extension and regeneration. These findings suggest that the 3D printing process allows for the precise fabrication of hydrogels with microarchitectural features that are crucial for applications in spinal cord tissue engineering.

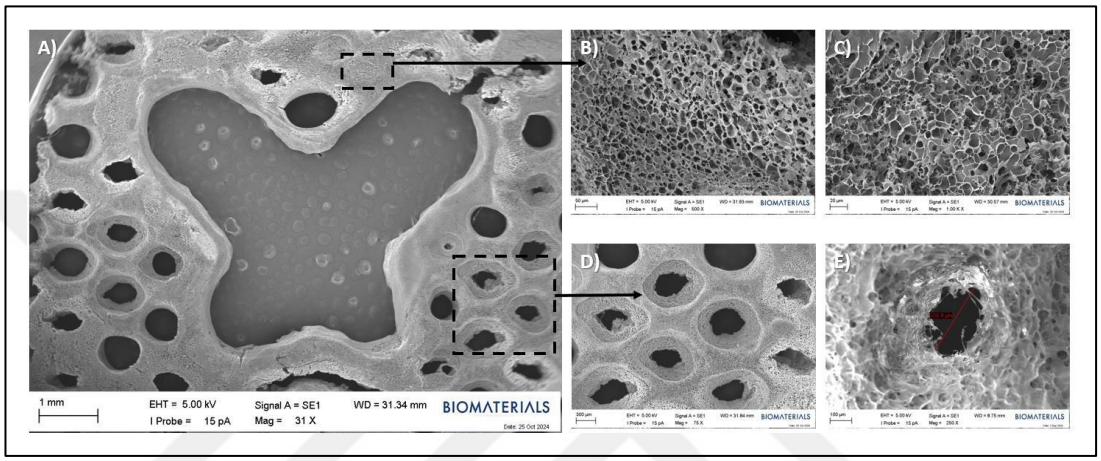

Figure 33. SEM images of the GelMA-HA-CS-Lmn 3D printed hydrogels. (A) top-view 31X. Microporous bulk: (B) 500 X, (C) 1000 X. Channels (D) 75X and (E) 250X.

4.3.3 *In Vitro* studies

4.3.3.1 Culture of SVG p12 cells

Morphological analysis of the cultured SVG p12 cells revealed that their morphology was consistent with descriptions in the literature, confirming that the cells maintained their expected structural characteristics under the applied culture conditions. This morphological consistency underscores the reliability of the culture protocol and the suitability of the experimental setup for further investigations.

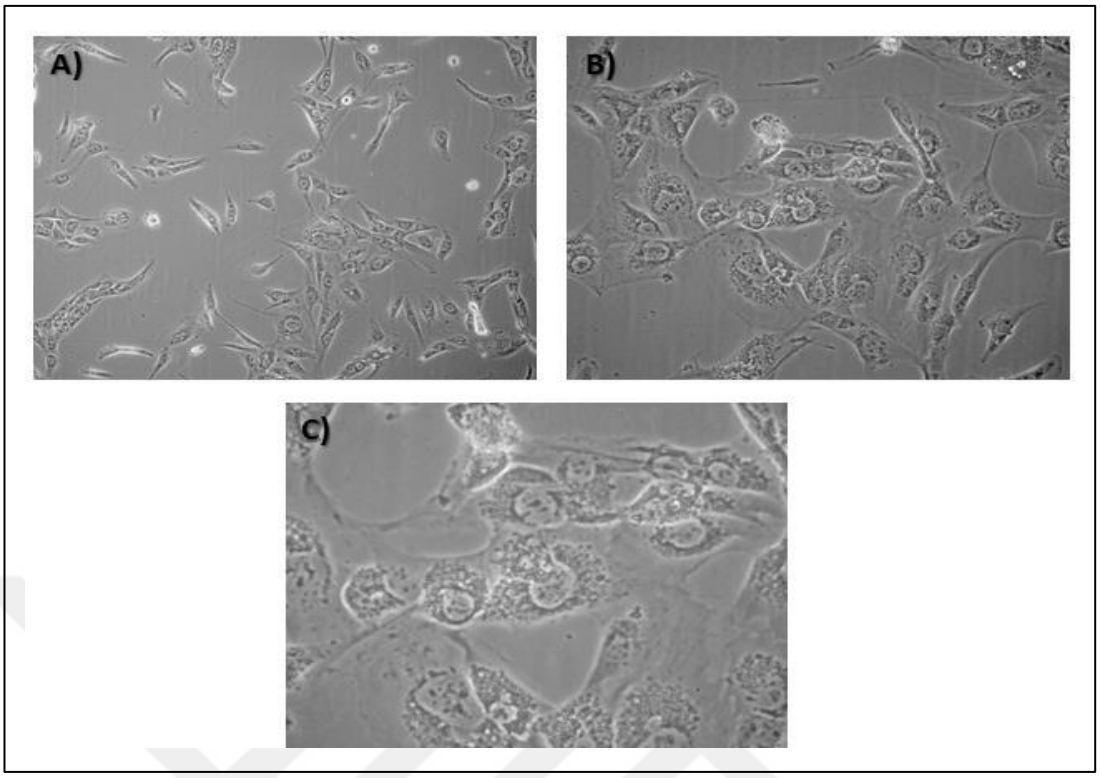

Figure 34. Light microscope images of SVG p12 cells on TCPs at different magnifications: (A) 10X, (B) 20X, and (C) 40X.

4.3.3.2 Culture of PC 12 cells

PC 12 Cells grown on fibronectin coated TCPs in the presence of NGF demonstrated a notable tendency to extend, forming longer and more prominent cell projections. This suggests that the fibronectin coating, combined with NGF, promotes cellular extension. In contrast, cells cultured on uncoated TCPs, whether with or without NGF, exhibited less pronounced extension, indicating the importance of both substrate coating and NGF in facilitating cell outgrowth.

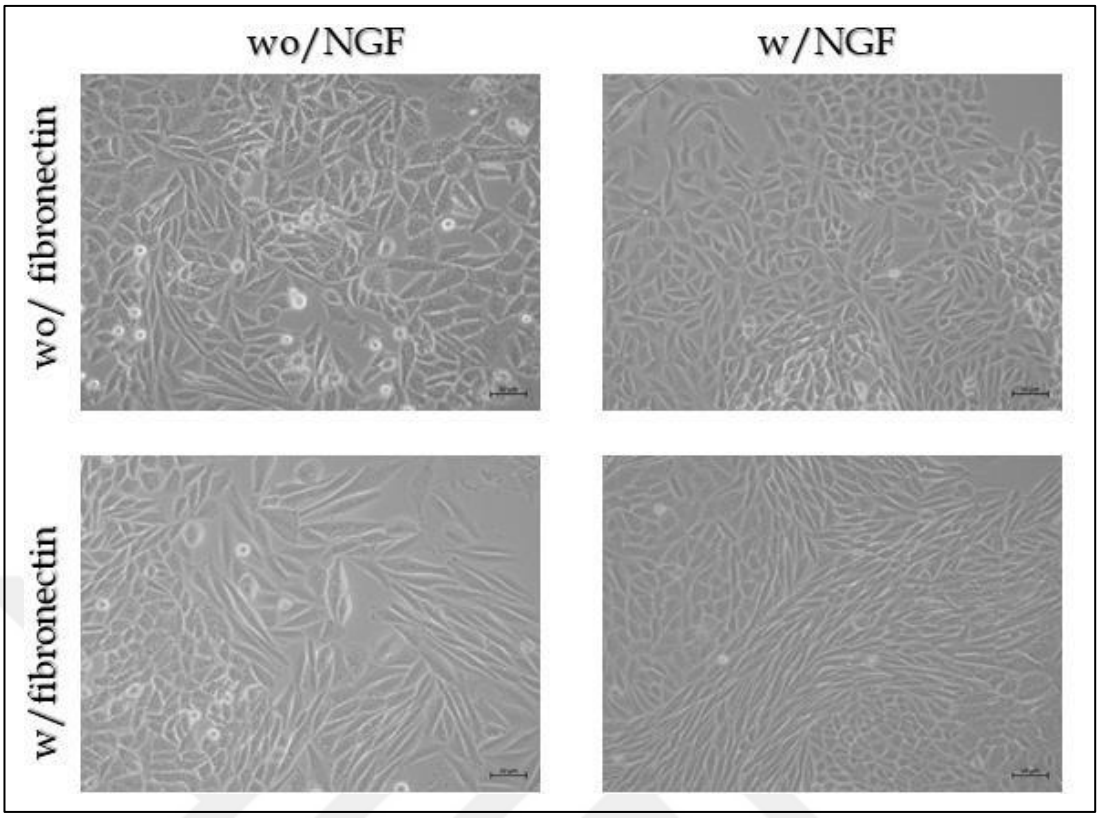

Figure 35. Light microscopy images of PC 12 cells under different culture conditions: in the absence and presence of fibronectin, in the absence and presence of NGF (20X magnification)

4.3.4 Cell response and functional evaluation of 3D bioprinted hydrogel

4.3.4.1 Preparation of cell loaded hydrogels

For the fabrication of cell-laden 3D scaffolds initially the hydrogel composition consisting of GelMA, HA, CS, and Laminin (15:1:1:0.2) was prepared under sterile conditions. The hydrogel solution was homogenized using gentle stirring and subjected to UV sterilization. Subsequently, printing parameters such as extrusion pressure, printing speed, nozzle diameter, and temperature were optimized to preserve cell viability during the printing process. Given that shear stress during extrusion can negatively impact cell health, a balance between print fidelity and cell survival was achieved by adjusting the nozzle diameter and extrusion speed accordingly. The temperature of the printing chamber and print bed was controlled allowing for immediate gelation post-printing. To further optimize the internal architecture, various

infill patterns and pore sizes were evaluated, aiming to enhance nutrient diffusion and promote neuronal attachment and axon extension. The bioprinting process was conducted under sterile conditions within a biosafety cabinet, and all printed constructs were immediately transferred into cell culture media cell survival and proliferation. Overall, these preparation steps ensured the creation of viable, structurally stable, and biologically relevant 3D hydrogel scaffolds suitable for *in vitro* neuronal studies.

4.3.4.2 Cell proliferation with alamar blue assay

Alamar Blue assays on 3D printed SVG p12 cells and slab PC 12 cell cultures were performed to evaluate cell proliferation. The assays were conducted on Days 1, 7, and 14, with three replicates for each condition (n=5). The percentage of reduced resazurin was calculated using the equation provided in Section 3.2.4.5.1, and the results were plotted (Figure 36).

During the 21 days of culture, the cells exhibited linear growth. The results indicated that the cells were able to proliferate within both the 3D printed hydrogel structure and the slab with the rate with SVG p12 being higher.

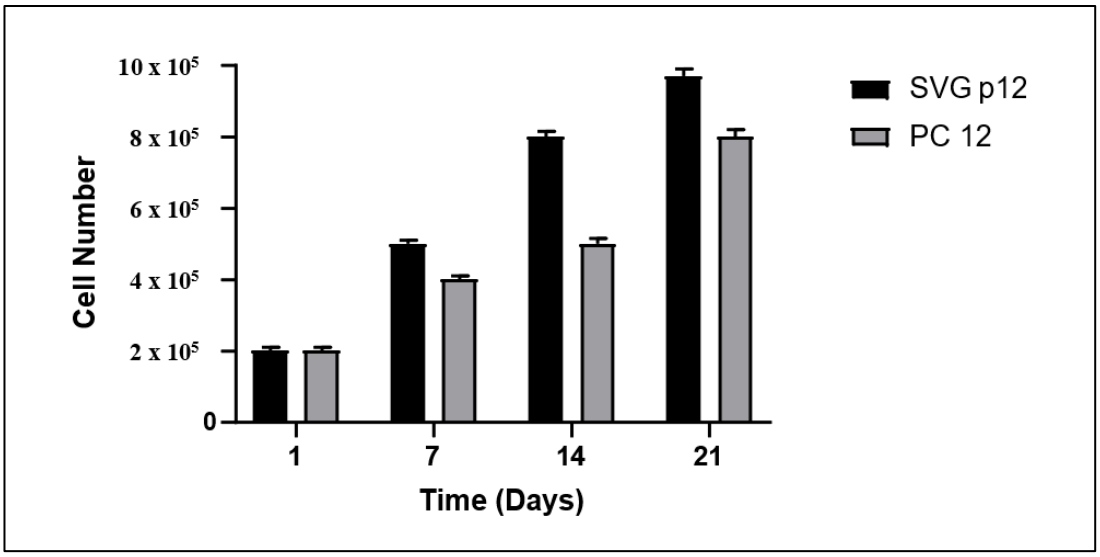

Figure 36. Alamar Blue cell proliferation assay of SVG p12 (black) and PC 12 (grey) cells in 3D bioprinted hydrogel and slab.

While SVG p12 cells were cultured within the 3D bioprinted hydrogel construct, PC12 cells were cultured separately in the slab form of the same hydrogel. As illustrated in Figure 36, both SVG p12 and PC12 cells exhibited consistent cell proliferation over a 21-day culture. However, the proliferation rate of PC12 neuronal cells was noticeably lower compared to that of SVG p12 glial cells. This discrepancy in proliferation rates can be attributed to the distinct biological characteristics of the two cell types. Specifically, SVG p12 cells exhibit a doubling time of approximately 24 hours, whereas PC12 cells have a significantly longer doubling time of around 48–72 hours. This difference highlights the inherent variations in growth kinetics between these cell lines, contributing to the observed differences in proliferation rates. Neuronal cells, such as PC12, require extensive cell-to-cell communication and interaction for optimal proliferation. Establishing these connections is crucial, as they enable the formation of functional neural networks essential for neuronal survival.

Neuronal cells are inherently sensitive and rely heavily on environmental cues provided by their surrounding microenvironment. In the 3D hydrogel matrix, PC12 cells exhibited a delayed proliferation pattern because they required additional time to locate and interact with neighboring cells (147). This delay can be explained by the necessity for axonal and dendritic extensions, which facilitate intercellular communication. In contrast, SVG p12 glial cells are more robust and adaptable, enabling them to proliferate more rapidly without the same level of dependency on direct cell-to-cell contact. The glial cells' ability to provide supportive functions, such as trophic factor secretion and extracellular matrix remodeling, may have further contributed to their enhanced proliferation (148).

Moreover, the architectural features of the 3D bioprinted hydrogel played a critical role in influencing cellular behavior. The hydrogel’s porosity, pore size, and interconnected channel structures significantly impacted nutrient diffusion, waste removal, and cellular migration. For neuronal cells, these structural properties are particularly important as they facilitate directional growth and alignment necessary for neural tissue formation. The observed lower proliferation of PC12 cells suggests that the current hydrogel design could be further optimized to enhance neuronal axon like

extensions. Adjustments in pore size, incorporation of guidance cues, or the addition of bioactive molecules such as neurotrophic factors could accelerate neuronal network formation and improve proliferation outcomes.

Additionally, the mechanical properties of the hydrogel, such as stiffness and elasticity, may have influenced cell proliferation. Neuronal cells are highly mechanosensitive, responding to substrate stiffness by altering their growth and differentiation patterns. The hydrogel's mechanical profile may have been more conducive to glial proliferation while presenting a less favorable environment for neuronal cell growth. Future studies could explore tuning the mechanical properties of the hydrogel to better match the native spinal cord tissue, potentially enhancing neuronal proliferation.

In conclusion, while both SVG p12 and PC12 cells demonstrated the ability to proliferate within the hydrogel system, the lower proliferation rate of PC12 cells underscores the complexity of designing scaffolds that meet the distinct needs of different neural cell types. Optimizing hydrogel architecture to promote efficient neuronal growth, tailoring mechanical properties, and integrating biochemical cues could significantly enhance neuronal proliferation and functional neural network formation. These findings highlight the critical role of scaffold design in neural tissue engineering and its implications for developing effective treatments for spinal cord injuries.

4.3.4.3 Live-dead assay for cell viability

Live-Dead assay was conducted to also determine the viability of SVG p12 and PC 12 cells encapsulated in GelMA-HA-CS-Laminin hydrogels. After 21 day culture, the hydrogels were subjected to the Live-Dead assay, as in section 3.2.7.4. Live cells retain the green fluorescent dye Calcein-AM within their cytoplasm, while dead cells permit the entry of Ethidium Homodimer-1 (EthD-1), which binds to DNA and emits red fluorescence (Figure 37, 38).

In order to determine viability of the cells extrapped in the hydrogels, live-dead assay was performed and confocal laser scanning microscopy (CLSM) was used to capture the fluorescent dyes high-resolution images of the cell-loaded hydrogels.

The Live-Dead assay performed on day one provided significant insights into the initial viability of SVG p12 glial cells and PC12 neuronal cells within the hydrogel environment. The results demonstrated that SVG p12 cells exhibited a viability rate of 81%, reflecting their robust nature and ability to adapt to the *in vitro* hydrogel environment. This high viability rate is indicative of the glial cells' inherent resilience and adaptability, allowing them to survive and function effectively within the 3D bioprinted hydrogel. SVG p12 cells are known for their supportive role in neural tissue by secreting trophic factors and remodeling the extracellular matrix, which likely contributed to their higher survival rate.

In contrast, the viability rate of PC12 neuronal cells on day one was calculated to be 79%. Although the difference between the two cell types appears minimal, it highlights the heightened sensitivity of neuronal cells to their surrounding microenvironment. Neuronal cells depend heavily on specific environmental cues, including appropriate substrate stiffness, biochemical signals, and the ability to establish functional networks through axonal and dendritic extensions. The slight reduction in viability suggests that PC12 cells faced additional challenges during the initial seeding and encapsulation processes, possibly due to the mechanical stress or lack of immediate intercellular interactions.

The observed difference in viability between the two cell types can also be linked to the hydrogel's architectural features. The porosity, pore size, and interconnected channel structures of the hydrogel play essential roles in nutrient diffusion, waste removal, and cellular migration. While these features were sufficient to support the survival of glial cells, neuronal cells may require more refined microarchitectural conditions to enhance their initial viability.

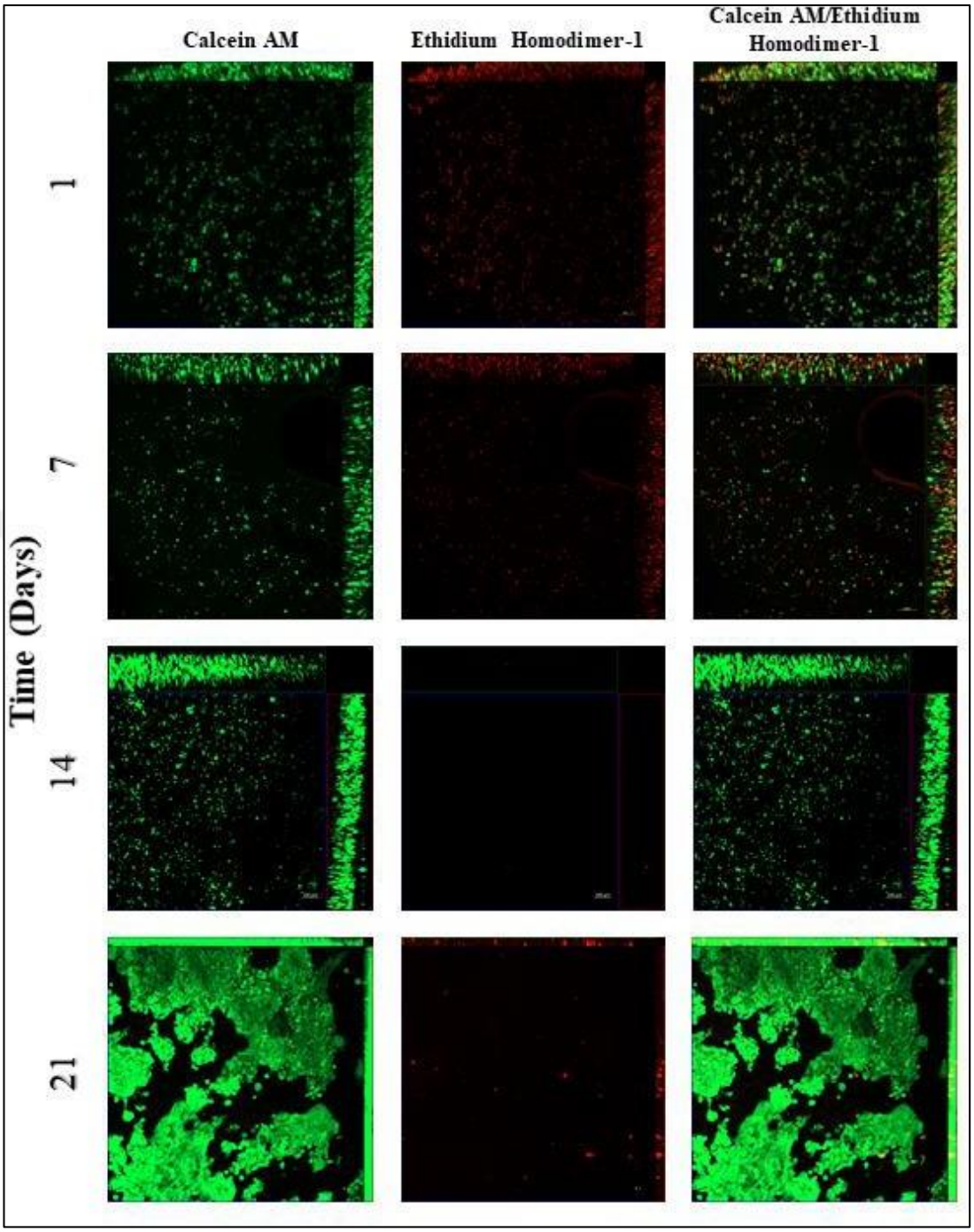

Figure 37. Live-Dead test of SVG p12 cells in 3D Bioprinted structure. Calcein AM stains live cells green, while Ethidium Homodimer-1 stains dead cells red. (scale bar: 50 μm)

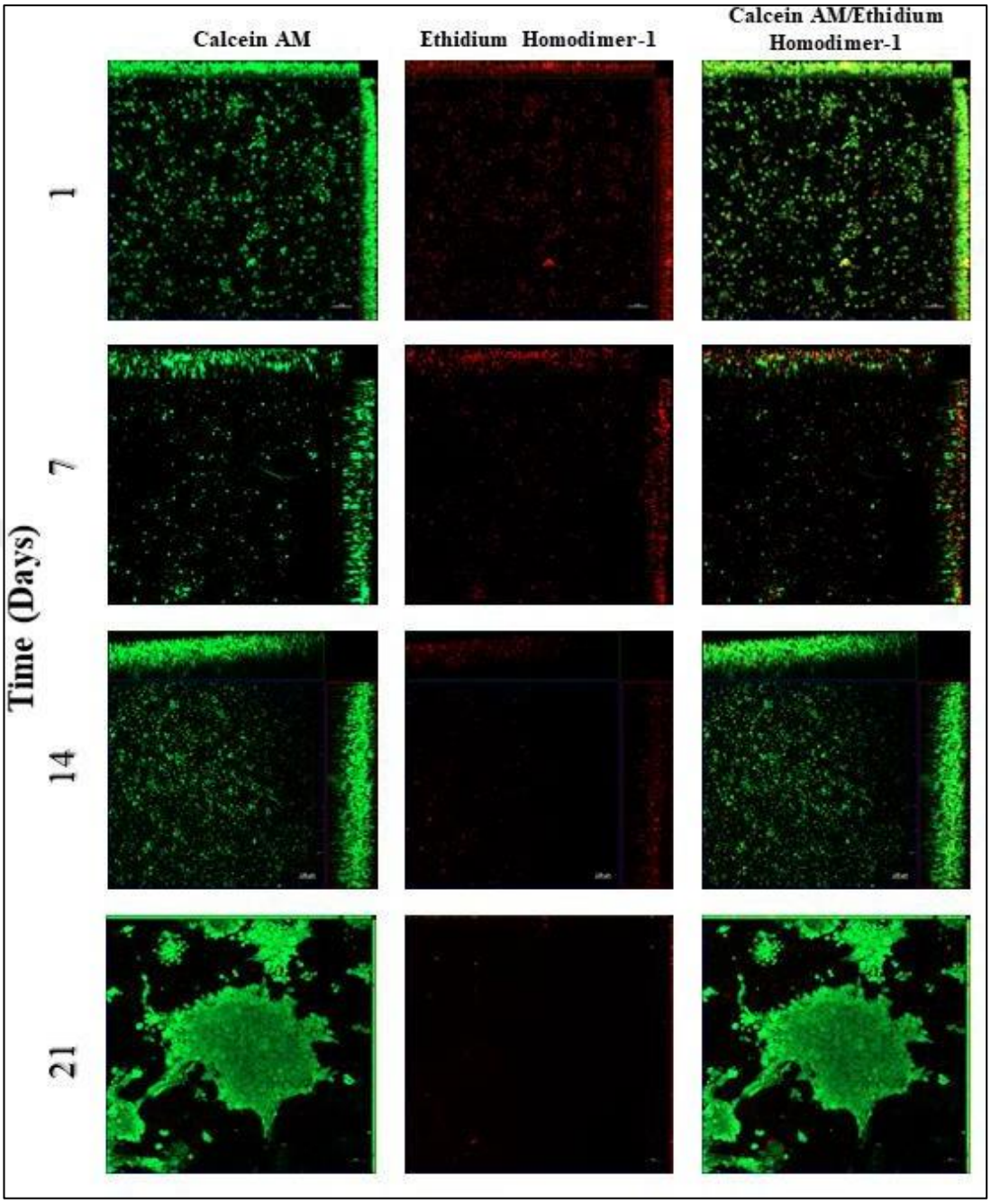

Figure 38. Live-Dead assay of PC 12 loaded in the hydrogel slab Calcein AM stains live cells green, while Ethidium Homodimer-1 stains dead cells red. (scale bar: 50 μm)

This finding suggests that further optimization of hydrogel design such as adjusting pore size, incorporating neurotrophic factors, or modifying mechanical properties could promote improved viability and functionality of neuronal cells.

The mechanical properties of the hydrogel, including its stiffness and elasticity, likely influenced the initial viability outcomes. Neuronal cells are particularly mechanosensitive and can alter their growth and differentiation in response to substrate stiffness. The current hydrogel composition may have provided a more favorable mechanical environment for glial cell survival, while presenting challenges for neuronal cell adaptation. Future research could focus on tuning these mechanical properties to better match the biomechanical characteristics of native spinal cord tissue, thereby enhancing neuronal viability and promoting neural network formation.

Furthermore, the delayed establishment of cell-to-cell interactions among PC12 cells could have contributed to their reduced viability. Neuronal cells rely on these connections for survival and differentiation, and the 3D hydrogel environment may have slowed this process. Strategies such as incorporating biochemical gradients or guidance cues could facilitate faster neuronal axonal growth, improving cell survival rates in the early stages of culture.

In conclusion, the Live-Dead assay results highlight the hydrogel's capacity to support the survival of both glial and neuronal cells, albeit with differences that reflect the unique physiological needs of each cell type. The initial viability rates of 81% for SVG p12 cells and 79% for PC12 cells underscore the importance of tailored scaffold design in neural tissue engineering. Enhancements in hydrogel architecture, mechanical properties, and biochemical cues could significantly improve the early viability of neuronal cells, contributing to more effective neural tissue regeneration and potential applications in spinal cord injury treatment.

4.3.4.4 Immunostaining

On day 21, both 3D-printed SVG p12 cells and slab-form PC 12 cells were stained with GFAP, beta III tubulin, and DAPI to evaluate neuronal extension. Confocal microscopy images were obtained and subsequently merged (Figure 39).

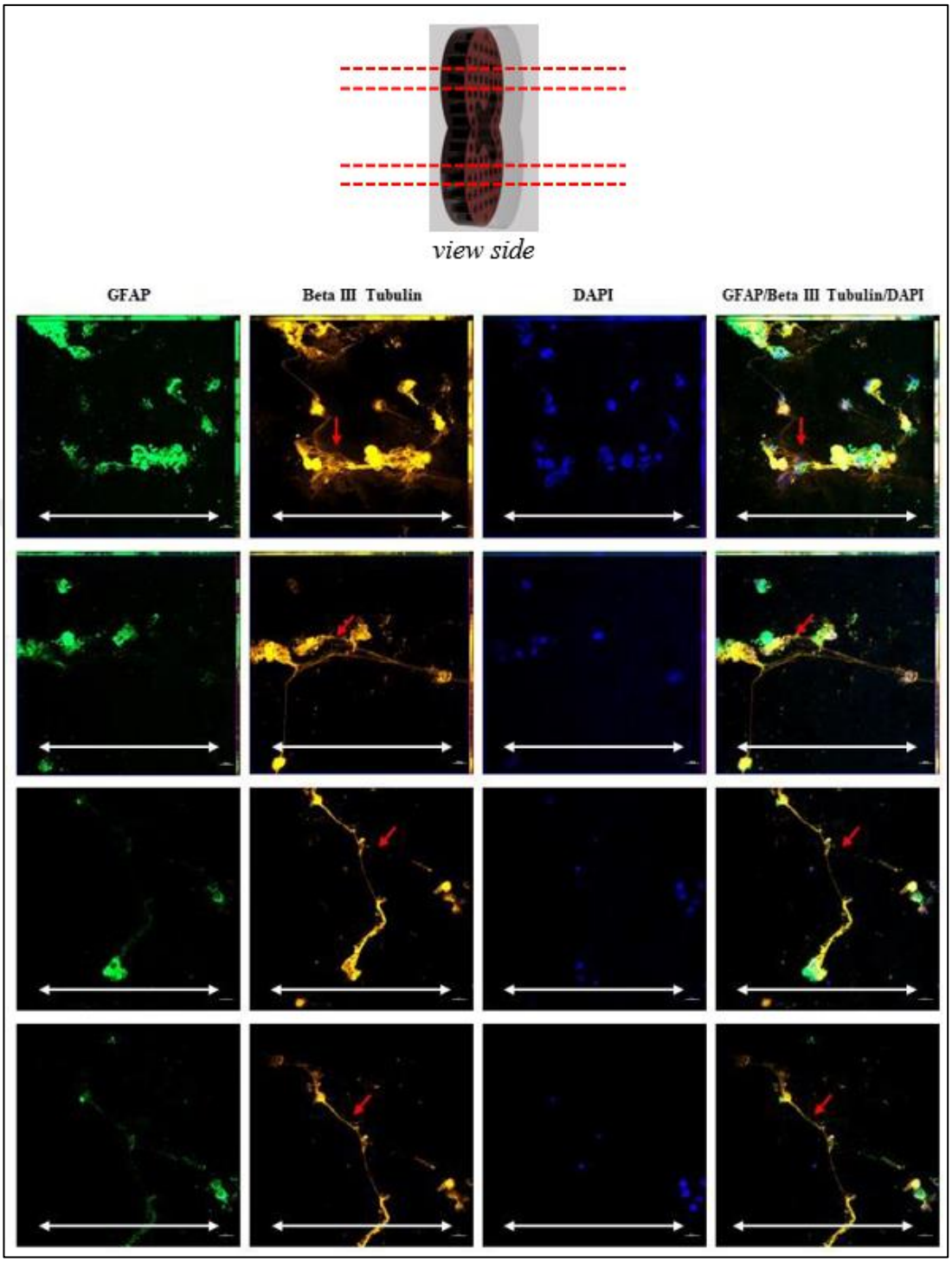

Figure 39. Merged confocal images of 3D-printed SVG p12 cells and slab-form PC 12 cells on day 21. GFAP staining (green) shows glial cells (SVG p12), Beta III tubulin staining (red) shows axonal extensions of PC 12, and DAPI staining (blue) labels cell nuclei of both. The merged images reveal axonal outgrowth in both cell types (scale bar: 20 μm). Red arrow: indicates the cell extention along the direction of channel. Two sided arrow shows the channel direction (horizontal)

The merged images revealed axon like extensions in neuronal cell types. GFAP staining (green) highlighted glial cells, while beta III tubulin staining (red) marked the presence of neuronal-like structures, particularly axons. The results indicated that PC 12 cells extended neuronal projections toward the channels of the 3D-printed structure containing SVG p12 cells, highlighting the scaffold's potential in guiding axonal growth and neuronal interactions. These findings underscore the role of the 3D printed environment in facilitating neuronal extension, providing valuable insights for tissue engineering applications aimed at neural regeneration.

Specifically, GFAP staining (green) confirmed the presence of glial cells (SVG p12), while Beta III tubulin staining (red) identified axonal extensions associated with PC12 neuronal cells. DAPI staining (blue) highlighted the nuclei of both cell types, enabling clear visualization of cellular organization and distribution within the hydrogel matrix. The merged images distinctly showed axonal outgrowth in PC 12 cell type, with red arrows indicating cell extensions aligned along the channels of the 3D-printed scaffold and two-sided arrows marking the channel direction. These observations suggest that the scaffold's architecture may play a role in guiding neuronal growth and supporting neural network formation.

The axonal extensions observed in the PC12 cells were notably aligned with the longitudinal channels designed into the 3D-printed structure. This alignment suggests that the hydrogel's topographical cues played a pivotal role in guiding axonal growth, a critical factor for establishing functional neural circuits. The Beta III tubulin-positive projections were observed to follow the scaffold’s channels, demonstrating that the hydrogel provided the necessary physical and biochemical microenvironment to support axon pathfinding. Such guidance is essential for the formation of coherent neural networks, which are fundamental for restoring neural function in regenerative medicine applications. Moreover, the presence of extended neuronal projections toward the regions populated by SVG p12 cells indicates effective neuron-glia interactions. These interactions are vital for neural survival, synapse formation, and functional integration within neural tissue constructs.

Interestingly, the co-localization of GFAP-positive glial cells and Beta III tubulin-positive neuronal projections in certain regions of the scaffold suggests a synergistic relationship between the two cell types (149, 150). Glial cells are known to secrete neurotrophic factors that promote neuronal survival and axonal growth. The observed proximity of glial cells to neuronal projections indicates that the glial population may have facilitated the directed growth of axons, enhancing overall neural network formation within the scaffold. This neuron-glia crosstalk is essential for maintaining homeostasis and promoting repair processes within neural tissues, further underscoring the scaffold's effectiveness in supporting complex neural architectures.

Moreover, the intensity of Beta III tubulin staining across the scaffold demonstrated heterogeneous axonal growth patterns, potentially influenced by variations in scaffold porosity and mechanical properties. Regions with higher porosity and optimal mechanical stiffness appeared to support more robust axonal outgrowth, suggesting that these parameters critically influence neuronal behavior. The results imply that strategic modifications in the scaffold design, such as adjusting pore size or incorporating additional biochemical cues, could further enhance axonal extension and neural connectivity.

The axonal growth along predetermined channels is a result of guidance of scaffold architecture in neural tissue engineering guidance. The ability to guide axonal growth is particularly important for spinal cord injury applications, where restoring neural connectivity is essential for functional recovery. These findings suggest that the 3D- printed hydrogel scaffold developed in this study could serve as a promising platform for neural tissue engineering, capable of supporting neuron-glia interactions, guiding axonal extension, and ultimately promoting functional neural regeneration if proven to repeat the axon extension shown here.

In conclusion, the immunostaining analysis implied that the 3D-printed hydrogel scaffold effectively supported the survival and differentiation of both glial and neuronal cells. The observed axonal extensions aligned along the scaffold channels confirm the scaffold's role in providing physical guidance for neuronal growth, a

critical requirement for neural tissue engineering applications. The co-localization of glial and neuronal markers further emphasizes the scaffold's ability to promote neuron-glia interactions, essential for neural tissue function and regeneration.

4.3.4.5 Phalloidin-DAPI staining

On day 7, both 3D-printed SVG p12 cells and slab-form PC12 cells were stained with phalloidin and DAPI, and confocal microscopy was employed to assess cellular morphology, cytoskeletal organization, and spatial distribution within the constructs. The phalloidin staining highlighted the actin cytoskeleton, revealing well-defined cell extensions, intricate network formations, and filamentous structures in both cell types. The DAPI staining effectively labeled the cell nuclei, allowing for high-contrast visualization of nuclear distribution and alignment throughout the 3D and 2D environments. The combination of these staining techniques enabled a comprehensive evaluation of cellular architecture and the influence of scaffold geometry on cell behavior.

In the 3D-printed SVG p12 cell culture, the cells demonstrated a robust, three-dimensional network of interconnected extensions spanning multiple layers of the hydrogel scaffold. These well organized cytoskeletal arrangements suggest that the 3D-printed environment provided spatial cues for cells to extend processes in three dimensions, promoting the formation of cellular networks that resemble *in vivo* neural tissue architecture. Furthermore, the uniform distribution of DAPI-stained nuclei throughout the scaffold indicated effective cellular infiltration and colonization, suggesting that the 3D environment facilitated cellular migration—an essential factor for successful neural tissue regeneration.

In contrast, the slab-form PC12 cells displayed a more planar organization of the actin cytoskeleton. The phalloidin staining revealed elongated actin filaments characteristic of neuronal differentiation, including axonal-like projections. However, these structures were predominantly aligned along a single plane, suggesting limited vertical extension and spatial complexity. This planar organization reflects the inherent

limitations of 2D culture systems, which fail to provide the necessary topographical cues required for complex neuronal network formation. Although distinct cellular projections were observed, their two-dimensional alignment contrasts sharply with the intricate, multidimensional organization seen in the 3D printed SVG p12 cultures. The DAPI staining further highlighted these differences, with nuclei in the slab-form cultures appearing more clustered, indicating limited migration and suggesting that the planar environment restricted cellular dispersion and interaction.

Additionally, the interaction between SVG p12 glial cells and PC12 neuronal cells in the 3D environment demonstrated the scaffold's ability to support complex cellular relationships. The scaffold's topographical features likely provided physical guidance cues that facilitated directional axonal extension, critical for the establishment of functional neural circuits. These observations underscore the role of the 3D-printed hydrogel in replicating key aspects of neural tissue microenvironments, crucial for successful regeneration strategies.

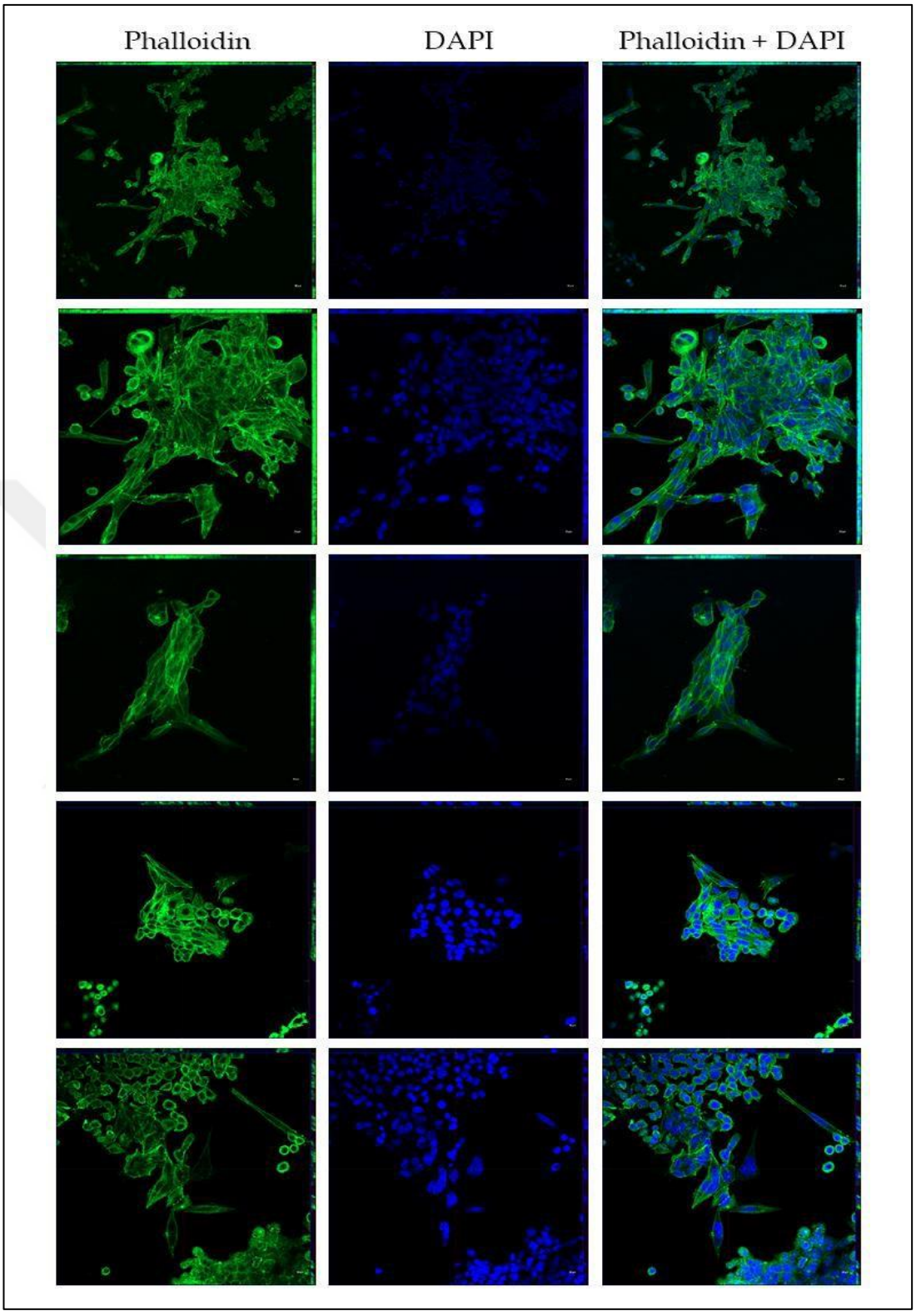

Figure 40. Phalloidin and DAPI staining of SVG p12 cells and PC12 cells at the junction of 3D bioprinted construct and slab between the two structures on day 7. Phalloidin staining highlights the actin cytoskeleton (green), while DAPI staining labels the cell nuclei (blue). (Scale bar: 20 μm)

In conclusion, the phalloidin and DAPI staining results in the 3D scaffold showed the cellular morphology, organization, and interaction. These results provide evidence for the potential application of such 3D-printed scaffolds in neural regeneration therapies, particularly for treating spinal cord injuries, and suggest future research directions focused on optimizing scaffold design to enhance neural axonal growth and function.

5 DISCUSSION

In this thesis focused on the development and comprehensive characterization of a 3D bioprinted hydrogel model designed to mimic the structural and functional complexity of spinal cord gray and white matter.

Characterization of the hydrogel's physical properties, including equilibrium water content (EWC) of 89%, revealed that the system exhibited excellent water retention. These properties are critical for maintaining a hydrated, stable environment that promotes cell survival and function, mimicking the natural extracellular matrix (ECM) of spinal cord tissue. Enzymatic degradation studies showed a 24% weight reduction after 2 hours of collagenase incubation, indicating low biodegradability suitable for long-term scaffold applications in SCI. The hydrogel demonstrated the capability to withstand degradation over a 21-day period, reinforcing its potential as a long-term scaffold for tissue regeneration.

The mechanical properties were assessed through compression tests, revealing an initial stiffness of 145±11 kPa, aligning closely with native spinal cord tissue. Rheological assessments demonstrated elastic and viscous moduli of 103 Pa and 100 Pa, respectively, indicating viscoelastic properties suitable for neural tissue applications. The 3D-printed constructs featured honeycomb and butterfly-like patterns resembling the microarchitecture of the spinal cord, with distinct regions mimicking the structural heterogeneity of gray and white matter. The longitudinal channels designed in the white matter region facilitated the alignment and extension of cellular processes, a critical factor in neural tissue engineering. These intricate patterns were achieved through precision bioprinting, enabling adequate nutrient diffusion and cellular communication while mimicking native spinal cord architecture.

Biological performance was confirmed through *in vitro* studies. The Alamar Blue assay demonstrated cell proliferation for both SVG p12 glial cells, which are involved in neural support, and PC12 neuronal cell lines, suggesting that the scaffold can support both cell types. The Live-Dead assay showed more than 90% cell viability,

confirming the suitability of the hydrogel. Immunostaining highlighted an indication of axonal extensions marked by Beta III tubulin expression, while Phalloidin-DAPI staining confirmed cytoskeletal organization and cell attachment. Confocal microscopy revealed co-localization of neuronal and glial cells, for functional recovery in SCI.

The inclusion of Laminin significantly enhanced cell adhesion and neurite outgrowth, consistent with its known role in neural tissue engineering.

Although the results are promising, several limitations were noted. Long-term electrophysiological assessments and synapse formation evaluations, critical for functional recovery, were not performed. While enzymatic degradation profiles were assessed *in vitro*, *in vivo* dynamics may differ. Mechanical properties, though suitable for *in vitro* conditions, may require further optimization for *in vivo* applications. Future studies should incorporate electrophysiological assessments, evaluate synaptic connectivity, and perform *in vivo* testing to assess functional regeneration. Advanced bioprinting techniques should introduce vascularization and gradient structures that better mimic native spinal cord architecture. Co-culture systems involving multiple neural cell types could further enhance neural network modeling.

In conclusion, the 3D bioprinted GelMA/HA/CS/Lmn hydrogel model developed in this study supports neural cell viability, axonal growth, and mechanical stability. The scaffold's ability to sustain both glial and neuronal cells, along with its precise structural architecture and controlled degradation profile, positions it as a platform for SCI research.

6 CONCLUSION

This study successfully demonstrated the development and application of a hydrogel- based 3D-bioprinted model that mimics the structural properties spinal cord tissue. Incorporating both gray and white matter architectures, this model aimed to provide the intricate microenvironment essential for the interaction and regeneration of glial and neuronal cells. The comprehensive characterization results not only confirmed the mechanical integrity of the hydrogel but also validated its biological compatibility, highlighting its potential for use in spinal cord tissue engineering applications.

The *in vitro* findings were particularly promising, providing robust evidence of the model's exceptional cell response and its capacity to support cellular processes such as survival, proliferation, and differentiation. These outcomes reinforce the feasibility of utilizing this hydrogel as a reliable platform for investigating SCI mechanisms and evaluating innovative therapeutic strategies aimed at enhancing spinal cord repair. The observed cellular responses further demonstrated the hydrogel's ability to sustain the regenerative potential of both glial and neuronal cells, which are crucial for the recovery of spinal cord function.

This research marks an attempt at development of tissue-engineered models, and mimic the different conditions created by different parameters to test hypotheses on neural and cancer research in addition to many others. By offering a scalable and reproducible model, this hydrogel-based system can serve as a key tool in the exploration of novel SCI treatments and regenerative therapies. These studies also pave the way for the translation of the findings into clinical applications, potentially leading to more effective strategies for spinal cord repair and regeneration. Ultimately, this work lays the groundwork for future innovations in spinal cord tissue engineering, offering new avenues for the development of personalized therapies tailored towards individual patient needs.

7 REFERENCES

1. Ahuja CS, Nori S, Tetreault L, Wilson J, Kwon B, Harrop J, et al. Traumatic Spinal Cord Injury-Repair and Regeneration. Neurosurgery. 2017;80(3S):S9-S22.
2. Who. International Perspectives on Spinal Cord Injury. International Perspectives on Spinal Cord Injury. 2013:1-231.
3. Wang H, Song G, Chuang H, Chiu C, Abdelmaksoud A, Ye Y, et al. Portrait of glial scar in neurological diseases. International journal of immunopathology and pharmacology. 2018;31:2058738418801406.
4. Fawcett JW, Asher RA. The glial scar and central nervous system repair. Brain Res Bull. 1999;49(6):377-91.
5. McDonald JW, Sadowsky C. Spinal-cord injury. The Lancet. 2002;359(9304):417-25.
6. Yuan TY, Zhang J, Yu T, Wu JP, Liu QY. 3D Bioprinting for Spinal Cord Injury Repair. Front Bioeng Biotech. 2022;10.
7. Bedir T, Ulag S, Ustundag CB, Gunduz O. 3D bioprinting applications in neural tissue engineering for spinal cord injury repair. Mat Sci Eng C-Mater. 2020;110.
8. Han Y, Sun MY, Lu XC, Xu KL, Yu MF, Yang HY, et al. A 3D printable gelatin methacryloyl/chitosan hydrogel assembled with conductive PEDOT for neural tissue engineering. Compos Part B-Eng. 2024;273.
9. Janig W, Habler HJ. Specificity in the organization of the autonomic nervous system: a basis for precise neural regulation of homeostatic and protective body functions. Prog Brain Res. 2000;122:351-67.
10. Nieuwenhuys R, Voogd J, Van Huijzen C. The human central nervous system: a synopsis and atlas: Springer Science & Business Media; 2007.
11. Sultana OF, Bandaru M, Islam MA, Reddy PH. Unraveling the complexity of human brain: Structure, function in healthy and disease states. Ageing Res Rev. 2024;100.
12. Harrow-Mortelliti M, Reddy V, Jimsheleishvili G. Physiology, Spinal Cord. StatPearls. Treasure Island (FL)2025.
13. Nógrádi A, Nógrádi A, Vrbová G. Anatomy and physiology of the spinal cord. Transplantation of neural tissue into the spinal cord. 2006:1-23.
14. Brown AG. Organization in the spinal cord: the anatomy and physiology of identified neurones: Springer Science & Business Media; 2012.
15. Filley CM, Fields RD. White matter and cognition: making the connection. J Neurophysiol. 2016;116(5):2093-104.
16. Stadelmann C, Timmler S, Barrantes-Freer A, Simons M. Myelin in the Central Nervous System: Structure, Function, and Pathology. Physiol Rev. 2019;99(3):1381-431.
17. Sengul G, Watson C. Ascending and descending pathways in the spinal cord. The rat nervous system: Elsevier; 2015. p. 115-30.

18. Catala M, Kubis N. Gross anatomy and development of the peripheral nervous system. Handbook of clinical neurology. 2013;115:29-41.
19. Waxenbaum JA, Reddy V, Varacallo M. Anatomy, autonomic nervous system. 2019.
20. Banerjee D, Das PK, Mukherjee J. Nervous System. Textbook of Veterinary Physiology: Springer; 2023. p. 265-93.
21. Brodal P. The central nervous system: oxford university Press; 2010.
22. Araque A, Navarrete M. Glial cells in neuronal network function. Philosophical Transactions of the Royal Society B: Biological Sciences. 2010;365(1551):2375-81.
23. Allen NJ. Astrocyte regulation of synaptic behavior. Annu Rev Cell Dev Biol. 2014;30:439-63.
24. Bradl M, Lassmann H. Oligodendrocytes: biology and pathology. Acta neuropathologica. 2010;119:37-53.
25. Norris GT, Kipnis J. Immune cells and CNS physiology: Microglia and beyond. Journal of experimental medicine. 2019;216(1):60-70.
26. Pannese E. Neurocytology: fine structure of neurons, nerve processes, and neuroglial cells: Springer; 2015.
27. Verkhratsky A, Rodríguez JJ, Parpura V. Neurotransmitters and integration in neuronal-astroglial networks. Neurochemical research. 2012;37:2326-38.
28. Almeida RG, Lyons DA. On myelinated axon plasticity and neuronal circuit formation and function. Journal of Neuroscience. 2017;37(42):10023-34.
29. Del Bigio MR. Ependymal cells: biology and pathology. Acta neuropathologica. 2010;119:55-73.
30. Prinz M, Priller J. Microglia and brain macrophages in the molecular age: from origin to neuropsychiatric disease. Nature Reviews Neuroscience. 2014;15(5):300-12.
31. Stevens CF. The neuron. Scientific American. 1979;241(3):54-65.
32. Arbib MA, Szentágothai J. Neural organization: Structure, function, and dynamics: MIT press; 1998.
33. Varma S. Neurone–basic functional unit of the nervous system. Pain Management E-Book: Pain Management E-Book. 2008:6.
34. Debanne D, Campanac E, Bialowas A, Carlier E, Alcaraz G. Axon physiology. Physiol Rev. 2011;91(2):555-602.
35. Hess A, Young JZ. The nodes of Ranvier. Proceedings of the Royal Society of London Series B-Biological Sciences. 1952;140(900):301-20.
36. Hammell KW. Exploring quality of life following high spinal cord injury: a review and critique. Spinal cord. 2004;42(9):491-502.
37. Hou S, Rabchevsky AG. Autonomic consequences of spinal cord injury. Compr Physiol. 2014;4(4):1419-53.
38. Borgens RB, Liu-Snyder P. Understanding secondary injury. The Quarterly review of biology. 2012;87(2):89-127.
39. Straley KS, Foo CWP, Heilshorn SC. Biomaterial design strategies for the treatment of spinal cord injuries. Journal of neurotrauma. 2010;27(1):1-19.

40. Chen H-C, Yen T-H, Chang K-H, Lin Y-N, Wang Y-H, Liou T-H, et al. Developing an ICF core set for sub-acute stages of spinal cord injury in Taiwan: a preliminary study. Disability and Rehabilitation. 2015;37(1):51-5.
41. ang Zhang Y, huan Wu Z, feng Wu J, dong Li T, gui Jiang F, Yang B. Current multi-scale biomaterials for tissue regeneration following spinal cord injury. Neurochemistry International. 2024:105801.
42. Yates AG. The contribution of the systemic inflammatory response to the outcome of spinal cord injury: University of Oxford; 2021.
43. Hong JY-L. A Comparison Between Cervical and Thoracic Spinal Cord Injury: Critical Level-dependent Differences in Pathobiology: University of Toronto (Canada); 2020.
44. Ditunno Jr JF, Formal CS. Chronic spinal cord injury. New England Journal of Medicine. 1994;330(8):550-6.
45. Houle JD, Tessler A. Repair of chronic spinal cord injury. Experimental neurology. 2003;182(2):247-60.
46. Raspa A, Pugliese R, Maleki M, Gelain F. Recent therapeutic approaches for spinal cord injury. Biotechnology and bioengineering. 2016;113(2):253-9.
47. Fiani B, Arshad MA, Shaikh ES, Baig A, Farooqui M, Ayub MA, et al. Current updates on various treatment approaches in the early management of acute spinal cord injury. Reviews in the Neurosciences. 2021;32(5):513-30.
48. Cadotte DW, Fehlings MG. Spinal cord injury: a systematic review of current treatment options. Clinical Orthopaedics and Related Research®. 2011;469:732-41.
49. Carlson GD, Gorden C. Current developments in spinal cord injury research. The Spine Journal. 2002;2(2):116-28.
50. Lanza R, Langer R, Vacanti JP, Atala A. Principles of tissue engineering: Academic press; 2020.
51. Loh QL, Choong C. Three-dimensional scaffolds for tissue engineering applications: role of porosity and pore size. Tissue Engineering Part B: Reviews. 2013;19(6).
52. Liao S, Chan CK, Ramakrishna S. Stem cells and biomimetic materials strategies for tissue engineering. Materials Science and Engineering: C. 2008;28(8):1189-202.
53. Henkel J, Hutmacher DW. Design and fabrication of scaffold-based tissue engineering. BioNanoMaterials. 2013;14(3-4):171-93.
54. Li Q, Ma L, Gao C. Biomaterials for in situ tissue regeneration: development and perspectives. Journal of Materials Chemistry B. 2015;3(46):8921-38.
55. Nguyen MK, Alsberg E. Bioactive factor delivery strategies from engineered polymer hydrogels for therapeutic medicine. Progress in polymer science. 2014;39(7):1235-65.
56. Quanjin M, Rejab M, Idris M, Kumar NM, Abdullah M, Reddy GR. Recent 3D and 4D intelligent printing technologies: A comparative review and future perspective. Procedia Computer Science. 2020;167:1210-9.
57. Zhang BG, Quigley AF, Myers DE, Wallace GG, Kapsa RM, Choong PF. Recent advances in nerve tissue engineering. The International journal of artificial organs. 2014;37(4):277-91.

58. Subramanian A, Krishnan UM, Sethuraman S. Development of biomaterial scaffold for nerve tissue engineering: Biomaterial mediated neural regeneration. Journal of biomedical science. 2009;16:1-11.
59. Olson L. Regeneration in the adult central nervous system: experimental repair strategies. Nature medicine. 1997;3(12):1329-35.
60. Sensharma P, Madhumathi G, Jayant RD, Jaiswal AK. Biomaterials and cells for neural tissue engineering: Current choices. Materials Science and Engineering: C. 2017;77:1302-15.
61. Wang A, Tang Z, Park I-H, Zhu Y, Patel S, Daley GQ, et al. Induced pluripotent stem cells for neural tissue engineering. Biomaterials. 2011;32(22):5023-32.
62. Khademhosseini A, Ashammakhi N, Karp JM, Gerecht S, Ferreira L, Annabi N, et al. Embryonic stem cells as a cell source for tissue engineering. Principles of tissue engineering: Elsevier; 2020. p. 467-90.
63. Bottai D, Fiocco R, Gelain F, Defilippis L, Galli R, Gritti A, et al. Neural stem cells in the adult nervous system. Journal of hematotherapy & stem cell research. 2003;12(6):655-70.
64. Wang H, Yang Y, Liu J, Qian L. Direct cell reprogramming: approaches, mechanisms and progress. Nature Reviews Molecular Cell Biology. 2021;22(6):410-24.
65. Hirschi KK, Li S, Roy K. Induced pluripotent stem cells for regenerative medicine. Annual review of biomedical engineering. 2014;16(1):277-94.
66. Fitzsimmons RE, Mazurek MS, Soos A, Simmons CA. Mesenchymal stromal/stem cells in regenerative medicine and tissue engineering. Stem cells international. 2018;2018(1):8031718.
67. Campana WM. Schwann cells: activated peripheral glia and their role in neuropathic pain. Brain, behavior, and immunity. 2007;21(5):522-7.
68. Duncan I, Hoffman R. Schwann cell invasion of the central nervous system of the myelin mutants. Journal of anatomy. 1997;190(1):35-49.
69. Bunge RP. Glial cells and the central myelin sheath. Physiol Rev. 1968;48(1):197-251.
70. Amini S, Salehi H, Setayeshmehr M, Ghorbani M. Natural and synthetic polymeric scaffolds used in peripheral nerve tissue engineering: Advantages and disadvantages. Polymers for Advanced Technologies. 2021;32(6):2267-89.
71. Kaewkhaw R, Scutt AM, Haycock JW. Integrated culture and purification of rat Schwann cells from freshly isolated adult tissue. Nature protocols. 2012;7(11):1996-2004.
72. Sanchez Rezza A, Kulahci Y, Gorantla VS, Zor F, Drzeniek NM. Implantable biomaterials for peripheral nerve regeneration–technology trends and translational tribulations. Front Bioeng Biotech. 2022;10:863969.
73. Yamanaka S. Induced pluripotent stem cells: past, present, and future. Cell stem cell. 2012;10(6):678-84.
74. Wobus AM, Boheler KR. Embryonic stem cells: prospects for developmental biology and cell therapy. Physiol Rev. 2005;85(2):635-78.
75. Rodríguez-Pizà I, Richaud-Patin Y, Vassena R, González F, Barrero MJ, Veiga A, et al. Reprogramming of human fibroblasts to induced pluripotent stem cells under xeno-free conditions.

Stem Cells. 2010;28(1):36-44.
76. Hynes K, Menicanin D, Mrozik K, Gronthos S, Bartold PM. Generation of functional mesenchymal stem cells from different induced pluripotent stem cell lines. Stem cells and development. 2014;23(10):1084-96.
77. Griffin TA, Anderson HC, Wolfe JH. Ex vivo gene therapy using patient iPSC-derived NSCs reverses pathology in the brain of a homologous mouse model. Stem cell reports. 2015;4(5):835-46.
78. Stern S, Zhang L, Wang M, Wright R, Rosh I, Hussein Y, et al. Monozygotic twins discordant for schizophrenia differ in maturation and synaptic transmission. Molecular Psychiatry. 2024;29(10):3208-22.
79. Qian L, Tcw J. Human iPSC-based modeling of central nerve system disorders for drug discovery. International Journal of Molecular Sciences. 2021;22(3):1203.
80. Wang J, Chen S, Pan C, Li G, Tang Z. Application of small molecules in the central nervous system direct neuronal reprogramming. Front Bioeng Biotech. 2022;10:799152.
81. Mohamed N-V, Larroquette F, Beitel LK, Fon EA, Durcan TM. One step into the future: new iPSC tools to advance research in Parkinson's disease and neurological disorders. Journal of Parkinson's disease. 2019;9(2):265-81.
82. Vizziello A, Magarini M, Savazzi P, Galluccio L. Intra-body communications for nervous system applications: Current technologies and future directions. Computer Networks. 2023;227:109718.
83. Doblado LR, Martínez-Ramos C, Pradas MM. Biomaterials for neural tissue engineering. Frontiers in Nanotechnology. 2021;3:643507.
84. Lendahl U, McKay RD. The use of cell lines in neurobiology. Trends in neurosciences. 1990;13(4):132-7.
85. Xie D, Deng T, Zhai Z, Sun T, Xu Y. The cellular model for Alzheimer's disease research: PC12 cells. Frontiers in molecular neuroscience. 2023;15:1016559.
86. Biazar E, Khorasani M, Montazeri N, Pourshamsian K, Daliri M, Khoshzaban A, et al. Types of neural guides and using nanotechnology for peripheral nerve reconstruction. International journal of nanomedicine. 2010:839-52.
87. Lopes CD, Gonçalves NP, Gomes CP, Saraiva MJ, Pêgo AP. BDNF gene delivery mediated by neuron-targeted nanoparticles is neuroprotective in peripheral nerve injury. Biomaterials. 2017;121:83-96.
88. Malafaya PB, Silva GA, Reis RL. Natural–origin polymers as carriers and scaffolds for biomolecules and cell delivery in tissue engineering applications. Advanced drug delivery reviews. 2007;59(4-5):207-33.
89. Gu X, Ding F, Williams DF. Neural tissue engineering options for peripheral nerve regeneration. Biomaterials. 2014;35(24):6143-56.
90. Wang KK, Nemeth IR, Seckel BR, Chakalis- Haley DP, Swann DA, Kuo JW, et al. Hyaluronic acid enhances peripheral nerve regeneration in vivo. Microsurgery. 1998;18(4):270-5.
91. Wang X, He J, Wang Y, Cui F-Z. Hyaluronic acid-based scaffold for central neural tissue

engineering. Interface focus. 2012;2(3):278-91.
92. Melrose J, Hayes AJ, Bix G. The CNS/PNS extracellular matrix provides instructive guidance cues to neural cells and neuroregulatory proteins in neural development and repair. International Journal of Molecular Sciences. 2021;22(11):5583.
93. Hussein RK, Mencio CP, Katagiri Y, Brake AM, Geller HM. Role of chondroitin sulfation following spinal cord injury. Frontiers in cellular neuroscience. 2020;14:208.
94. Asghari F, Samiei M, Adibkia K, Akbarzadeh A, Davaran S. Biodegradable and biocompatible polymers for tissue engineering application: a review. Artificial cells, nanomedicine, and biotechnology. 2017;45(2):185-92.
95. Gentile P, Chiono V, Carmagnola I, Hatton PV. An overview of poly (lactic-co-glycolic) acid (PLGA)-based biomaterials for bone tissue engineering. International journal of molecular sciences. 2014;15(3):3640-59.
96. Malikmammadov E, Tanir TE, Kiziltay A, Hasirci V, Hasirci N. PCL and PCL-based materials in biomedical applications. Journal of Biomaterials science, Polymer edition. 2018;29(7-9):863-93.
97. Subramanian A, Krishnan UM, Sethuraman S. Fabrication, characterization and in vitro evaluation of aligned PLGA–PCL nanofibers for neural regeneration. Annals of biomedical engineering. 2012;40:2098-110.
98. Seal B, Otero T, Panitch A. Polymeric biomaterials for tissue and organ regeneration. Materials Science and Engineering: R: Reports. 2001;34(4-5):147-230.
99. Hasanzadeh E, Seifalian A, Mellati A, Saremi J, Asadpour S, Enderami SE, et al. Injectable hydrogels in central nervous system: Unique and novel platforms for promoting extracellular matrix remodeling and tissue engineering. Materials Today Bio. 2023;20:100614.
100. Abidian MR, Daneshvar ED, Egeland BM, Kipke DR, Cederna PS, Urbanchek MG. Hybrid conducting polymer–hydrogel conduits for axonal growth and neural tissue engineering. 2012.
101. Boni R, Ali A, Shavandi A, Clarkson AN. Current and novel polymeric biomaterials for neural tissue engineering. Journal of biomedical science. 2018;25:1-21.
102. Gao Y, Zhang X, Zhou H. Biomimetic hydrogel applications and challenges in bone, cartilage, and nerve repair. Pharmaceutics. 2023;15(10):2405.
103. Bell JH, Haycock JW. Next generation nerve guides: materials, fabrication, growth factors, and cell delivery. Tissue Engineering Part B: Reviews. 2012;18(2):116-28.
104. Limongi T, Rocchi A, Cesca F, Tan H, Miele E, Giugni A, et al. Delivery of brain-derived neurotrophic factor by 3D biocompatible polymeric scaffolds for neural tissue engineering and neuronal regeneration. Molecular neurobiology. 2018;55:8788-98.
105. Mahar M, Cavalli V. Intrinsic mechanisms of neuronal axon regeneration. Nature Reviews Neuroscience. 2018;19(6):323-37.
106. Nasrolahi A, Javaherforooshzadeh F, Jafarzadeh-Gharehziaaddin M, Mahmoudi J, Asl KD, Shabani Z. Therapeutic potential of neurotrophic factors in Alzheimer's Disease. Molecular biology reports. 2022:1-13.
107. Zhang Q, Wu P, Chen F, Zhao Y, Li Y, He X, et al. Brain derived neurotrophic factor and glial

cell line-derived neurotrophic factor-transfected bone mesenchymal stem cells for the repair of periphery nerve injury. Front Bioeng Biotech. 2020;8:874.

108. Berry A, Bindocci E, Alleva E. NGF, brain and behavioral plasticity. Neural plasticity. 2012;2012(1):784040.
109. Navarro X, Vivó M, Valero-Cabré A. Neural plasticity after peripheral nerve injury and regeneration. Progress in neurobiology. 2007;82(4):163-201.
110. Hussain G, Wang J, Rasul A, Anwar H, Qasim M, Zafar S, et al. Current status of therapeutic approaches against peripheral nerve injuries: a detailed story from injury to recovery. International journal of biological sciences. 2020;16(1):116.
111. Rossi F, Gianola S, Corvetti L. Regulation of intrinsic neuronal properties for axon growth and regeneration. Progress in neurobiology. 2007;81(1):1-28.
112. Chuang J-H, Tung L-C, Lin Y. Neural differentiation from embryonic stem cells in vitro: An overview of the signaling pathways. World Journal of Stem Cells. 2015;7(2):437.
113. Terenghi G. Peripheral nerve regeneration and neurotrophic factors. The Journal of Anatomy. 1999;194(1):1-14.
114. Fernyhough P, Ishii DN. Nerve growth factor modulates tubulin transcript levels in pheochromocytoma PC12 cells. Neurochemical research. 1987;12:891-9.
115. Li Y, Ma Z, Ren Y, Lu D, Li T, Li W, et al. Tissue engineering strategies for peripheral nerve regeneration. Frontiers in neurology. 2021;12:768267.
116. Lotfi L, Khakbiz M, Moosazadeh Moghaddam M, Bonakdar S. A biomaterials approach to Schwann cell development in neural tissue engineering. Journal of Biomedical Materials Research Part A. 2019;107(11):2425-46.
117. Singh G, Sikder A, Phatale V, Srivastava S, Singh SB, Khatri DK. Therapeutic potential of GDNF in neuroinflammation: Targeted delivery approaches for precision treatment in neurological diseases. Journal of Drug Delivery Science and Technology. 2023;87:104876.
118. Duarte Azevedo M, Sander S, Tenenbaum L. GDNF, a neuron-derived factor upregulated in glial cells during disease. Journal of clinical medicine. 2020;9(2):456.
119. Zuccaro E, Piol D, Basso M, Pennuto M. Motor neuron diseases and neuroprotective peptides: A closer look to neurons. Frontiers in Aging Neuroscience. 2021;13:723871.
120. Sariola H, Saarma M. Novel functions and signalling pathways for GDNF. Journal of cell science. 2003;116(19):3855-62.
121. Zhang L, Ma Z, Smith GM, Wen X, Pressman Y, Wood PM, et al. GDNF- enhanced axonal regeneration and myelination following spinal cord injury is mediated by primary effects on neurons. Glia. 2009;57(11):1178-91.
122. Tran AP, Warren PM, Silver J. The biology of regeneration failure and success after spinal cord injury. Physiol Rev. 2018;98(2):881-917.
123. Liu Y, Wang H. Peripheral nerve injury induced changes in the spinal cord and strategies to counteract/enhance the changes to promote nerve regeneration. Neural regeneration research. 2020;15(2):189-98.

124. Numakawa T, Suzuki S, Kumamaru E, Adachi N, Richards M, Kunugi H. BDNF function and intracellular signaling in neurons. Histology and histopathology. 2010.
125. Gordon T. The role of neurotrophic factors in nerve regeneration. Neurosurgical focus. 2009;26(2):E3.
126. Colucci-D'Amato L, Speranza L, Volpicelli F. Neurotrophic factor BDNF, physiological functions and therapeutic potential in depression, neurodegeneration and brain cancer. International journal of molecular sciences. 2020;21(20):7777.
127. Carvalho CR, Oliveira JM, Reis RL. Modern trends for peripheral nerve repair and regeneration: beyond the hollow nerve guidance conduit. Front Bioeng Biotech. 2019;7:337.
128. Johnson EO, Charchanti A, Soucacos PN. Nerve repair: experimental and clinical evaluation of neurotrophic factors in peripheral nerve regeneration. Injury. 2008;39(3):37-42.
129. Lucini C, D'Angelo L, Cacialli P, Palladino A, De Girolamo P. BDNF, brain, and regeneration: insights from zebrafish. International journal of molecular sciences. 2018;19(10):3155.
130. Merighi A. Brain-Derived neurotrophic factor, nociception, and pain. Biomolecules. 2024;14(5):539.
131. Dunkel P, Chai CL, Sperlágh B, Huleatt PB, Mátyus P. Clinical utility of neuroprotective agents in neurodegenerative diseases: current status of drug development for Alzheimer's, Parkinson's and Huntington's diseases, and amyotrophic lateral sclerosis. Expert opinion on investigational drugs. 2012;21(9):1267-308.
132. Zhang H, Guo J, Wang Y, Shang L, Chai R, Zhao Y. Natural polymer- derived bioscaffolds for peripheral nerve regeneration. Advanced Functional Materials. 2022;32(41):2203829.
133. Wang J, Hu W-W, Jiang Z, Feng M-J. Advances in treatment of neurodegenerative diseases: perspectives for combination of stem cells with neurotrophic factors. World journal of stem cells. 2020;12(5):323.
134. Zhang Z, Hao Z, Xian C, Fang Y, Cheng B, Wu J, et al. Neuro-bone tissue engineering: multiple potential translational strategies between nerve and bone. Acta Biomaterialia. 2022;153:1-12.
135. Lu D, Yang Y, Zhang P, Ma Z, Li W, Song Y, et al. Development and application of three-dimensional bioprinting scaffold in the repair of spinal cord injury. Tissue Engineering and Regenerative Medicine. 2022;19(6):1113-27.
136. Ning L, Zhu N, Smith A, Rajaram A, Hou H, Srinivasan S, et al. Noninvasive three-dimensional in situ and in vivo characterization of bioprinted hydrogel scaffolds using the X-ray propagation-based imaging technique. ACS Applied Materials & Interfaces. 2021;13(22):25611-23.
137. Prendergast ME, Burdick JA. Recent advances in enabling technologies in 3D printing for precision medicine. Advanced Materials. 2020;32(13):1902516.
138. Ravanbakhsh H, Karamzadeh V, Bao G, Mongeau L, Juncker D, Zhang YS. Emerging technologies in multi- material bioprinting. Advanced Materials. 2021;33(49):2104730.
139. Richard C, Neild A, Cadarso VJ. The emerging role of microfluidics in multi-material 3D bioprinting. Lab on a Chip. 2020;20(12):2044-56.
140. Liu W, Zhang YS, Heinrich MA, De Ferrari F, Jang HL, Bakht SM, et al. Rapid continuous

multimaterial extrusion bioprinting. Advanced materials. 2017;29(3):1604630.

141. Zarepour A, Hooshmand S, Gökmen A, Zarrabi A, Mostafavi E. Spinal cord injury management through the combination of stem cells and implantable 3D bioprinted platforms. Cells. 2021;10(11):3189.

142. Ju D, Dong C. The combined application of stem cells and three-dimensional bioprinting scaffolds for the repair of spinal cord injury. Neural Regeneration Research. 2024;19(8):1751-8.

143. Giger RJ, Hollis ER, Tuszynski MH. Guidance molecules in axon regeneration. Cold Spring Harbor perspectives in biology. 2010;2(7):a001867.

144. Hoang DM, Pham PT, Bach TQ, Ngo AT, Nguyen QT, Phan TT, et al. Stem cell-based therapy for human diseases. Signal transduction and targeted therapy. 2022;7(1):272.

145. Jain P, Kathuria H, Dubey N. Advances in 3D bioprinting of tissues/organs for regenerative medicine and in-vitro models. Biomaterials. 2022;287:121639.

146. Han X, Alu A, Liu H, Shi Y, Wei X, Cai L, et al. Biomaterial-assisted biotherapy: A brief review of biomaterials used in drug delivery, vaccine development, gene therapy, and stem cell therapy. Bioactive materials. 2022;17:29-48.

147. Zhang Z, Chai Y, Zhao H, Yang S, Liu W, Yang Z, et al. Crosstalk between PC12 cells and endothelial cells in an artificial neurovascular niche constructed by a dual-functionalized self-assembling peptide nanofiber hydrogel. Nano Research. 2022;15:1433-45.

148. Tewari BP, Chaunsali L, Prim CE, Sontheimer H. A glial perspective on the extracellular matrix and perineuronal net remodeling in the central nervous system. Frontiers in cellular neuroscience. 2022;16:1022754.

149. Jurga AM, Paleczna M, Kadluczka J, Kuter KZ. Beyond the GFAP-astrocyte protein markers in the brain. Biomolecules. 2021;11(9):1361.

150. Terry S, Ploussard G, Allory Y, Nicolaiew N, Boissiere-Michot F, Maille P, et al. Increased expression of class III β-tubulin in castration-resistant human prostate cancer. British journal of cancer. 2009;101(6):951-6.

8 CURRICULUM VITAE